



**Core-shell nanoparticles - Synthesis and Applications in
Catalysis and
Electrocatalysis**

Journal:	<i>Chemical Society Reviews</i>
Manuscript ID:	CS-REV-04-2015-000343.R2
Article Type:	Review Article
Date Submitted by the Author:	23-Jul-2015
Complete List of Authors:	Gawande, Manoj; Palacky University, Regional Center of Advanced Technologies and Materials Goswami, Anandarup; Palacky University, Regional Center of Advanced Technologies and Materials Asefa, Tewodros; Rutgers University, Department of Chemistry and Chemical Biology Guo, Huizhang; Xiamen University, Department of Materials Science and Engineering Biradar, Ankush; National Chemical Laboratory, Catalysis Division Peng, Dong-Liang; Xiamen University, Department of Materials Science and Engineering Zboril, Radek; Palacky University, Regional Center of Advanced Technologies and Materials Varma, Rajender; U.S. Environmental Protection Agency, National Risk Management Research Laboratory

Core-shell nanoparticles: synthesis and applications in catalysis and electrocatalysis

Manoj B. Gawande,^{a*} Anandarup Goswami,^{a,b,c} Tewodros Asefa,^{b,c} Huizhang Guo,^d Ankush V. Biradar,^e Dong-Liang Peng,^d Radek Zboril,^{a*} and Rajender S. Varma^{f*}

^a Regional Centre of Advanced Technologies and Materials, Faculty of Science, Department of Physical Chemistry, Palacky University, Šlechtitelů 11, 783 71, Olomouc, Czech Republic.

^b Department of Chemistry and Chemical Biology, Rutgers, The State University of New Jersey, 610 Taylor Road, Piscataway, New Jersey 08854, USA.

^c Department of Chemical and Biochemical Engineering, Rutgers, The State University of New Jersey, 98 Brett Road, Piscataway, New Jersey 08854, USA.

^d Department of Materials Science and Engineering, College of Materials, Xiamen University, Xiamen 361005, People's Republic of China.

^e Catalysis Division, CSIR-National Chemical Laboratory, Dr. Homi Bhabha Road, Pune 411008, India.

^f Sustainable Technology Division, National Risk Management Research Laboratory, US Environmental Protection Agency, 26 West Martin Luther King Drive, MS 443, Cincinnati, Ohio, 45268, USA.

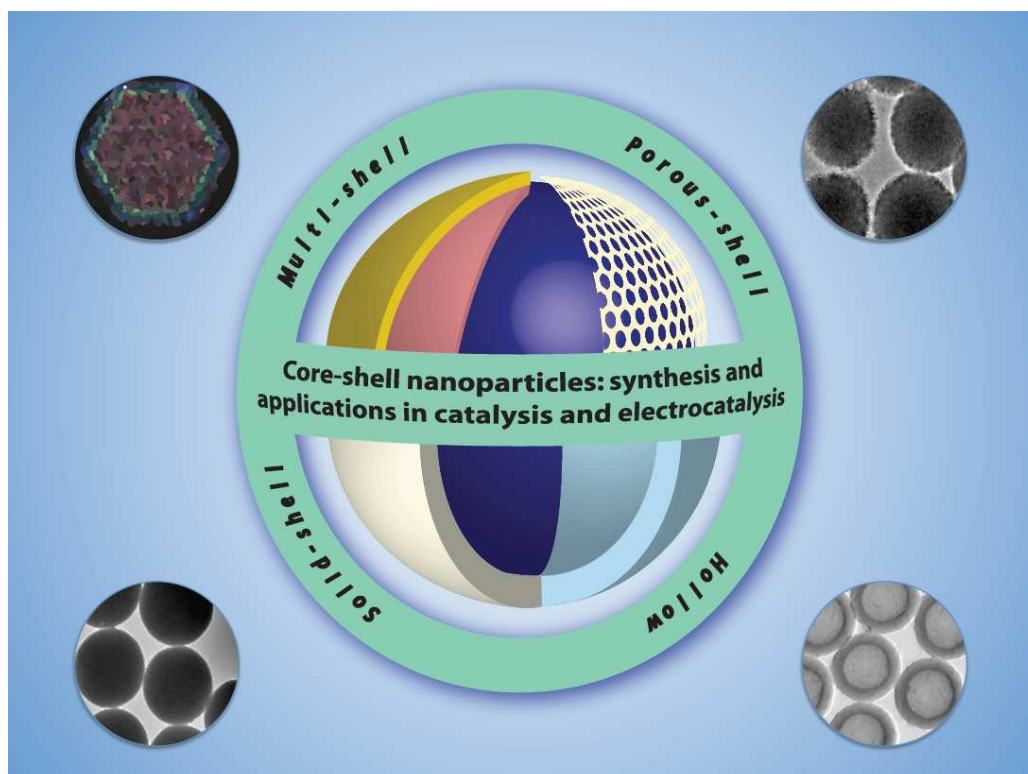


Table of Content

1. Introduction
- 5 2. Focus of review
3. Synthetic and characterization techniques of core–shell nanoparticles
 - 3.1. Synthesis of core–shell nanocatalysts
 - 3.1.1. Classification
 - 3.1.1.1. Organics
 - 10 3.1.1.2. Inorganics
 - 3.1.1.3. Classification based on shell properties
 - 3.1.1.3.1. Hollow-core-shell NPs
 - 3.1.1.3.2. Core-Multishell NPs
 - 3.1.1.3.3. Core-porous-shell NPs
 - 15 3.2. Characterization techniques for core–shell nanoparticles
 4. Applications of core–shell nanoparticles in catalysis
 - 4.1. Hydrogenation reactions
 - 4.1.1. Chemoselective reduction reaction
 - 4.1.2. Semihydrogenation of alkynes by Pd@MPSO/SiO₂
 - 20 4.1.3. Reduction reactions with magnetically separable core–shell nanocatalysts
 - 4.1.4. Asymmetric transfer hydrogenation of aromatic ketones on immobilized rhodium catalyst
 - 4.1.5. Vapor-phase cyclohexene hydrogenation by Au–Rh core–shell nanoparticles
 - 4.1.6. Hydrogenation of alkenes by SiO₂/Pd/SiO₂ type core–shell–shell microspheres
 - 25 4.1.7. Magnetic core–shell Au nanocatalyst for the reduction of 4-nitrophenol
 - 4.2. Oxidation reactions
 - 4.2.1. One-pot oxidation of sulfides by Pd/SiO₂@TiMS core–shell nanocatalyst
 - 4.2.2. Oxidation of alcohols on Fe₃O₄@MgAl-LDH@Au core–shell nanocatalyst
 - 4.2.3. Oxidation of benzyl alcohol by gold–palladium core–shell nanocrystals
 - 30 4.2.4. Lab-in-a-shell approach for selective catalysis
 - 4.2.5. CO oxidation with core–shell nanoparticles
 - 4.2.6. CO oxidation on sinter-resistant Au–mesoporous-silica core–shell nanoparticles
 - 4.3. Coupling Reactions
 - 4.3.1. Au–Pd core–shell catalyzed Suzuki–Miyaura reaction
 - 35 4.3.2. Suzuki–Miyaura reaction catalyzed by Ni/Pd core–shell nanoparticles

- 4.3.3. Sonogashira coupling reaction catalyzed by inside-out type core-shell nanoparticles
- 4.4. Ammonia decomposition reaction with iron-based core-shell nanoparticles
- 4.5. Tandem deprotection-Knoevenagel and Henry reaction by core-shell nanocatalysts
- 5 4.6. CO adsorption on Pd- and Pt-based core-shell nanocatalysts
- 4.7. Aerobic oxidative esterification by AuNiO_x/SiO₂-Al₂O₃-MgO catalysts
- 4.8. Catalytic applications of Al₂O₃@Fe₂O₃ CSNs for the synthesis of adipic acid
- 4.9. Heterogeneously exposed core-shell Pt@TiO₂ catalysts
5. Electrocatalysis by core-shell nanocatalysts
- 10 6. Perspectives and future prospects
7. Concluding remarks

Abstract

15 Core-shell nanoparticles are a class of nanostructured materials that have recently received increased attention owing to their interesting properties and broad range of applications in catalysis, biology, materials chemistry and sensors. By rationally tuning the cores as well as the shells of such materials, a range of core-shell nanoparticles (CSNs) can be produced with tailorable properties that can play important roles in various catalytic processes and offer sustainable solutions to current
20 energy problems. Various synthetic methods for preparing different classes of CSNs, including the Stöber method, solvothermal method, one-pot synthetic method involving surfactants, *etc.*, are briefly mentioned here. The roles of various classes of CSNs are exemplified for both catalytic and electrocatalytic applications, including oxidation, reduction, coupling reactions, *etc.*

25 1. Introduction

Nanomaterials have attracted enormous attention owing to their interesting properties as well as utility in the diverse areas including nanocatalysis,^{1, 2} magnetite-supported catalysis,³⁻⁵ nanoelectronics,⁶⁻¹⁰ integrated catalysis,¹¹ *etc.*¹²⁻²⁰ Rapid development of nanotechnology over the past few decades has allowed researchers to view conventional heterogeneous catalysts from a new
30 perspective.²¹⁻²⁴ In particular, catalytic materials can now be prepared with greater precision *via* nanotech-enabled processes.²⁵⁻²⁷ Noble metal nanoparticles (NPs), which often serve as active catalytic components, can now be routinely synthesized with well-defined sizes, shapes, crystal facets, structure and composition.^{28,29} Such controllability over materials' structures could potentially lead to the development of new technologies for applications in green, sustainable and
35 economically-viable chemical processes, which are currently regarded as among the most desirable yet challenging areas in chemistry.³⁰⁻³³ Besides offering solutions to the traditional demands for

catalysts to be efficient and selective for a particular catalytic reaction that will transform raw materials into valuable chemicals, such as pharmaceuticals and fuels, these nanomaterials could assist in the development of green chemistry, offering the advantages of waste reduction, atomic efficiency, higher reaction rates and also facile catalyst recovery.³⁴⁻³⁷

5 Traditional composite nanomaterials constructed with cores (inner material) and shells (outer layer material), both at nanoscale, are broadly defined as CSNs (or core-shell nanostructured materials).³⁸ Though, historically, the term was coined for the concentric multilayer semiconductor nanoparticles^{39,40} with the advancement in the field of core-shell nanomaterials, the definition of the core-shell nanomaterials can be extended to the class of nanomaterials having distinct boundary
10 materials covering (either fully or partially) the inner component as long as they can be separately identified. Depending on the compositions and arrangements of the two components in the materials, core-shell nanostructures can be divided into several classes, including inorganic/inorganic, inorganic/organic, organic/inorganic and organic/organic type CSNs.⁴¹⁻⁴³ As interest in task-specific nanomaterials with multi-functional capabilities and/or enhanced properties
15 is increasing, core-shell nanostructures are increasingly attracting attention because of their conducive and versatile compositions and structures to serve such purposes.⁴⁴⁻⁴⁷ In addition, CSNs may have properties that are synergistic between the cores and shells and/or offer new properties depending on the interactions between the cores and shells.⁴⁸⁻⁵² Such unique, useful and tailorable properties have also advanced CSNs as a very important class of emerging nanomaterials for a wide
20 range of applications in, for instance, bio-nanotechnology,⁵³⁻⁵⁵ enhanced optical devices,^{56,57,58} tailored magnetic devices,⁵⁹⁻⁶³ electronic optical devices,⁴² bioimaging systems,^{64, 65} energy storage materials,⁶⁶ genetic engineering and stem cells,^{67,68} fuel cell labeling,^{69,70} dye sensitized solar cells⁷¹ and many important catalytic processes⁷²⁻⁸² (Fig. 1).

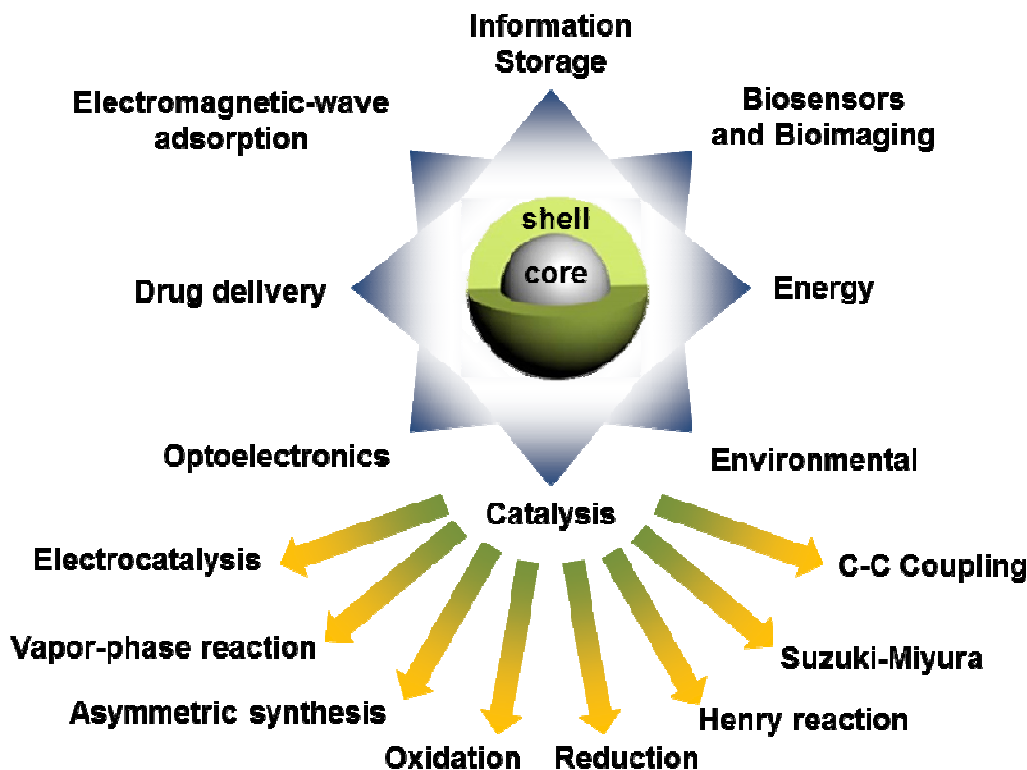


Fig. 1 Applications of CSNs in various areas of modern technology especially in the field of catalysis.

One important challenge, often faced by chemists working in the area of catalysis, is the development of highly active and selective, robust, low-cost and environmentally benign catalytic systems. This issue, as a whole or in part, could be addressed by developing catalytic systems with core-shell structural features. Among the possible advantages that these types of nanomaterials can offer, three major ones can be highlighted: 1) the use of the core as a support allowing the specific surface(shell) nanoarchitecture in terms of porosity, surface area etc. thus resulting in superior catalytic performance of such a layer/shell, 2) synergism between the shell and the core enabling to achieve higher efficiency/yield/selectivity in catalytic applications and 3) combination of the properties of the core and shell towards improved/combined applications (e.g. magnetically separable nanocatalysts with the possibility of the repetitive use without the loss of the catalytic efficiency).

The catalytic and electrocatalytic activity of such catalyst depends on its synergistic interactions between the core and shell. Primarily there are three major effects (and in most cases a single, combined one) that can play important roles in deciding the catalytic/electrocatalytic activity of a particular materials: (a) ligand effect, which involves the interaction between the core and the shell because of atomic vicinity affecting the charge transfer between the components by altering the band-structures; (b) ensemble effects, which is governed by the material's adsorption

on the surface due to the presence of distinct atomic groups, and finally (c) geometric effects, originates from the difference in reactivity of the surface atoms because of their three dimensional structural constraints (e.g. surface strain).”

For instance, by coating precious metal catalysts (e.g., Au, Pt or Pd), as a monolayer on the surfaces of non-precious based nanometal (e.g., Ni, Fe or Co), atom-economical and cost effective CSNs with good catalytic efficiency can be produced. This strategy has been successfully exploited by Son *et al.* via Ni@Pd core-shell NP-based catalysts that displayed high catalytic activity for the Sonogashira coupling reactions.⁸³ Similarly, carbon-supported Pd@Co CSNs were synthesized by Wang *et al.* and used as electrocatalysts for the oxygen reduction reaction (ORR).⁸⁴ In addition to decreasing the amount of expensive material used in the catalytic system by placing Pt only as a shell monolayer over Co and Fe surfaces, the composite materials (Pt₃Co and Pt₃Fe) could result in improved oxygen adsorption energy, and thereby enhanced catalytic activity and stability.^{85, 86}

Additionally, rational design and applications of CSNs with tailored structures and efficient catalytic activity can often be investigated by applying density functional theory (DFT) and other theoretical considerations.^{49, 87-89} DFT studies, which have been successfully used to model various chemisorption and desorption processes, primarily involve the d-band center model.⁹⁰ In such a model, the ligand and strain effect from the core to the shell components are assumed to affect the d-band width or d-band filling.^{91, 92} By harnessing such theoretical designs, supported by experiments, CSNs catalysts can be prepared with enhanced activity and selectivity.⁹³

Recently, Tedsree *et al.* synthesized Ag NPs coated with a thin layer of Pd atoms, which showed significantly enhanced catalytic activity toward H₂ evolution from formic acid at ambient temperature.⁹⁴ The improved catalytic activity of the materials was attributed to the fact that the Pd shell contains terrace sites and is electronically promoted by the Ag core. Meanwhile, lattice strain has been found to be advantageous for tuning the catalytic activity of core-shell structure.⁹⁵ Xu⁷⁵ and Li⁹⁶ designed and synthesized Au@Co CSNs that have efficient catalytic activity for the hydrolytic dehydrogenation of ammonia borane. Similarly, Ag@Ni CSNs synthesized *via* a one-pot synthetic procedure showed enhanced catalytic activity towards hydrogen evolution from the dehydrogenation of sodium borohydride in aqueous solutions⁹⁷ and transfer hydrogenation reactions of aromatic nitro and carbonyl compounds.⁹⁸ In another example, alumina-supported Cu@Ni and Ni@Cu CSNs were shown to have comparable catalytic activity towards water-gas-shift reaction, giving significantly low undesirable methanation side-reaction, than conventional supported Ni catalyst.⁷² In other words, the selectivity of the water-gas-shift reaction was improved by using CSNs catalysts. By incorporating magnetic materials, multifunctional CSNs with catalytic as well as magnetic properties (the latter being useful for the ease of recyclability/magnetic

separation of the CSNs after the reaction), could be synthesized in an analogous manner.⁹⁹ This synthetic strategy has been widely applied for the fabrication of various bifunctional nanomaterials, *e.g.*, magnetic and optically/photocatalytically active Fe₃O₄@ZnS NPs.⁵⁷ Stark and co-workers have reviewed nanomaterials comprising ferrite NPs and their use as semi-heterogeneous catalyst supports.¹⁰⁰

Overall, the variety of CSNs with different sizes (5 - 500 nm), morphologies (spherical, honeycomb, hollow, etc.), compositions (organic, inorganic etc.), and their catalytic applications in various types of catalytic processes, organic reactions and electrocatalysis are presented in detail. For instance, Fe₂O₃@Au CSNs,¹⁰¹ carbon-coated cobalt,¹⁰² FeCo/graphitic core-shell nanocrystals,⁵⁵ and FePt@ZnO CSNs¹⁰³ exhibit promising catalytic properties for various reactions. The noble metal (Au and Pt)-supported magnetic CSNs not only have strong magnetic properties allowing excellent recovery of the catalysts after its use *via* magnetic separation but also exhibit enhanced catalytic properties. The advantages pertinent to both shell and the core materials, in addition to their nanoscale structures, has motivated worldwide research in the synthesis and investigation of multifunctional CSNs for the catalysis of various chemical reactions (Fig. 1).^{104-118,119-121}

2. Focus of review

The focus of the present review is to provide an up-to-date appraisal of CSNs and their potential applications in catalysis and electrocatalysis, encompassing oxidation, reduction, semi-hydrogenation, carbon-carbon coupling reactions, oxygen storage, *etc.*

In addition, the structure-property relationships of the materials, especially the effect of shape, size, core and shell on the properties of the materials and their effects on catalysis are discussed. The detailed preparative procedures for various types of CSNs have been omitted in this review as they have been extensively covered earlier.¹²² However, representative methods, including basic general procedures for various classes of CSNs, are briefly mentioned, followed by more detailed description of a modern classification approach with recent examples.¹²³⁻¹³⁰ Moreover characterization techniques for CSNs are also mentioned only briefly.

3. Synthetic and characterization techniques of core-shell nanoparticles

As mentioned earlier, the recent upsurge in the field of CSNs can be attributed to their diverse applications because of their unique structural, physical and chemical properties.^{122,131-133} Although the review primarily focuses on the catalytic properties of CSNs, the synthetic strategies and different characterization techniques used to make assemblies of CSNs are briefly described in the following sections.

3.1. Synthesis of core–shell nanocatalysts

As far as synthesis is concerned, the techniques that have been used to synthesize nanomaterials can often be extended to generate the core and/or shell components of CSNs. Although “top-down” approaches are possible, in which external controls like microfabrication techniques, mechanical stress, *etc.* are utilized to break down the bulk materials to obtain the desired nanomaterials with desired shapes and sizes, “bottom-up” techniques are mostly preferred. In the latter case, the materials are synthesized from molecular or atomic building blocks, relying on the inherent chemical properties of the individual constituents and their mutual interactions to allow control over the shape and size of the nanomaterials. Using bottom-up synthetic methods, core and shell(s) of CSNs can be synthesized either in a stepwise or one-pot fashion. Both of these approaches have been used for the synthesis of CSNs. However, other new and modified procedures are continuously being developed and reported in the literature.

3.1.1. Classification

Inspired by the classification developed by Paria,¹²² the current section focuses on the synthesis of different CSNs according to type (rather than the procedures employed to make them) and categorizes CSNs in two main classes: organics (3.1.1.1) and inorganics (3.1.1.2) (Fig. 2).¹³⁴ The “organic” materials are related to carbon-based materials (mostly polymers), whereas the “inorganic” class includes metal, metalloid and metal salt NPs. Synthetic methods employed for each of these categories are discussed in this review with recent examples. Towards the end, a modern classification approach based on the shell properties of the core–shell nanomaterials is included in view of the increasing importance of nanocatalysis (3.1.1.3).

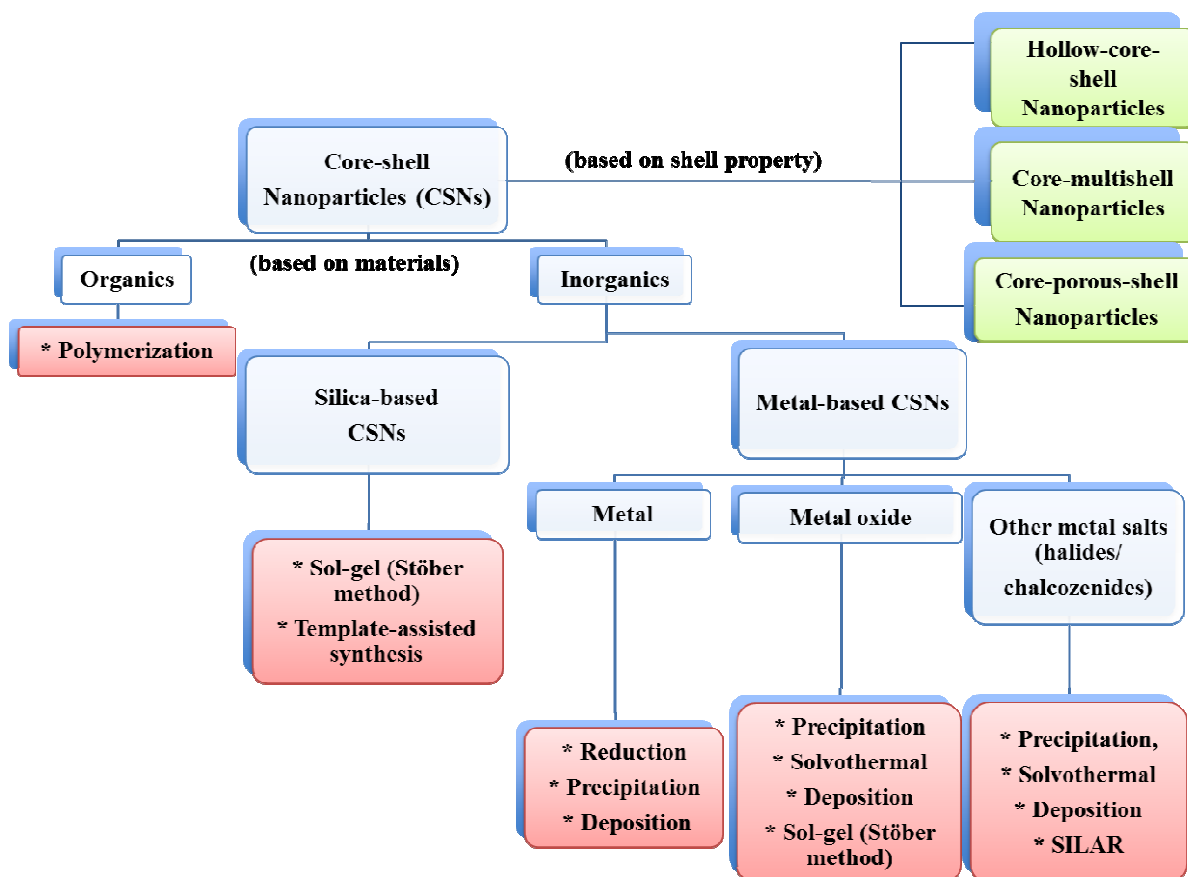


Fig. 2 General classification of CSNs based on material-type (along with the most prevalent synthetic methods) and properties of their shells.

3.1.1.1. Organics

Although these types of CSNs are relatively new compared to conventional CSNs, the advantages of using carbon-based compounds, particularly with regard to the stability/biocompatibility of the material, have generated a great deal of interest.¹³⁵ The syntheses of such materials mostly rely on polymerization techniques to prepare the organic core, shell or both. The basic strategy of polymerization involves formation of 3D network-like structures *via* addition of several units of appropriate monomeric substrates with key functionalities. Although organic cores are often synthesized first, organic shells can also be prepared *in situ*. Additionally, surface modifiers, such as surfactants, polyelectrolytes, *etc.*, can be used to improve the coating efficiency and stability. Recently, Asefa and co-workers successfully demonstrated the preparation of polyaniline (PANI) inside mesoporous channels of amine-functionalized SBA-15 using persulfate as an oxidant and used the resulting composite core-shell nanostructures to produce mesoporous carbons that can serve as an efficient metal-free electrooxidation catalyst for various reactions.^{15, 136} Chen and co-workers demonstrated facile syntheses of shells around metallic

systems using 1) amphiphilic block copolymers (polystyrene-*block*-poly(acrylic acid) (PSAA)), and 2) conductive polymers (such as PANI, polypyrrole (PPy), *etc.*) to develop metal-based CSNs.³⁸ Other carbon-based materials, such as fullerenes, carbon nanotubes (single-walled or multi-walled), *etc.*, have also been harnessed for different catalytic transformations. Detailed discussion on the syntheses of these materials is beyond the scope of this section. However, in brief, most of them are prepared *via* doping or functionalization of carbon materials with different active species, which can also ultimately result in hollow CSNs after removal of organic part either *via* extraction or calcination;¹³⁷⁻¹⁴⁰ recent examples from the literature are described in Section 3.1.3.

3.1.1.2. Inorganics

The “inorganic” materials can be categorized further into two main sub-categories, namely (a) silica-based CSNs and (b) metal-based CSNs.

Almost all the silica-based CSNs are synthesized using sol-gel chemistry, historically known as the Stöber method.¹⁴¹ This wet chemical method entails the hydrolysis and subsequent condensation of silicon alkoxides or silicon halides in alcohol, water or a mixture thereof in the presence of a base catalyst, such as ammonia, to afford uniform colloidal microspheres. Because of its simplicity, reproducibility as well as versatility, this method has been applied to synthesize different types of silica-based CSNs with great success. Although most of the CSNs prepared using this method involve solid, non-porous SiO₂, newer strategies have now been developed to generate porous materials using either template-based techniques or post-synthetic modifications. This, in turn, allows not only increased surface area of the resulting CSNs but also better accessibility of the cores as well as shells themselves. Moreover, the pores of the materials can further be modified with different functional groups, providing the materials with multi-functionality for various catalytic applications.

The broad class of “metal-based CSNs” requires further sub-classification as it covers the entire range of metal, metal alloys, metal oxides, metal salts, *etc.* and can thus be sub-divided into three parts: i) metallic NPs, ii) metal oxides, and iii) metal salts.

In general, metallic NPs are synthesized *via* reduction of their corresponding metal-salts, either using external reducing agents (such as NaBH₄, hydrazine, *etc.*) or *via* trans-metallation utilizing the intrinsic redox properties of the metal precursors. The reaction medium, temperature and type of reducing agent influence the reaction kinetics and any manipulation of these parameters may lead to significant differences in particle growth, size, shape, and thereby different chemical, physical, optical and biological properties.

Among the metal oxide NPs, titania-based materials, often obtained *via* the “sol-gel” method (similar to silica), possess a range of chemical, physical and optical properties that render

them useful in photo-, bio- and energy-related applications. Additional actions such as “thermal-treatment” may allow tuning of the structures, physical robustness or porosity of the materials. In general, the kinetics of the synthesis of titania-based materials is faster than for silica-based materials due to the relatively higher reactivity of the precursors in the former case. Nevertheless, because of the availability of various structurally and electronically different precursors, as well as the interesting phase-behavior, the final structure and reactivity of the precursors can be modulated to produce different types of structures. In the context of CSNs, several examples have recently been reported where TiO_2 in different forms was used as one of the components (mostly as shell).¹³³ Apart from the sol-gel method, co-precipitation or thermal decomposition methods are also used to access other metal oxides depending on the chemical properties of the metal precursors. Whereas the co-precipitation technique is mainly used for metal oxides (hydroxides) that can be precipitated under basic conditions, thermal decomposition involves high temperature treatment or thermolysis of organometallic precursors in the presence of oxygen or air to afford the final product. Pertinent examples of the latter case include magnetic core-shell nanocatalysts where the core is synthesized using a combination of hydrolysis and thermal treatment of Fe-precursors.¹⁴²⁻¹⁴⁴ In addition, chemical vapor deposition (CVD) and pulse layer deposition (PLD) have also been employed to prepare metal oxides from gaseous precursors and are often applied for the *in situ* synthesis of metal oxides.

In the class of “metal-salt”-based CSNs, metal chalcogenides/halides have found a range of applications in semiconducting devices and (bio)imaging. They are commonly synthesized by precipitating metal salts from a mixture of metal precursors and desired counter ions in the presence of stabilizer/capping agents. In this case, the inherent reactivity of metal salts toward external parameters (*e.g.*, oxygen, temperature, *etc.*) sometimes plays an important role, rendering further modification. A relatively new method, named as “successive ionic layer adsorption and reaction” (SILAR, first developed by Ristov¹⁴⁵ but its acronym coined by Nicolau¹⁴⁶) has been developed to synthesize metal-salt-based CSNs, mainly for their semiconductor and photovoltaic-related properties. This method allows uniform and isotopic growth of shell materials covering the core particles and minimizes the formation of unwanted nanocrystals (NCs) of just the shell material. Additionally, annealing between successive depositions (which is particularly important for making multishell NPs) allows elimination of the possible biasness that might generate from either the core or shell materials. The progress on different SILAR techniques have also been reviewed by Tolstoy.¹⁴⁷

Beyond such classifications and the aforementioned methods, depending on the applications as well as availability of sophisticated techniques, alternate energy inputs, such as ultrasound-, and microwave-irradiation, electrodeposition, *etc.*, have been used for the synthesis of various CSNs. In

the case of sonochemical synthesis, varying the sound frequency helps to i) form local microreactors/cavities in which reaction can occur, ii) promote better mixing (therefore less agglomeration), and iii) produce a short-lived shock wave, which can generate localized heating in order to produce smaller particles. The electrodeposition method generally involves deposition of the substrate/core material on the surface of an electrode or supported matrix from a bulk electrolyte solution using an electric field, followed by further decoration of the shell either by using different electrolytes or by varying the synthetic strategy. Last, but not least, recent developments in microwave technology have enabled the synthesis of either component of CSNs in shorter time with moderate to large control over structural properties.¹⁴⁸⁻¹⁵⁰

In addition to such classifications, some of the hybrid-structures (e.g. metal-organic-frameworks,¹⁵¹ zeolite-based structures,¹⁵² covalent-organic-frameworks,¹⁵³ etc.) have also been introduced recently in the literature, and hopefully a special classification and major discussion may be warranted in future for these classes.

3.1.1.3. Classification based on shell properties

Given the current status of core-shell nanocatalysis, we envision that a modern classification based on the shell properties of the materials would be beneficial, particularly for comparison of different synthetic strategies leading to varied shell properties. Broadly, these materials can be divided into three major categories: 1) hollow-core-shell, 2) core-multishell, and 3) core-porous-shell, each of which is discussed briefly in the following sections.

3.1.1.3.1. Hollow-core-shell NPs

Although not essentially CSNs by definition, hollow-core-shell type nanomaterials need to be mentioned here as the first step in their preparation is analogous to the one used for making normal CSNs described earlier. Once, the CSNs have been synthesized, the core is sacrificed using a variety of conditions specific to the core materials: organic core materials are removed either by calcination or dissolution in organic solvents, whereas inorganic core(s) are purged with strong acid or base. The removal of core materials offers some additional advantages depending on its application. In the case of multiple shells (described later), the inner shells can also be removed using specific methods.

Possibly the most common examples of this category are the inorganic oxide shell-based hollow core-shell particles, which are prepared from their precursors either separately or during calcination of the organic cores. Silica, titania or ceria (sometimes in combination) are often used because of their versatility in crafting different nanostructures. For example, Zhang *et al.* utilized a combination of sol-gel and hydrothermal action to synthesize Pd@hCeO₂ (Pd NPs embedded in a

hollow shell of CeO₂) starting from carbon microspheres and using the latter as a sacrificial core;¹⁵⁴ Pd NPs prepared *via* reduction (using alcohol) in the presence of poly-vinylpyrrolidone (PVP) as capping agent were first adsorbed on carbon microspheres (generated *via* thermal treatment of glucose). Hydrothermal treatment was then employed to coat CeO₂ outside the Pd-NP-grafted carbon sphere, followed by calcination in presence of air to remove the carbon core (Fig. 3). The resulting Pd@hCeO₂ was shown to be highly active toward the thermal and photocatalytic reduction of aromatic nitro compounds with excellent recyclability.

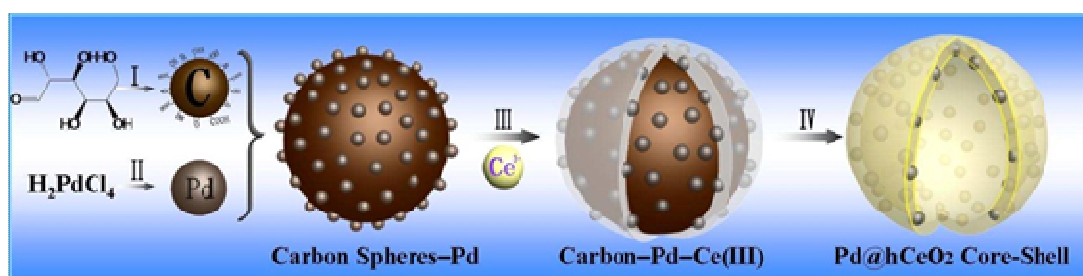


Fig. 3 Schematic illustration of the fabrication of Pd@hCeO₂ core-shell nanocomposite particles.
 10 Reprinted with permission from ref.¹⁵⁴ Copyright 2013 American Chemical Society.

The presence of the shell in Pd@hCeO₂ prevents leaching and aggregation of the Pd-NPs in the catalytic reaction. Following an analogous pathway, core-void-shell anatase TiO₂ was prepared *via* solvothermal treatment of sucrose and TiO₂, followed by removal of the carbon-precursor *via* calcination.¹⁵⁵ The final material showed enhanced photocatalytic activity for the degradation of rhodamine B and improved lithium storage capacity. A slightly different approach for the preparation of hollow-core-shell mesoporous TiO₂ has been reported¹⁵⁶ by a stepwise protocol based on seed-emulsion-polymerization, followed by coating of the Ti-precursor and subsequent calcination to generate hollow TiO₂ materials for electrophoretic studies.^{157,158} Ohtani and co-workers adopted a similar procedure involving solvothermal and calcination techniques for the synthesis of SiO₂/void/TiO₂ (and also platinumized SiO₂/void/TiO₂).^{159, 160} These photocatalytically active materials were used in the stereoselective synthesis of pipercolinic acid. In a related example, SiO₂/Mg(OH)₂ spheres have been prepared using a combination of a modified Stöber method (to prepare SiO₂ spheres or cores) followed by polyethyleneglycol (PEG) and sodium dodecyl benzene sulfonate (SDBS) mediated coating of Mg(OH)₂ onto the SiO₂ spheres;¹⁶¹ depending on the ratio of precursors, different morphologies, including hollow core-shell and honeycombed structures, were obtained. Apatite-type La_{9.33}(SiO₄)₆O₂ hollow nanosphere catalysts were synthesized using a protocol that included a combination of hydrothermal synthesis (to prepare the cores), modified Stöber method (to coat the cores with silica shells), thermal treatment (to form a hollow structure *via* decomposition of cores) and finally solvothermal treatment (for controlled etching of the silica

layers); the resulting material was shown to catalyze oxidative coupling of methane.¹⁶² Another major class of oxides, *i.e.*, zeolites (aluminosilicates), has also been used as a component of numerous CSNs. Recently, morphological control of zeolites has been achieved using a polymer network with special attention to the synthesis of hollow/core–shell structures.¹⁶³

5 Besides silica, ceria or titania, other metal oxides have been explored for synthesizing hollow CSNs. For instance, the synthesis of hollow core–shell $\text{ZrO}_2@\text{void}@\text{BiVO}_4$ NPs that can serve as visible light photocatalysts for the photodegradation of methylene blue has been investigated.¹⁶⁴ Their synthetic strategy involved initial hydrothermal treatment of aqueous $\text{Bi}(\text{NO}_3)_3$ and NH_4VO_3 to synthesize BiVO_4 core, followed by successive coating of carbon (glucose as
10 carbon precursor) and ZrO_2 (using ZrOCl_2). Finally calcination in the presence of air removed the carbon layer to afford $\text{ZrO}_2@\text{void}@\text{BiVO}_4$. Zhang *et al.* described a novel, one-pot synthesis of an iodine incorporated (core) BiOCl shell structure. Depending on the ratio of inorganic precursors, they obtained hierarchical and pure hollow-structures, which showed catalytic activity towards the photodegradation of phenol and rhodamine B.^{165, 166} Fan and co-workers reported a combination of
15 hydrothermal, atomic-layer-deposition (ALD) and solvothermal synthetic methods (to remove the sacrificial middle layer), followed by annealing to procure the porous material to produce a hollow-core–shell microstructure (Fig. 4).¹⁶⁷ In that case, a CoO precursor was first synthesized on a nickel foam using a hydrothermal process, followed by coating of the “as-grown CoO nanostructure” with Al_2O_3 and then with TiO_2 using ALD method. The removal of sacrificial Al_2O_3 with strong base
20 and subsequent annealing afforded $\text{CoO}@\text{TiO}_2$ CSNs that showed enhanced activity as supercapacitor electrodes. The ALD method provides better control on over the thickness of the resulting coating compared to other methods – an aspect particularly important for catalysis. A detailed study of the solvothermal synthesis of $\text{Co}(\text{OH})_2$ based flowerlike hollow core–shell structures has also been reported.¹⁶⁸ Plasma polymerization was also used to prepare hollow NPs
25 from simple organic substrate.¹⁶⁹

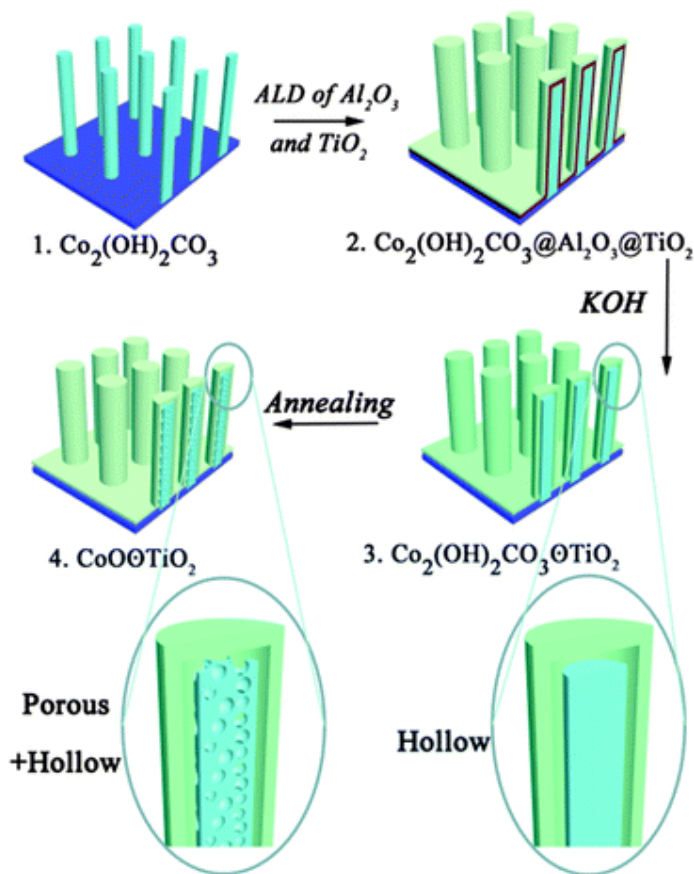


Fig. 4 Illustration of the fabrication process of the “wire-in-tube” type $\text{CoO}@\text{TiO}_2$ nanostructure. Reprinted with permission from ref. ¹⁶⁷. Copyright 2012 Royal Society of Chemistry.

5

In another example related to biosensing, a “nano-sheet”-based titania microsphere encapsulating horseradish peroxidase (HRP) was synthesized by a hydrothermal method followed by trapping of the enzyme *via* adsorption.¹⁷⁰ The resulting material was used for mediator-free biosensing of H_2O_2 aided by the redox-active HRP enzyme. The structure of the material was shown to be dependent on the reaction time, while its hollow structure enabled better electron transfer as well as higher stability of the material. In a related example, the facile synthesis of a hollow core-shell NiO microsphere has been reported, where hexamethylenetetramine was used as sacrificial carbon source. A lamellar template-based mechanism involving Ni^{2+} ions, sodium citrate and ethanol leading to intercalated Ni-hydroxide layers during an alkalization process was suggested (Fig. 5);¹⁶⁶

10

15 the final product, obtained *via* calcination in the presence of air, was shown to have excellent supercapacitive properties.

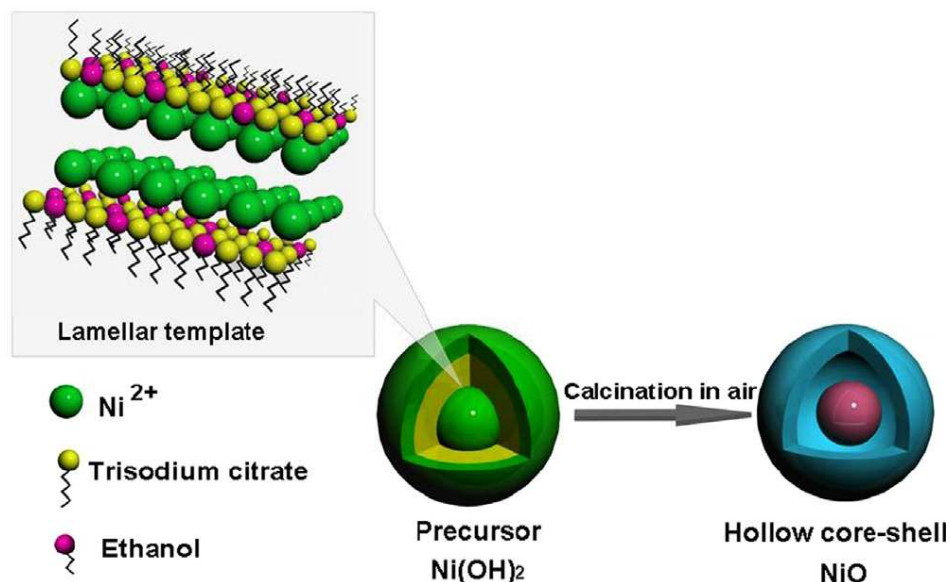


Fig. 5 Schematic of the theoretical model for the lamellar template and morphology evolution of hollow core-shell NiO. Reprinted with permission from ref. ¹⁶⁶. Copyright 2013 Elsevier Ltd.

The advantages of utilizing the intrinsic magnetic properties have been thoroughly demonstrated for Fe-oxide based materials. For instance, a two-step solvothermal synthetic method has been developed to synthesize ferrimagnetic bisphthalonitrile-Fe₃O₄-hollow-core-shell microspheres.¹⁴⁹ In the first step, Fe₃O₄ NPs were formed by the reduction of FeCl₃ using ethylene glycol in an autoclave; high boiling ethylene glycol was used because of its ability to reduce the metal-salts, whereas sodium acetate and polyethylene glycol (PEG) were added to prevent particle agglomeration. Next, bisphthalonitrile (BPHR) solution and Fe₃O₄ NPs were stirred to coat the Fe₃O₄ with BPHR molecules *via* physical adsorption, followed by another solvothermal procedure to polymerize BPHR molecules into iso-indole on the surface of Fe₃O₄. During this process, aggregation of Fe₃O₄ NPs resulted in hollow hybrid microspheres. Earlier, a less complicated synthesis was reported to synthesize hollow core-shell α -Fe₂O₃ hierarchical nanostructures, which were used for the photocatalytic degradation of phenol.¹⁷¹ A similar synthetic strategy was also reported for the synthesis of magnetic hollow core-shell structures for drug delivery, where their formation was suggested to occur *via* a possible Ostwald ripening mechanism (Fig. 6).¹⁷²

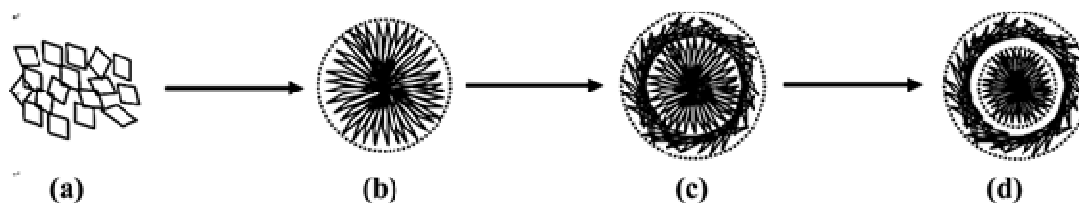


Fig. 6 Illustration of the possible formation mechanism of core/shell hierarchical nanostructures *via*

Ostwald ripening process in the presence of various precursors. Reprinted with permission from ref.
172 Copyright 2008 American Chemical Society.

The synthesis of iron oxides@SnO₂ “quasi” hollow-structures has been reported using a
seed-mediated hydrothermal method to produce a material with photocatalytic activity.¹⁷³ In
another study, Fe₃O₄-embedded hollow polymer spheres were synthesized using a combination of
various techniques: polymerization (to synthesize the cores), adsorption (to graft the Fe₃O₄ NPs on
the cores), encapsulation (*via* a second polymerization to make outer shells), and finally selective
dissolution (of the core).¹⁷⁴ A template-based synthetic method was used (involving emulsion
polymerization and subsequent hydrothermal technique) to synthesize hollow core-shell
microspheres of spinel ferrites (MFe₂O₃, where M = Zn, Co, Ni, Cd).¹⁷⁵

In addition to metal oxides, different metal-based hollow core-shell structures have been
synthesized. Ye *et al.* demonstrated the phase-transfer based synthesis of Ag@Ru hydrosol (with
ruthenium shell) *via* a ligand exchange reaction.¹⁷⁶ The Ag-core was finally removed by treatment
of the material with aqueous NaCl solution, which was followed by an additional phase-transfer
recovery step to afford hollow Ru NPs. Niu and co-workers reported the synthesis of hollow
Ag@Pd core-shell nanowires (NWs) that can catalyze formic acid oxidation. The material was
synthesized using a seed-mediated growth method (successive chemical reduction), in which
inherent galvanic displacement was suggested to be responsible for the formation of the hollow-
structure in the material.¹⁷⁷ A similar strategy was employed to synthesize hollow Au@Pd and
Au@Pt core-shell nanocatalysts for ethanol oxidation.¹⁷⁸ A one-step pyrolysis method was
developed for the synthesis of hollow carbon nanospheres with a supported PtRu electrocatalyst for
methanol oxidation.^{179, 180} The synthesis of hollow core-shell and flower-like Au-TiO₂
nanocomposite materials with photocatalytic activity towards adsorption and photon-assisted
desorption of thiol is another example, where a simple, controllable, wet chemical synthetic method
was employed.¹⁸¹

One of the major applications of the hollow-core-shell architecture is in the development of
anode materials for lithium ion batteries. Li and co-workers have summarized recent progress in the
synthesis of Si@C core-shell composite materials, particularly for lithium ion battery applications,
with an additional discussion on their future perspectives.¹⁸² Owing to the potential of hollow core
(silicon)-shell (carbon) nanocomposites as an anode material in lithium ion batteries, several
variants of similar structures have been prepared.¹⁸³ First Si nanospheres were calcined in the
presence of air to coat their surfaces with an oxide layer. Next, carbon was coated using chemical
vapor deposition method.¹⁸³ Finally, etching of the silica layers around the NPs delivered hollow
Si@C nanocomposite particles. A coaxial electrospinning method has also been employed to

synthesize Si(core)-hollow carbon nanofibers (sheath), which were shown to be a promising anode material in lithium-ion batteries.¹⁸⁴ The mechanistic details of the core-shell interaction in coaxial electrospinning were previously explored,¹⁸⁵ focusing mainly on carbon nanotubes (CNTs). Beyond silicon, by combining alcoholysis and subsequent calcination involving SnCl₂ and glycerol as metal and carbon precursors, respectively, hollow SnO₂@C CSNPs, with enhanced lithium-ion battery storage capacity successfully been synthesized.¹⁸⁶ A similar synthetic method has been used to make Sn@carbon NPs in bamboo-like carbon nanofibers for a similar potential application in lithium-ion batteries (Fig. 7).¹⁸⁷ Lately, “dealloying” of Li from a Li-Sn alloy using an electrochemical method produced hollow CSNs along with other different bicontinuous microstructures depending upon the composition, size of particles and also kinetics of the process.¹⁸⁸

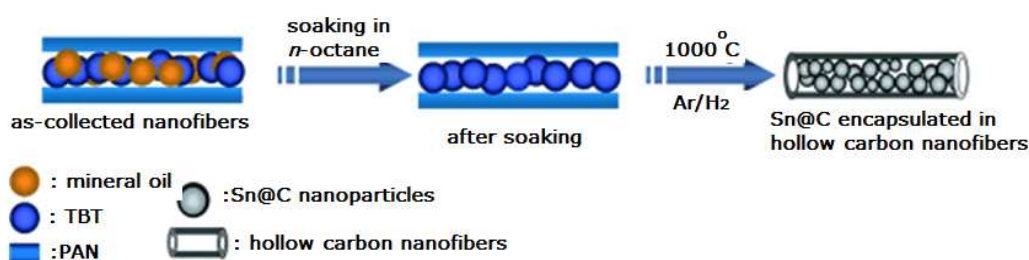


Fig. 7 Preparation of Sn@carbon NPs encapsulated in hollow carbon nanofibers. Reprinted with permission from ref. ¹⁸⁷. Copyright 2009 WILEY-VCH Verlag GmbH & Co. KGaA, Weinheim.

15

Apart from the conventional “inorganic” precursors based techniques, an “all-organic” based synthesis of hollow NPs has been reported, which involved synthesis of poly(N-isopropylacrylamide) (PNIPAM) cores by controlled heating (above the LCST, lower critical solution temperature) of polymers in the presence of a small amount of sodium dodecyl sulfate, followed by the formation of shells *via* radical copolymerization of 2-hydroxyethyl methacrylate (HEMA) and poly(ethylene glycol) dimethacrylate (PEG-DMA) as cross-linking agents.¹⁸⁹ Subsequent partial removal of the PNIPAM cores by dialysis resulted in the final material. In another study, the synthesis of two-layered hollow chiral NPs using a combination of polymerization, sol-gel, and extraction methods has been reported and the materials have been employed in the enantioselective crystallization of alanine. Hollow nanostructures were also synthesized by employing biopolymeric systems as precursors. Lipid-polymer-lipid-hybrid hollow nanostructures were synthesized using a combination of a double-emulsion and solvent evaporation technique and self-assembly route.¹⁹⁰ Another study described the synthesis of a pH-sensitive hollow polymer microcapsule *via* sequential steps involving two-stage distillation, precipitation polymerization, followed by removal of the core.¹⁹¹ Nakashima and co-workers reported several synthetic routes involving core-shell-corona type polymeric micelles as a versatile template for the

synthesis of inorganic hollow nanospheres.¹⁹²

More sophisticated techniques were recently developed for the assembly of unique nanostructures. For example, He *et al.* used γ -ray assisted polymerization (Fig. 8).¹⁹³ By applying a combination of laser-induced deposition and self-assembly synthetic procedures, Lei reported carbon nitride-based materials with different microstructures, including flower-like, hollow core-shell and nanorod structures.¹⁹⁴

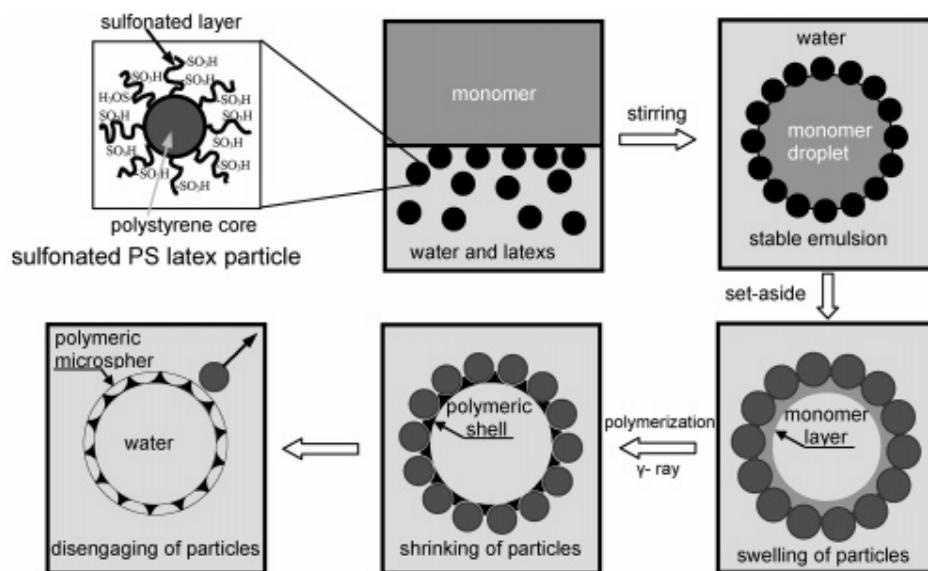


Fig. 8 Schematic illustration of the synthesis of polymer microspheres with a hollow core/porous shell structure. Reprinted with permission from ref.¹⁹³. Copyright 2005 American Chemical Society.

Though, the detailed discussion is out of the scope of this current manuscript, multiwalled carbon nanotubes (MWCNT) can be combined with various materials to produce diverse hollow CSNs displaying interesting properties. Since the initial discovery of single and multiwalled carbon nanotubes, interest in this class of materials has increased because of their potential applications, ranging from catalysis to nanoelectronics, and also option for affixing various classes of functional groups *via* chemical or physical methods.¹⁹⁵⁻¹⁹⁷ As far as syntheses of such materials are concerned, arc-discharge, laser-ablation, electrolysis, chemical-vapor-deposition and, to some extent, sonochemical and hydrothermal procedures have been deployed depending on the desired application; further modifications are possible.¹⁹⁸

Another similar hollow CSNs involving fullerenes (another form of carbon nanomaterials) can be made using aforementioned technologies. Although typical synthetic procedures mostly rely on arc-discharge, different metals can be incorporated either *via* vapor or solution phase doping.¹⁹⁹ Encapsulation of various molecules inside the fullerene cage (known as “endohedral fullerenes”) has recently been exploited and the synthetic approaches mainly entail trimetallic-template, ion-

bombardment, high-pressure and the relatively new CAPTEAR (chemically adjusting plasma temperature, energy, and reactivity) synthetic methods to produce carbon-based core-shell type nanostructures.²⁰⁰

3.1.1.3.2. Core-Multishell NPs

In lieu of removing some parts of the materials for forming “hollow NPs”, coating the core materials successively with similar or different types of materials can result in so-called “core-multishell NPs”, which have been explored recently for a number of applications ranging from catalysis to biology. These types of NPs are generally synthesized in a stepwise manner and mostly designed to utilize different functionalities of the multishell rather than just to protect the core materials. Furthermore, the inner layers of such NPs can sometime shield the core from outer layers, which may otherwise not be compatible with each other.

Until recently, most of the research efforts on core-multishell nanomaterials were concentrated on applications based on the optical and electronic properties of the materials rather than catalysis. As a consequence, most of the materials belong to the inorganic type and are mainly synthesized using strategies similar to those described in earlier sections. In addition, due to the advancement and availability of various sophisticated instrumentation, many other novel materials with unique properties can also be made. In the following section, recent examples of core-multishell nanomaterials along with their respective synthetic strategies are documented to provide a holistic picture of this important area.

Perhaps the most prevalent literature under this category belongs to quantum dots (QDs), which are NPs mostly synthesized by the approach termed SILAR, in which individual layers are synthesized starting with metal-salts/ metal-chalcogenides on the core materials. The first synthesis of multilayered QDs was reported by Shi and co-workers,²⁰¹ subsequently followed by several synthetic strategies for preparing multishell QDs. For example, the Park group have incorporated a $\text{Pb}_x\text{Cd}_{1-x}\text{S}$ interlayer between a PbS and CdS layer in a PbS/CdS/ZnS quantum-dot-sensitized solar cell using the SILAR method.²⁰² A more complex CdSe/CdS/CdS/ $\text{Cd}_{0.75}\text{Zn}_{0.25}\text{S}$ / $\text{Cd}_{0.5}\text{Zn}_{0.5}\text{S}$ / $\text{Cd}_{0.25}\text{Zn}_{0.75}\text{S}$ /ZnS/ZnSQDs/PMMA bulk nanocomposite has been synthesized using a combination of SILAR method (to prepare layered QDs) and photopolymerization (to synthesize the outer organic shell) using 2,4,6-trimethylbenzoyldiphenylphosphine oxide as the initiator (Fig. 9).²⁰³ In their synthetic scheme, the authors reported modification of the QDs with the amphiphilic polymer poly(ethylene glycol)-oleate (PEG-oleate) in order to make a homogeneous dispersion. Meyer also reported a similar approach to synthesize QDs followed by photopolymerization of the shell materials on a glass surface and showed the application of the materials as solar-concentrators.²⁰⁴ Peng,²⁰⁵ Li,²⁰⁶⁻²⁰⁹

Han,²¹⁰ Masumoto,^{211, 212} Hollingsworth,²¹³ Dai,²¹⁴ Cho²¹⁵ and Mews²¹⁶ have employed similar stepwise successive deposition methods to synthesize QDs for different photovoltaic applications. Gamelin and co-workers reported an analogous technique for Mn-based water-soluble dual-emitting core-multishell QD nanocrystals (NCs) for optical thermometry applications.²¹⁷ A combination of MW-assisted synthesis and the SILAR method was employed to generate core-shell and core-multishell materials, and the final NCs were shown to be useful for cell imaging applications.¹⁴⁸ The surface chemistry of core-multishell InP QDs (comprising an InP core coated with a zinc blende bulk structure surrounded by an organic coating), prepared *via* the SILAR method was extensively studied by Chaudret to explore the intricate interaction between the different layers.²¹⁸

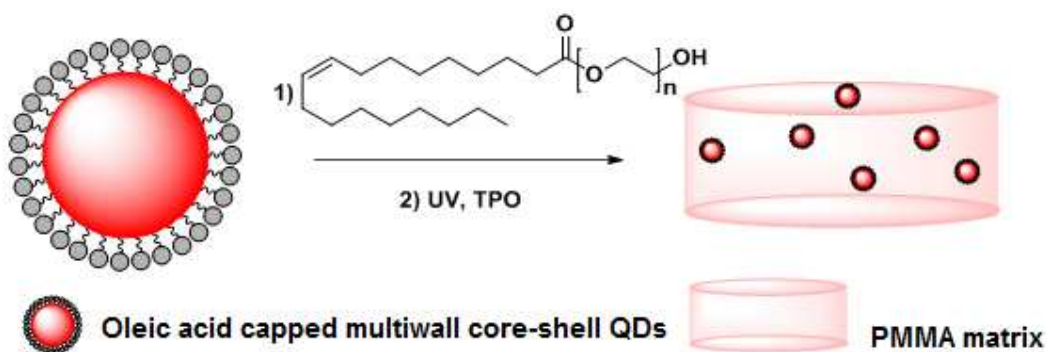


Fig. 9 *In situ* polymerization method for the generation of transparent QDs/PMMA nanocomposites. Adapted with permission from ref. ²⁰³. Copyright 2009 WILEY-VCH Verlag GmbH & Co. KGaA, Weinheim.

15

Another method of utilizing the above-mentioned “layer-by-layer” approach for generating multishell materials involves successive deposition of either a liquid or vapor of the materials onto a surface. Vertical heterostructures, composed of core-multishell Ga(In)P/GaAs/GaP grown on a flat Si(111) surface, were synthesized by a layer-by-layer vapor-liquid-solid (VLS) synthetic method involving a conventional bottom-up approach.²¹⁹ A successive layer-by-layer (SLBL) strategy was also employed to fabricate core-multishell NPs using Re-OA (rare-earth metal chlorides in oleic acid at 140 °C to make the cores) and Na-TFA-OA (sodium trifluoroacetate dissolved in oleic acid at room temperature to make the shells) (Fig. 10).²²⁰ In the latter case, the authors showed the versatility of the synthetic method, accommodating different phases as well as allowing better control over the shell thickness and dopant positions *via* simple variation of the reaction conditions and precursor solutions.

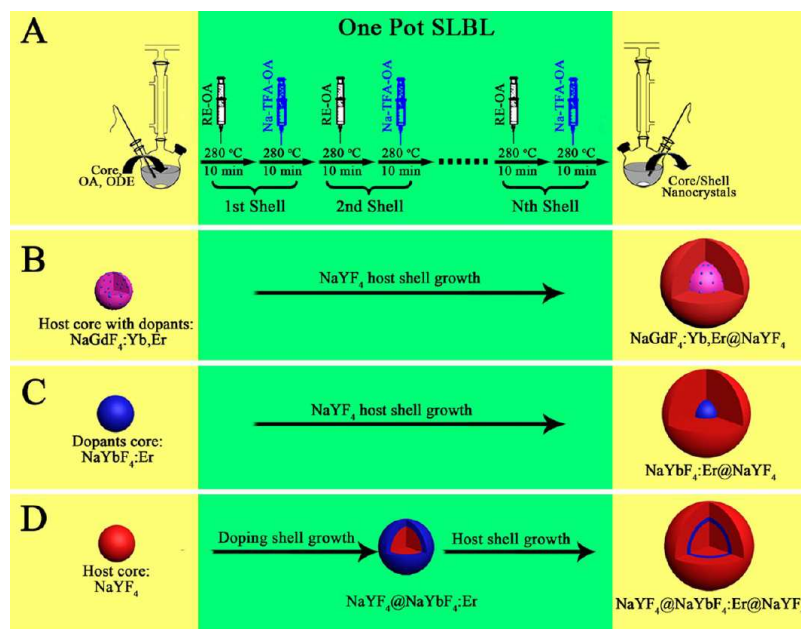


Fig. 10 (A) SLBL synthetic procedure for core@shell UCNPs. (B–D) Schematic of the synthesis of shell thickness controllable β -NaGdF₄:Yb,Er@NaYF₄ CSNs. Reprinted with permission from ref. ²²⁰. Copyright 2013 American Chemical Society.

5 Takashi and co-workers used a phosphine-free method entitled “Selective Area Metal Chemical Vapor Epitaxy (SA-MOVPE)” (a variation of chemical vapor deposition for achieving selective and controlled deposition) to synthesize core-multishell NWs involving In, Ga, As, Si, P, *etc.* for solar cell, photoluminescence and other photovoltaic applications.^{221–228} An analogous synthetic approach for generating epitaxial core-multishell nanopillars based on GaAs (doped with

10 nitrogen and phosphorous) and InGaP has been described.²²⁹ A similar approach was adopted by Tegude for the synthesis of n-GaAs/InGaP/p-GaAs core-multishell nanowire diodes,²³⁰ and Lieber to prepare an n-GaN core and In_xGa_{1-x}N/GaN/p-AlGa_{1-x}N/p-GaN shells.^{42, 231} A thermoresponsive chemical connector based on Ge/perylene/PNIPAM (PNIPAM = poly(N-isopropylacrylamide)) was developed by Javey and co-workers *via* a combined deposition and photopolymerization

15 method (Fig. 11).²³² Solid-state lithium-ion nanobatteries were synthesized using a combination of gold-catalyzed growth of Si-NWs followed by stepwise coating of different layers (10 nm Ti, 30 nm Pt, 40 nm Ti, and \approx 180 nm of LiCoO₂) by sputter deposition techniques under an inert atmosphere.²³³ Similar growth techniques have been used by Picraux^{234, 235} for making core/multishell germanium/silicon nanowire heterostructures and also by Patolsky for creating

20 wire-in-wire and/or tube-in-tube or wire-in-tube nanostructures.^{236, 237} Kempa *et al.* used a gold nanocluster catalyzed growth process to obtain coaxial Si- and B-based multishell NWs using SiH₄ as the silicon precursor, B₂H₆ as the p-type dopant and PH₃ as the n-type dopant for application as ultrathin photovoltaic materials.²³⁸

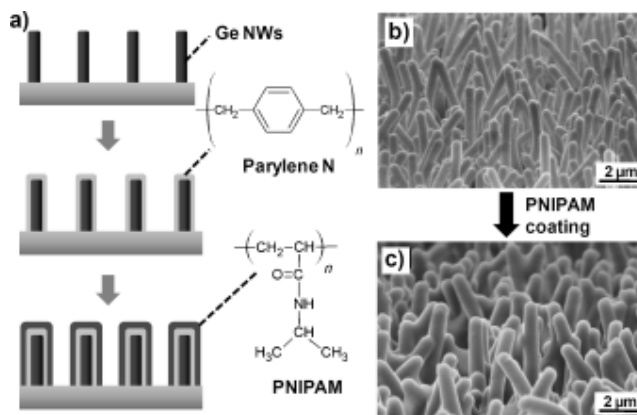


Fig. 11 (a) Fabrication procedure for a thermoresponsive NW forest, used as one mate of the proposed unisex fasteners. (b,c) Scanning electron microscopy (SEM) images of Ge/parylene NW forests before and after deposition of the PNIPAM outer shell. Reprinted with permission from ref. ²³². Copyright 2010 WILEY-VCH Verlag GmbH & Co. KGaA, Weinheim.

More traditional methods have also been used for synthesizing core-multishell nanomaterials. For example, $\text{Fe}_3\text{O}_4@Ag/\text{SiO}_2/\text{Au}$ microspheres were prepared starting from Fe_3O_4 (prepared *via* solvothermal method) and using reduction, sol-gel process and interfacial growth chemistry.²³⁹ In another example, CaCO_3 (PAH/astralen)_x/Ag (where $x = 1-3$, PAH = polyaniline hydrochloride) core-multishell microparticles composed of a solid carbonate core coated with silver NPs and astralen (polyhedral multishell fullerene-like structure) have also been synthesized using a conventional approach. The synthetic procedure involved precipitation (to make the CaCO_3 core) followed by layer-by-layer assembly of astralen with polyallylamine hydrochloride (PAH) and finally deposition of Ag-NPs by means of the silver mirror reaction.²⁴⁰ Xiong and co-workers²⁴¹ demonstrated that incorporation of “gain” material (fluorophore dye) into core-multishell Au/silica/silica spherical nanocavities allows resonance energy-transfer from the gain media to the plasmon, thereby compensating loss due to energy dissipation. In their synthesis, a Au-NP core was first synthesized using conventional reduction of a Au-salt by sodium citrate. This was followed by coating the surfaces of the Au-NPs with silica shells using a mixture of tetraethyl orthosilicate (TEOS) and 3-(aminopropyl)trimethoxysilane (APTMS). Then, using a controlled etching technique, by treating the sample with strong base at elevated temperature, allowed formation of a thin shell surrounding the Au-NP core. Finally, a modified Stöber method using a mixture of fluorophore dye and TEOS afforded the final product, where the dye particles were doped only in the outer layer (Fig. 12). In their recent report,^{242, 243} Catala *et al.* demonstrated a surfactant-free one-pot multistep procedure to obtain core-multishell magnetic/photomagnetic co-ordination NPs specifically composed of face-centered-cubic Prussian blue analogs (PBAs) of the general formula

$A^I x M^{II} [M^{III} (CN)_6]_{(2+x)/3}$, [where A is an alkali-metal cation and M^{II} and M^{III} are transition-metal ions].²⁴⁴ The particle-size (and also shell thickness) was shown to be easily controllable and in good agreement with calculated values. Zeng and co-workers reported the sol-gel synthesis of $Zn_{1-x}Co_xO/Co_{1-y}Zn_yO$ core-multishell NPs that could be used as a catalyst for CO oxidation at relatively low temperature.²⁴⁵

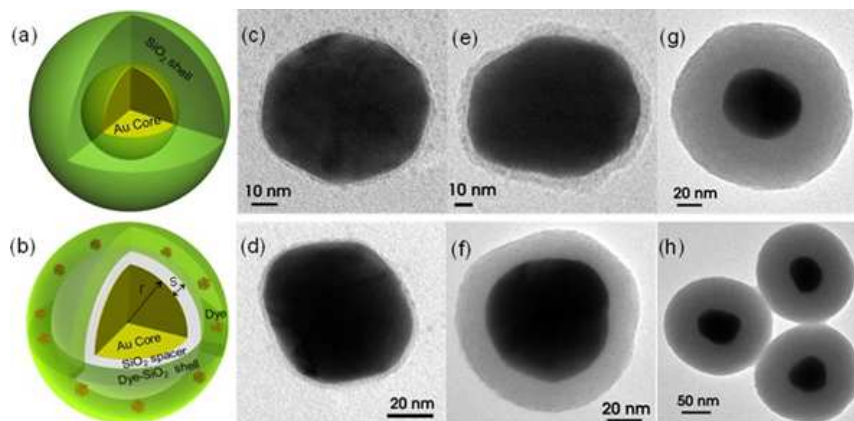


Fig. 12 Core-shell/multishell plasmodia nanocavities. Schematic of (a) Au (yellow)/silica (green) and (b) Au/silica/dye silica core-multishell nanostructures. Dye molecules (shown as red stars) are dispersed in the outermost silica shell (shown as green shell). (c–g) TEM images of Au/silica core-shell structures with different shell thickness. (h) TEM images of Au/silica/dye (rhodamine 6G) silica core-multishell nanostructures. Reprinted with permission from ref. ²⁴¹. Copyright 2012 American Chemical Society.

A step-by-step synthetic method has been used to obtain hetero-epitaxial growth of core-shell and core-multishell nanomaterials containing Pd and Au NPs.^{246,247} Ming and co-workers have reported the synthesis of silica/Ag/TiO₂ nanocomposites prepared by depositing Ag on silica supporting cores followed by additional coating of titania.²⁴⁸ First, silica microspheres were treated with a solution containing Sn²⁺ ions followed by another solution containing Ag⁺ ions to obtain silver NPs outside the core *via* galvanic replacement. Then electroless-plating using Ag⁺ and formaldehyde solution resulted in the formation of Ag shells outside the silica microspheres. The resulting NPs were then coated with titania shells *via* the traditional sol-gel method along using PVP (poly-vinylpyrrolidone) as stabilizer. A flow synthesis of core-double-shell Au/Ag/Au NPs with narrow size distribution has also been reported where tetradecane was used as carrier medium to generate segmented flow.²⁴⁹ Further, multishell hydrogel NPs with a Ag-NP core, protective citrate capping, pH indicator dye shell and polyacrylamide cladding have been prepared.²⁵⁰

Mainly comprising “organic” materials, special types of core-multishell NPs have been introduced recently involving supramolecular dendritic assemblies, which have potential

applications for drug/dye/metal ions delivery^{251, 252,253-257} catalysis,²⁵⁸⁻²⁶⁰ *etc.* In a typical synthetic procedure, a polar inner core (mostly PEG related materials, PEG = polyethylene glycol) was chemically attached (typically *via* simple esterification between mPEG (methoxypoly(ethylene glycol)) and diacid based linkers) to a non-polar intermediate shell. The ensuing material was then conjugated *via* amidation using EDC (1-ethyl-3-(3-dimethylaminopropyl)carbodiimide) coupling to a hydrophilic outer core (generally PEI, polyethyleneimine) to produce the final material (Fig. 13). This synthetic strategy is attractive, because depending on the desired application the synthetic procedure, polarity and sequence of layering can all be easily altered along with the chain-length and molecular weight of each of the precursors. Regarding catalysis, these dendritic core-multishell composites could be used to incorporate catalytic active metal ions/NPs for assorted organic transformations (including enantioselective reactions) with high reactivity and excellent recyclability.²⁵⁸⁻²⁶⁰

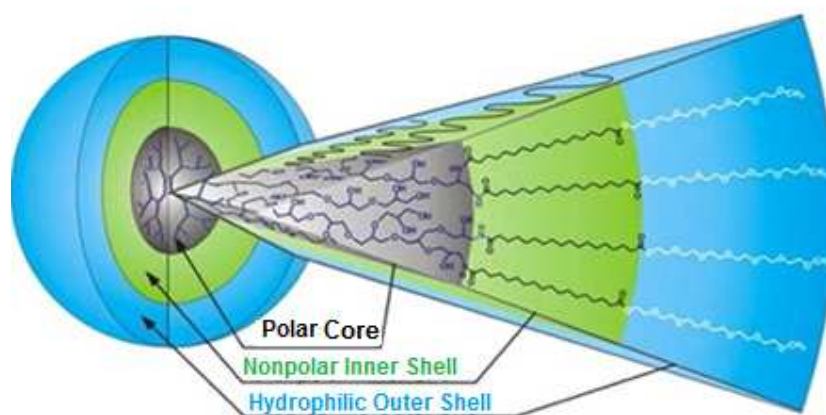


Fig. 13 Schematic of the structure of a core-multishell NP synthesized using a combination of esterification and amidation reactions. Reprinted with permission from ref. ²⁵¹. Copyright 2012 American Chemical Society.

3.1.1.3.3. Core-porous-shell NPs

Although it is difficult to completely separate the category “core-porous-shell” from the aforementioned two classes of CSNs because porosity in the materials can be brought about either directly or after synthesizing the particles using earlier described protocols, this section includes recent and exclusive examples of porous-shell NPs, the associated synthetic strategies and applications. In addition to chromatographic separation,²⁶¹⁻²⁶⁵ these particles have been explored for diverse catalytic applications.

The techniques for utilizing the pores of core-porous shell nanomaterials depend on the intrinsic chemical reactivity of the shells and compatibility with cores. In most cases, a mild variant

of the strategy employed to remove the shell completely (as described for hollow-shell nanomaterials) can be used to partially “etch” the shells to render them porous. The most prevalent examples here are the inorganic oxides, which can be easily etched by treatment with strong base/acid.

Asefa and co-workers have reported the synthesis of both core-shell and core-porous-shell type silica-based microparticles together with their applications for catalysis.^{266, 267} The synthesis involved a combination of 1) the Stöber synthesis of silica core microparticles, 2) grafting of different functional groups (*e.g.*, amine, thiol, amine based dendrimer, *etc.*) on the surfaces of the core NPs, 3) incorporation of metal-ions or metallic NPs by using the different surface functional groups of the microparticles as ligands, 4) coating the resulting materials with a layer of metal oxides using another sol-gel (Stöber-like) process, and finally 5) base-assisted partial etching of the metal oxide shells to produce porous shells. The pore size of the materials was shown to be easily controllable by varying external reaction parameters (*e.g.*, reaction temperature, etching time, *etc.*). The porous shells around the NPs thus enabled selective transport of substrates/product. Fig. 14 shows a schematic of the procedural route for porous SiO₂-AuNP-SiO₂ core-shell-shell materials,²⁶⁸ which were used for the selective oxidation of styrene with high recyclability and almost no leaching of the metals.



Fig. 14 Schematic representation of the synthesis of a porous SiO₂-AuNP-SiO₂ core-shell-shell microsphere catalyst. Reprinted with permission from ref.²⁶⁸. Copyright 2012 Springer.

In another related example, Yu *et al.* developed a synthetic strategy involving sol-gel, hydrothermal, polymerization, and carbonization to synthesize silicalite-1 (core)/mesoporous shell structures.^{269, 270} Chen and co-workers reported the synthesis of Pd/SiO₂ and Ca-Pd/SiO₂ egg-porous-shell nanomaterials *via* an impregnation method to explore their catalytic prowess in CO hydrogenation to methanol with high selectivity.²⁷¹ Porous Fe₃O₄/Fe/SiO₂ and Fe₃O₄/SnO₂ core/shell nanorods possessing magnetic and electromagnetic properties were synthesized by Chen and co-workers using a combination of hydrothermal, sol-gel, and annealing methods.^{150, 272} Commercially available films composed of Ag₆₅Au₃₅ (based on atom %) were used to synthesize nanoporous gold by chemical etching with 70% HNO₃ aqueous solution at room temperature. Subsequent controlled incorporation of Ag into the nanopores of the material was carried out using

an electroless-plating method.²⁷³ A combination of a hydrothermal and layer-by-layer deposition technique has also been applied to synthesize $\alpha\text{-Fe}_2\text{O}_3@\text{SnO}_2@\text{C}$ porous core-shell nanorods.²⁷⁴ The resulting materials showed excellent performance when used as an anode for lithium-ion batteries. Wang's group reported a simple oxidation-based method to generate porous core-shell structured Ni/NiO anode materials for lithium ion batteries.²⁷⁵ Using a similar approach, Mathur and coworkers synthesized porous Ni/Ni₃S₂ core-shell nanotubes *via* a hydrothermal method followed by controlled oxidation.²⁷⁶ A general galvanic displacement approach has also been employed to synthesize porous core-shell Au-M (M=Au, Pd, and Pt) nanostructures that served as efficient electrocatalysts for EtOH oxidation as well as the oxygen reduction reaction.²⁷⁷

10 The synthetic strategies for porous CSNs have been extended to relatively sophisticated unconventional methods. For example, the synthesis of hierarchical porous core-shell carbon nanostructures using detonation-assisted-chemical-vapor-deposition has been reported.²⁷⁸ In this process, picric acid was assumed to create the required high temperature environment by detonation, where the premixed carbon(phenol)/catalyst(cobalt acetate) precursors decompose to
15 form carbon nanostructures. In another study, a coaxial electrospinning system with a "water-immersed collector" was used to synthesize polycaprolactone and gelatin based highly porous core-shell nanostructures (Fig. 15).²⁷⁹ A combination of electrostatic spray deposition (ESD) and high temperature treatment was also successfully employed by Wang and co-workers to obtain three-dimensional porous core-shell Sn@carbon anode materials on nickel foam.²⁸⁰ Using a
20 protocol involving electrodeposition (to make Ni nanowire), plasma annealing (to make Ni@NiO) and finally hydrothermal reduction, one-dimensional Ni@NiO/Pt hybrid NWs were synthesized.²⁸¹ The resulting material showed excellent catalytic activity for the electrooxidation of ethanol in alkaline media and high tolerance against CO-poisoning. Porous metal oxide (Co₃O₄@NiO and ZnO@NiO) core-shell NWs with excellent supercapacitive properties have been prepared by Fan
25 and co-workers using hydrothermal, chemical bath deposition and finally thermal annealing.²⁸² A similar technique was used to synthesize Co₃O₄@NiO, which displayed a high catalytic efficiency towards methanol oxidation.²⁸³ Zhang's group made porous silica CSNs *via* the sol-gel method and used them as a fluorescent sensor for the detection of very low concentrations of Zn²⁺ ions by employing rhodamine 101 adsorbed on the solid cores and 8-aminoquinoline impregnated onto the
30 porous silica shells.²⁸⁴ Weitz and co-workers used a microfluidic and "porogen-templating" techniques to prepare NPs with a hydrophobic porous core and hydrophilic porous surface.²⁸⁵ While the hydrophilic surface allowed good dispersibility in water, the hydrophobic cores enabled adsorption of organic molecules into the NPs from the surrounding aqueous environment, thus enhancing their high adsorption capacity (Fig. 16).

35

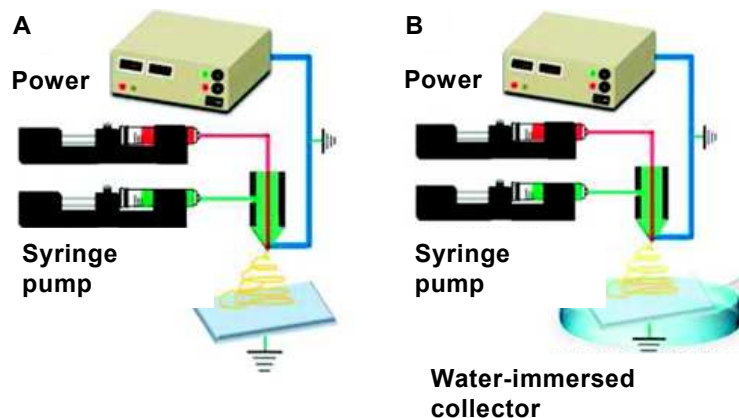


Fig. 15 Electrospinning system for creating core-shell and porous core-shell fiber networks. (A) core-shell electrospinning system for core-shell nanofibers. Scale bar is 2 μm . (B) Electrospinning setup in a water-immersed collector for preparing porous core-shell fiber networks. Scale bar is 10 μm . Reprinted with permission from ref. ²⁷⁹. Copyright 2011 American Chemical Society.

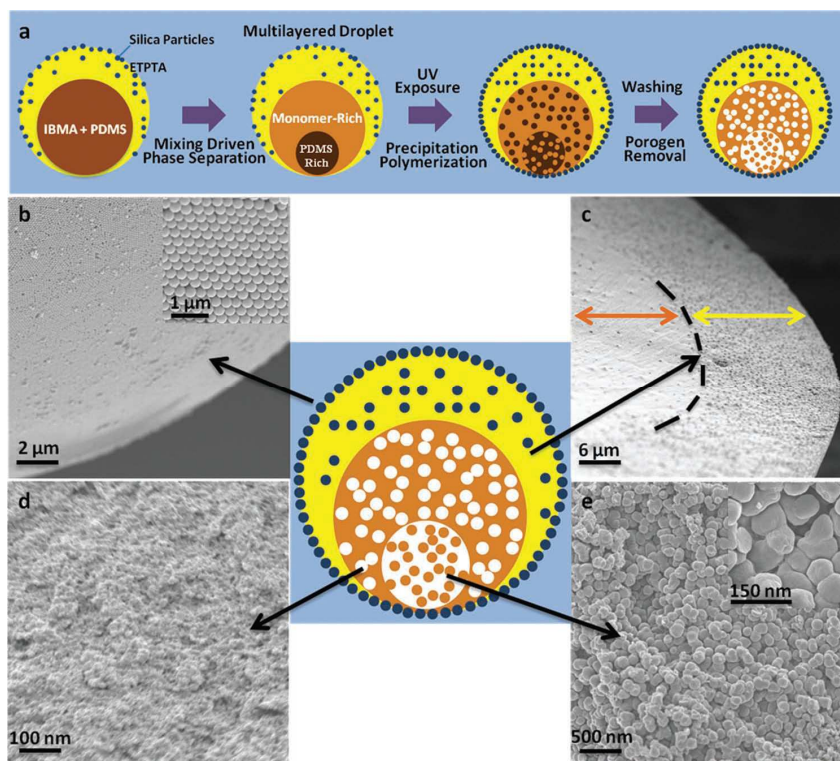


Fig. 16 (a) Schematic of the mechanism of mixing driven phase separation, precipitation polymerization and subsequent pore formation after removal of porogen PDMS oil. (b-e) SEM images of the surface and the three different layers within the porous particle. Reprinted with permission from ref. ²⁸⁵. Copyright 2013 WILEY-VCH Verlag GmbH & Co. KGaA, Weinheim.

As opposed to repeating the different synthetic strategies for core-shell nanoparticles, already extensively covered in other reviews, the aforementioned classification, followed by the extensive discussion, hopefully have provided some thoughts to the readers for possible extension/development in the field of core-shell nanocatalysts.

The above section described different synthetic strategies for the core-shell nanomaterials according to the types of materials. A novel classification system based on the shell-properties has been introduced considering recent upsurge in their applications. In contrast to the archaic literature precedence, most of the recent methods are primarily application-driven. Based on the compatibility between the layers as well as their utilizations, combinations of different synthetic methods or simplification of relatively complicated and time-consuming methods are becoming routine practices. With such enhanced synthetic prowess, core-shell nanomaterials with hybrid structures and unique functionalities can be obtained in a relatively shorter time which can find varied applications and especially in catalysis.

3.2. Characterization techniques for core-shell nanoparticles

The above sections described common synthetic strategies and some recent examples of different types of CSNs. However, before discussing the catalytic applications, it is important to provide an overview of the techniques available for characterizing such systems. In this section, some common techniques related to CSNs (or nanomaterials in general) are mentioned with some representative examples.

The properties and performance of nanomaterials, especially as nanocatalysts, relies heavily on their size, morphology, structure and composition. In the case of CSNs, the combination of the inner core and outer shell, dispersion of catalytic groups on the surface of the materials and diffusion of the NPs in the reaction has a crucial effect on their properties and catalytic activities. Therefore, characterization of CSNs and their structural features and physical properties are not only important for understanding their structure-catalytic activity relationships but also for gaining deeper insights into the catalytic mechanisms involving these nanosystems. Consequently, a range of parameters that define CSNs needs to be characterized and assessed (Fig. 17). To describe CSNs as completely as possible, it is necessary to elucidate the chemical and physical properties of the materials, *i.e.*, the size and shape of the particles, surface characteristics, nature of surface coating and presence of impurities/dopants (which are often incorporated by combining a series of complimentary analytical methods). Below, the major characterization techniques used to probe the structures, compositions and properties of CSNs are briefly described.

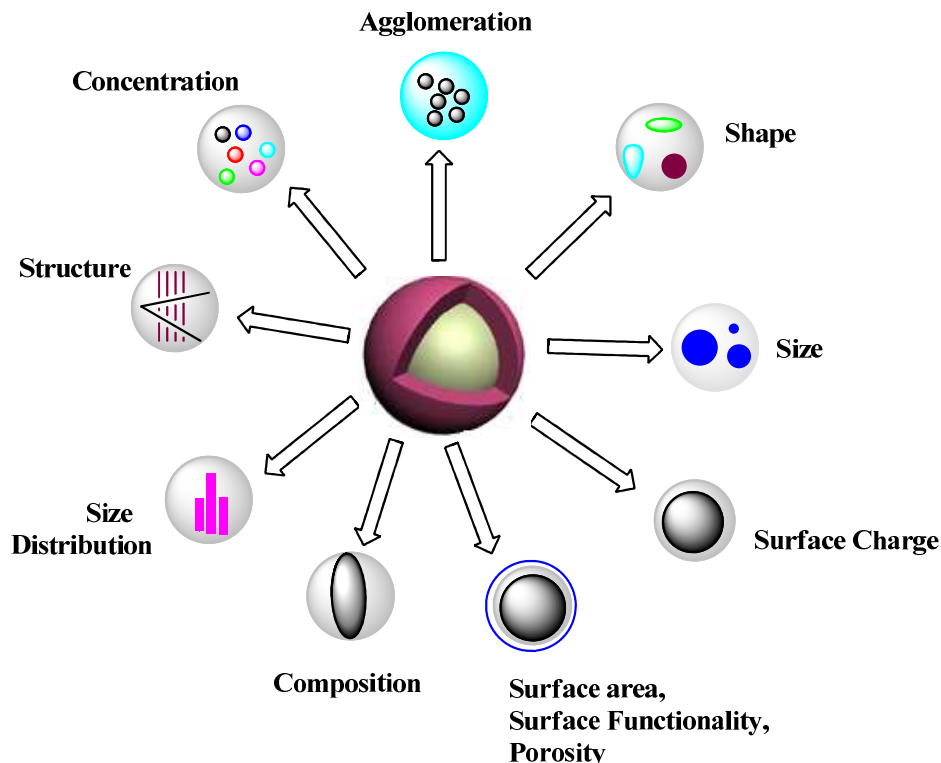


Fig. 17 Structural and compositional features of CSNs that can affect their catalytic properties.

X-ray diffraction (XRD) has long been the method of choice for studying the crystal phase
 5 or microstructures of a range of materials, including CSNs. Particularly for CSNs, XRD is an
 important tool that can, shed light on the presence of core-shell structures in the NPs. Even
 separated phases belonging to the core and shell could be detected simultaneously. Scanning
 electron microscopy (SEM) and transmission electron microscopy (TEM) images are usually used
 to determine the size, morphology and homogeneity of the NPs. However, because signal collection
 10 in SEM usually involves collecting secondary electrons, and therefore generates only a surface
 image, it is difficult to distinguish the core from the shell with SEM analysis. High resolution TEM
 (HRTEM) enables the simultaneous observation of lattice fringes with different spacings in the core
 and shell from a single particle. Additionally, HRTEM mode, energy dispersive spectrometry
 (EDS), which is typically attached as an accessory to TEM instruments, can serve as a powerful
 15 method for determining the distribution of elements within a single NP. Thus, EDS can be reliably
 used to characterize the chemical nature of the core and shell within a core-shell nanosystem.
 Another important technique used for core-shell nanomaterials, particularly for their composition,
 elemental mapping and also sometimes depth-profiling, is Electron Energy Loss Spectroscopy(
 EELS), which is often considered complimentary to EDS. This technique has been routinely used
 20 for core-shell nanocatalysts to obtain valuable information regarding their structure activity
 relationships (see part 5 on electrocatalysis). In high angle annular dark-field STEM (HAADF-
 STEM), regions with larger average atomic number are indicated by brighter contrast in images, as

long as this area has the same thickness. Therefore, *Z*-contrast (*Z* is the average atomic number) images can be used to detect the element distribution visually and directly. More advanced electron microscopy methods, such as aberration-corrected STEM operating at a lower voltage (100 kV), which can give atomic-resolution images, have recently been developed for special types of materials.²⁸⁶ In fact, annular dark field scanning transmission electron microscopy (ADF-STEM) and atomic-resolution spectroscopic mapping are nowadays routinely used under various suitable conditions. By taking advantage of the unique optical properties, such as plasmonic, absorption and emission properties, of NCs (which are quite sensitive to their surface modification), several spectroscopic techniques have been developed to directly or indirectly, characterize CSNs. UV-Vis spectroscopy is one of the most commonly used spectroscopic techniques for the analysis of different types of NPs, especially those capable of absorbing in the UV-Vis region of electromagnetic radiation. For organic type core@shell nanostructures, infrared spectroscopy can be used for the identification of the organic molecules/moieties present in the nanostructures.

Raman spectroscopy is also another important technique for studying the surface characteristics of core/shell nanomaterials. Additionally, surface enhanced Raman spectroscopy (SERS) can be used for studying CSNs containing SERS active metals, such as Au, Ag, and Cu, and for the detection and monitoring of surface processes relevant for catalysis by core-shell nanomaterials. Gas adsorption/desorption machinery equipped with an automated analyzer, which allows multilayer adsorption/desorption of gas (mostly nitrogen) over a material's surface as a function of relative pressure, is also useful for the characterization of core-shell nanomaterials, especially those containing porous structures. In particular, the Brunauer-Emmett-Teller (BET) method is commonly used for determination of the specific surface area of porous core-shell nanomaterials, whereas the Barrett-Joyner-Halenda (BJH) method can be employed to determine the pore volume and pore size of the materials; the choice being dictated by the pore sizes and structures in the materials.

The above section highlights the key tools used to characterize CSNs by providing information about their physicochemical properties. In the context of current review, these tools are also important for checking the integrity of the nanocatalysts after catalytic reactions and often provide insights into the interactions of different components of the catalyst with the reactant molecules.

4. Applications of core-shell nanoparticles in catalysis

The systematic design and synthesis of core-shell nanocatalysts comprising active metal NPs in the core and closely assembled structures with nano-gaps in the shell to permit substrates access to the core metal can enable highly selective catalysts to be achieved.²⁸⁷⁻²⁹⁷ In this section, various catalytic reactions by CSNs²⁹⁸ are described, such as transfer hydrogenation reactions,

oxidation reactions, cross-coupling reactions, tandem deprotection-Knoevenagel and Henry reactions, aerobic oxidative esterifications and synthesis of bulk chemicals (*e.g.*, adipic acid), *etc.*

4.1. Hydrogenation reactions

5 Hydrogenation reactions are important in the industrial syntheses of dyes, biologically active compounds, pharmaceuticals, rubber and agricultural chemicals.²⁹⁹⁻³⁰¹ Nanomaterial-catalyzed hydrogenations of alkynes, alkenes, aromatic nitro compounds and ketones have received much interest in the last decade because of their use in the synthesis of important raw materials along with the remarkable effectiveness of nanomaterials in catalyzing such reactions.^{300, 302-304}

10 Hydrogenation reactions are often performed using traditional catalysts for several important drug intermediates and pharmaceutical precursors,³⁰⁵⁻³⁰⁷ for which the selectivity of the reactions is the biggest concern. Among such processes, catalytic transfer hydrogenation (CTH) reaction is becoming increasingly popular because of their wide usage and versatility. The practical use of CSNs for CTH often stems from the fact that these materials offer high selectivity (both regio- and

15 chemo-selectivity) and their enhanced ease of separation and recyclability; several types of core-shell nanocatalysts have been successfully employed for various transfer hydrogenation reactions.³⁰⁸⁻³¹¹

4.1.1. Chemoselective reduction reaction

20 Kaneda and co-workers have reported the synthesis of Ag@CeO₂ core-shell nanocatalysts using the reverse micelle method and showed their catalytic properties in chemoselective reduction reactions.³¹² The material (denoted as the core-shell nanocomposite AgNPs@BM) consisted of AgNPs covered with a basic material (BM) (Fig. 18). It is worth emphasizing that a hydrogen molecule was cleaved heterolytically at the junction between AgNPs and basic sites (or BM) of the

25 materials, thereby suppressing the unfavorable homolytic fission of the hydrogen molecule on the bare AgNPs. The resultant Ag hydride and proton species enable the complete chemoselective reduction of nitro compounds while retaining the C=C bonds intact (Fig.19). Similarly, AgNPs@CeO₂ was shown to catalyze the deoxygenation of epoxides to alkenes with excellent (99%) selectivity (Fig. 20).

30

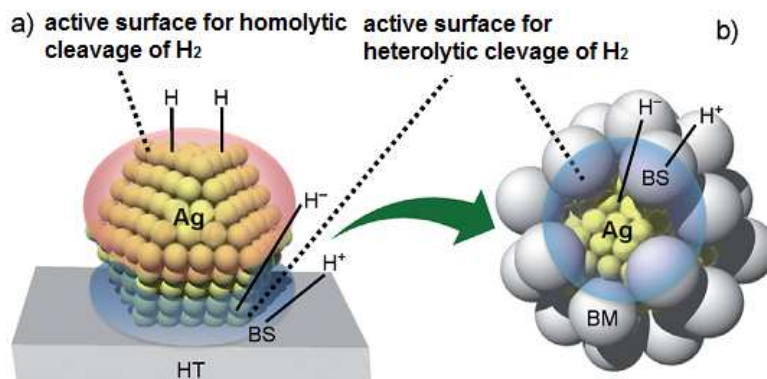


Fig. 18 (a) Representation of Ag/HT (HT represents hydrotalcite support) reacting with H₂; both polar and nonpolar hydrogen species are formed. (b) Representation of AgNPs@BM; AgNPs are covered with a basic material (BM), which reacts with H₂ to result in exclusive formation of polar hydrogen species. A basic site of HT and BM is represented by BS. Reprinted with permission from ref. ³¹². Copyright 2012 WILEY-VCH Verlag GmbH & Co. KGaA, Weinheim.

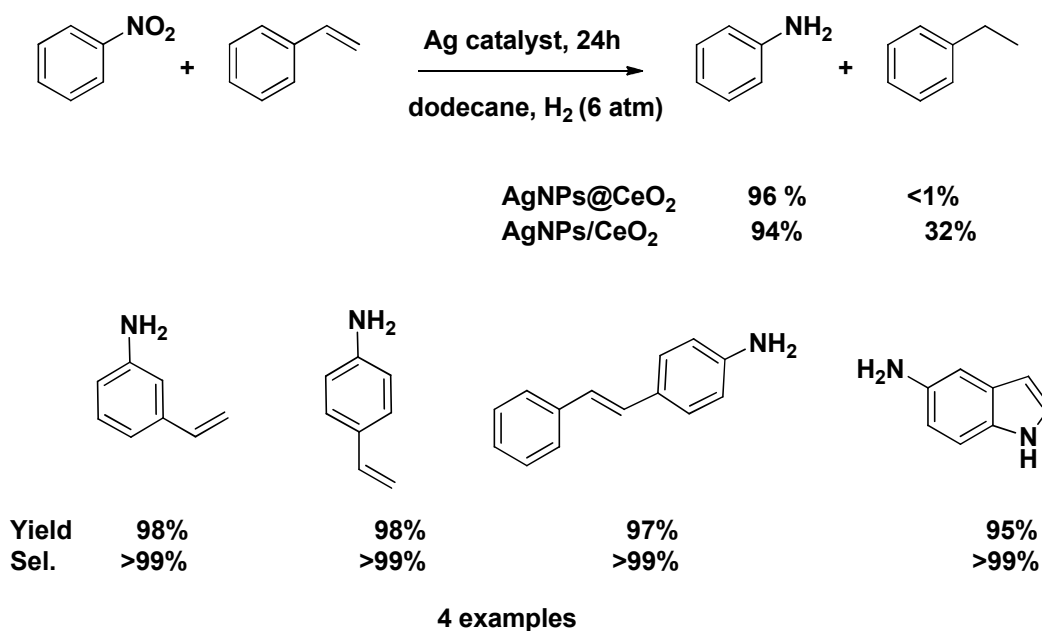


Fig. 19 Chemoselective reduction of various organic substrates on silver@cerium dioxide core-shell nanocatalyst.

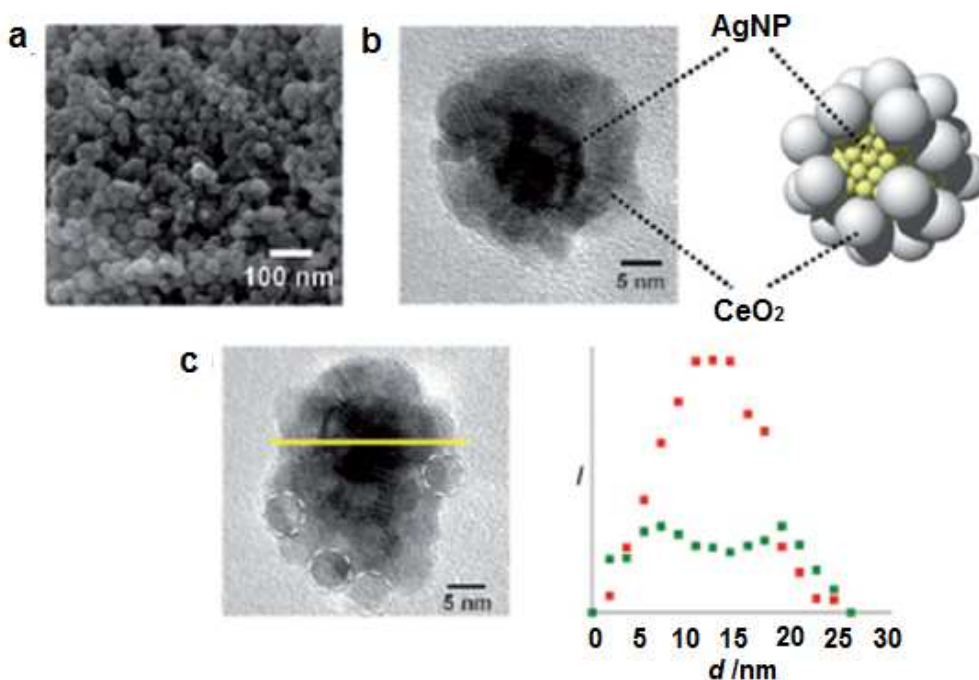


Fig. 20 Electron micrographs of AgNPs@CeO₂: (a) SEM and (b) HRTEM images of a AgNPs@CeO₂ nanocomposite particle, (c) Line-scan STEM-EDS across the AgNPs@CeO₂ nanocomposite (Ag: red squares, Ce: green squares). The circled areas correspond to the spherical CeO₂ NPs. Reprinted with permission from ref.³¹². Copyright 2012 WILEY-VCH Verlag GmbH & Co. KGaA, Weinheim.

AgNPs@CeO₂, has also been shown to catalyze the chemoselective reduction of unsaturated aldehydes to the corresponding unsaturated alcohols with H₂,³¹³ the nanogaps among adjacent CeO₂ NPs within the shell allow better access of reactants to the active Ag sites in the core. Exploiting the interaction between the basic sites of CeO₂ and Ag NPs effectively induced the heterolytic cleavage of H₂ to Ag-hydride and proton species, allowing the highly chemoselective reduction of unsaturated aldehydes to the corresponding allylic alcohols.

15

4.1.2. Semihydrogenation of alkynes by Pd@MPSO/SiO₂

The semihydrogenation of alkynes is an important synthetic protocol for preparing (*Z*)-alkenes, which are important building blocks for fine chemicals and pharmaceuticals, such as flavors, natural products and bioactive molecules.³¹⁴ A core-shell nanocatalyst consisting of Pd NPs shielded within a DMSO-type matrix on the surface of SiO₂ producing Pd@MPSO/SiO₂ CSNs (MPSO = methyl-3-trimethoxysilylpropylsulfoxide) has been designed and shown to catalyze the selective semihydrogenation of alkynes.³¹⁵ The shell containing an alkyl sulfoxide network acted as

a macroligand and permitted the selective entrance of alkynes to the active center of the Pd NPs, encouraging the selective semihydrogenation of alkynes (Fig. 21).^{315,316} Varying the molar ratios of MPSO to Pd during the synthesis resulted in two different core-shell nanocatalysts, namely Pd@MPSO/SiO₂-1 (where MPSO: Pd = 7:1) and Pd@MPSO/SiO₂-2 (where MPSO: Pd = 100:1). The material Pd@MPSO/SiO₂-1 was successfully employed as a catalyst for the semihydrogenation of a wide range of internal alkynes (aromatic and aliphatic alkynes) to the corresponding alkenes, affording > 97% yield (Table 1).

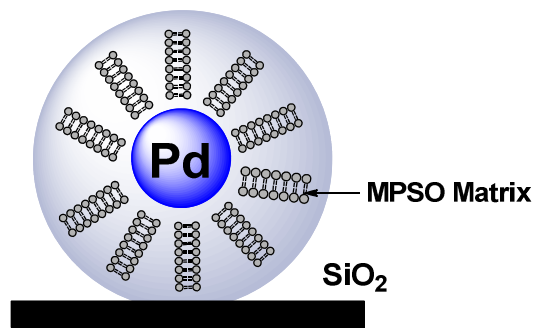
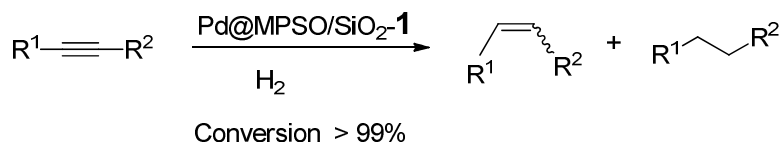


Fig. 21 Schematic showing the principles behind the synthesis of Pd@MPSO/SiO₂ core-shell nanocatalyst. Adapted from ref.³¹⁵.

Table 1. Semihydrogenation of internal alkynes using Pd@MPSO/SiO₂-1.^a



Entry	Alkyne	Product	T (h)	Alkenes	Yield ^b (%) Z:E	Alkanes
1			2	97	97:3	3
2 ^c			8	95	97:3	5
3 ^d			6	98	97:3	2
4 ^d			6	99	98:2	1
5 ^d			6	98	98:2	2
6 ^c			6	98	95:5	2
7 ^d			8	98	97:3	2

15

^a Reaction conditions: alkyne (0.5 mmol), Pd@MPSO/SiO₂-1 (0.02 g, Pd: 0.2 mol%) and MeOH (5 mL); ^bDetermined by Gas Chromatography (GC) yield using an internal standard; ^c Pd@MPSO/SiO₂-1 (0.1 g, Pd: 0.05 mol%), 1 (10 mmol), MeOH (40 mL), H₂ (1 atm.), 30 °C; ^d Reaction was conducted at 40 °C; and ^e THF was used as a solvent.

Pd@MPSO/SiO₂-2 also catalyzed the selective semihydrogenation of a variety of terminal alkynes, such as ethynyl benzenes, bearing electron-withdrawing and electron-donating groups to the corresponding terminal alkenes with excellent selectivities (Fig. 22).

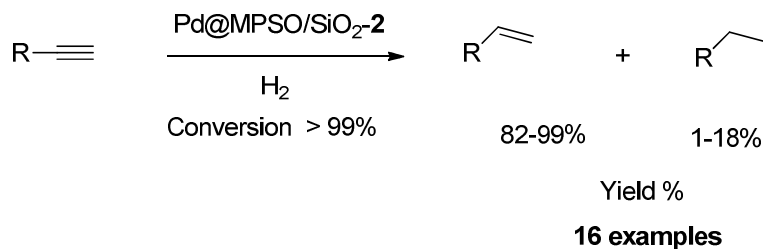


Fig. 22 Semihydrogenation of terminal alkynes using Pd@MPSO/SiO₂-2.

4.1.3. Reduction reactions with magnetically separable core–shell nanocatalysts

Magnetically separable NPs are increasingly used as robust catalysts for various organic transformations because they are easily recoverable and reusable as catalyst for multiple catalytic runs. Such nanomaterials can easily be synthesized *via* a stepwise synthetic method or *in-situ* approach. For example, a simple one-pot process has been developed where oleylamine serves as both solvent and reducing agent for the Ag⁺ and Ni²⁺ ions and triphenylphosphine as surfactant.⁹⁸ TEM images of the nanocatalyst showed particles with a spherical morphology, diameter of *ca.* 14.9 nm (Fig. 23A) and narrow size distribution ($\sigma = 1.14$ nm). The selected area electron diffraction (SAED) pattern (Fig. 23A, b) acquired for the NPs displayed diffraction rings, which could be indexed to face-centered cubic (fcc) corresponding to both Ni and Ag. The compositional scan profile (red line marked in the HAADF image (Fig. 23A (d)) on a single particle clearly showed strong Ni signals at the edge of the particle and strong Ag signals at the center of particle, typical of a core–shell structure.

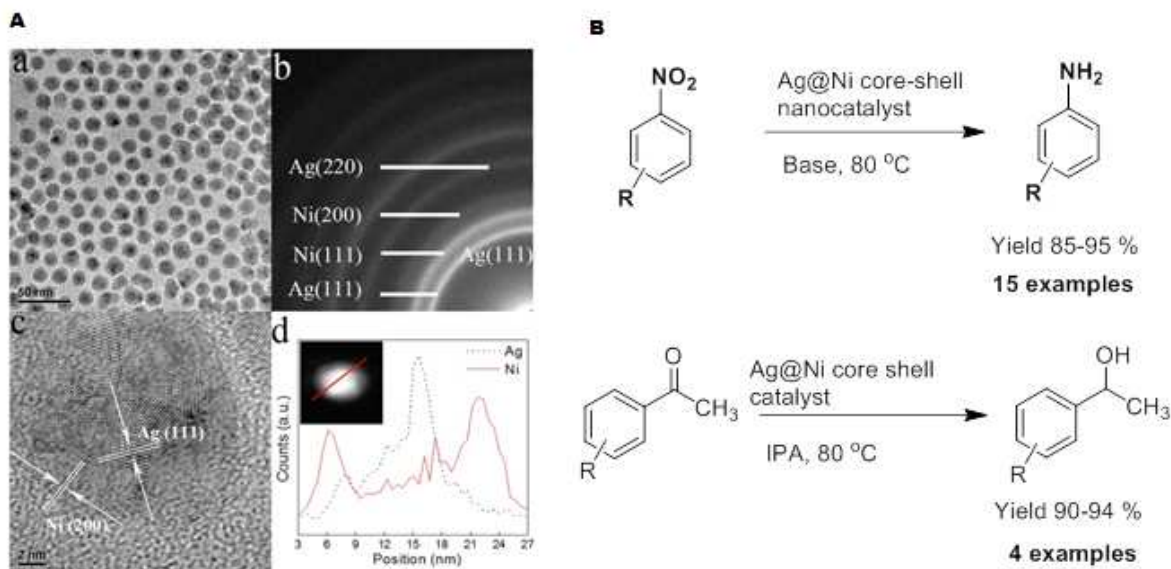


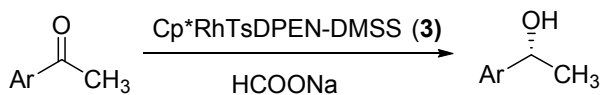
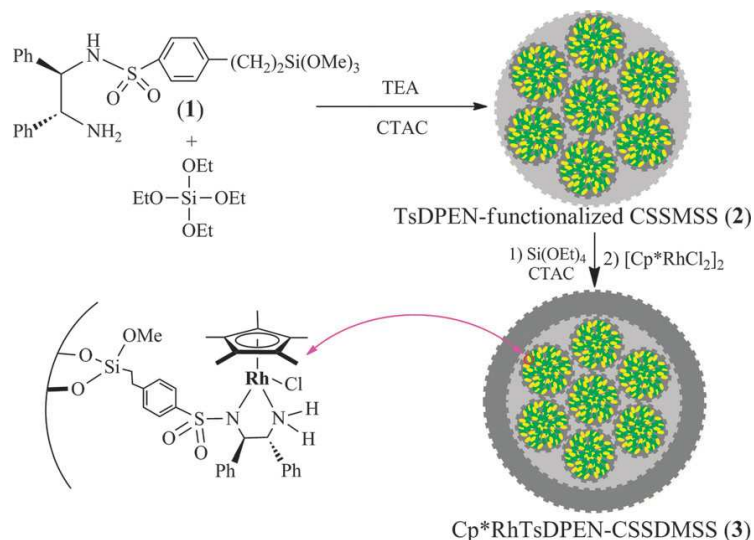
Fig. 23 (A) Ag–Ni CSNs: (a) Low-magnification TEM image (at 50 nm), (b) SAED pattern, (c) HRTEM image, and (d) EDS spectra recorded from the center. (B) Hydrogen transfer reactions of aromatic nitro and carbonyl compounds on Ag@Ni core–shell nanocatalyst. Reprinted with permission from ref. ⁹⁸. Copyright 2013 Royal Society of Chemistry.

The above mentioned nanomaterials can serve as catalysts for the reduction of functional groups in, *e.g.*, nitro, azido and carbonyl compounds; they are of high importance for organic synthesis^{300, 301, 317} and the synthesis of many biologically active compounds for medical applications. Specifically, Ag@Ni CSNs have been deployed for the hydrogen transfer reactions of aromatic nitro compounds (1) using isopropyl alcohol (IPA) as hydrogen donor (Fig. 24B, right); both, electron withdrawing and electron donating groups, such as -Cl, -Br, -F, and -OCH₃, were found to have no significant influence on the reaction. In addition, the catalytic performance of the CSNs was evaluated for the reduction of carbonyl compounds and found to provide good to excellent yields (90-94%).

4.1.4. Asymmetric transfer hydrogenation of aromatic ketones on immobilized rhodium catalyst

Core–shell nanostructured mesoporous silica microspheres have successfully been used as a support material for making nanocatalysts for asymmetric synthesis. The core of silica spheres enables the assembly of various chiral functionalities while the shell of silica spheres prevents leaching of chiral organometallics. Li and co-workers used such an immobilized rhodium catalyst for asymmetric transfer hydrogenation reaction,³¹⁸ wherein a chiral Cp*RhTsDPEN complex (Cp* = pentamethyl cyclopentadiene, TsDPEN = 4-methylphenylsulfonyl-1,2-diphenylethylenediamine) was assembled within the core of mesoporous silica spheres. The detailed synthetic protocol used

for making these core-shell nanostructured mesoporous silica nanospheres with Cp*RhTsDPEN functionality is shown in Fig. 24. First, the TsDPEN-functionalized internal core (**2**) was obtained *via* co-condensation of a chiral silica resource and tetraethoxysilane (TEOS) in the presence of a mixture of cetyltrimethylammonium chloride (CTAC) and triethanol amine (TEA). TEA helps to promote high nucleation and slow growth of the generated seeds, resulting in mesoporous silica NPs. The continuous growth of the external shell around the nanospheres was made possible by using additional TEOS along with CTAC. Finally, direct complexation of [Cp*RhCl₂]₂, followed by the removal of the CTAC templates *via* Soxhlet extraction afforded the mesoporous catalyst Cp*RhTsDPEN-CSSDMSS (**3**) as a light red-colored powdered material.



Ar = Ph, 4-MePh etc.

Conversion = 88 -99%
 Enantiomeric excess = 87-97%

Fig. 24 Synthesis of the heterogeneous catalyst Cp*RhTsDPEN-CSSDMSS (**3**). Reprinted with permission from ref. ³¹⁸. Copyright 2013 Royal Society of Chemistry.

The resulting nanocatalyst was successfully employed as a catalyst for the asymmetric transfer hydrogenation of aromatic ketones in aqueous medium in the absence of any phase transfer catalyst (PTC), affording excellent conversions and high enantioselectivities. The nanocatalyst demonstrated its versatility in accommodating various substrates with electron donating as well as electron withdrawing groups. Moreover, the catalyst was successfully recycled up to twelve times with no significant loss of catalytic activity.

20

4.1.5. Vapor-phase cyclohexene hydrogenation by Au–Rh core–shell nanoparticles

Humphrey and co-workers have reported a MW-assisted method for the synthesis of Au–Rh CSNs in which AuNP seeds were coated by Rh shells in a one-pot procedure.³¹⁹ The Au NPs were prepared by NaBH₄ reduction of HAuCl₄·H₂O in the presence of poly(vinylpyrrolidone) (PVP) in ethylene glycol at 150 °C for 30 min under MW irradiation and then left for an overgrowth step without further modification. Based on the desired thickness of the shell, a specific quantity of RhCl₃·xH₂O in ethylene glycol was added at a rate of 20.0 mL h⁻¹ to the suspended Au NPs under MW heating. In situ reduction of Rh(III) by ethylene glycol facilitated the isotropic overgrowth of Rh(0) onto the AuNP seeds under MW at 150 °C (Fig. 25).

10

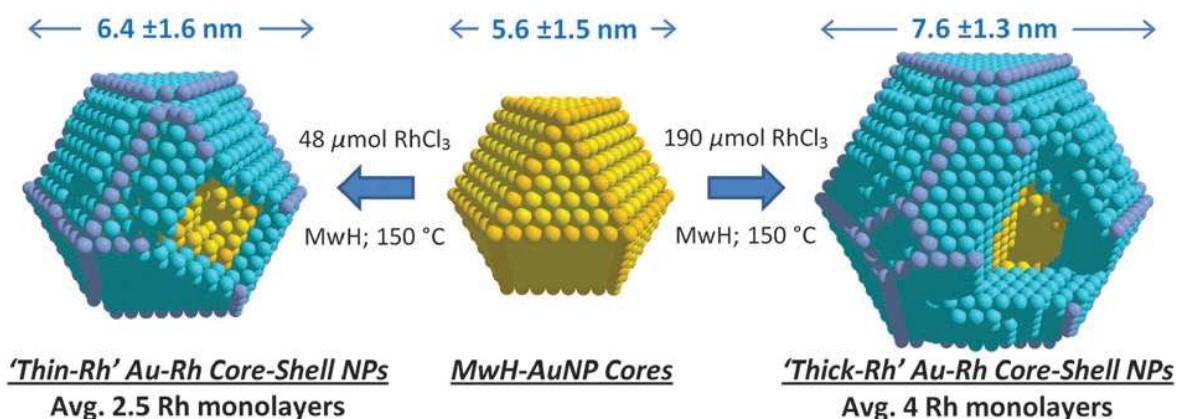


Fig. 25 Schematic of the synthesis of Au-Rh CSNs using a microwave (MW)-assisted synthetic method: yellow/orange = Au; blue/violet = Rh. Reprinted with permission from ref. ³¹⁹. Copyright 2013 Royal Society of Chemistry.

15

The catalytic activity of the resulting CSNs was assessed using vapor-phase cyclohexene hydrogenation as a model reaction in a down flow reactor. Before packing the catalyst in the reactor, Au, Rh and Rh-Au CSNs were supported on amorphous silica using the reported procedure.³²⁰ Next, a few milligrams of each catalyst (material) were studied using a single-pass reactor, in which a low pressure stream of H₂/He and cyclohexene were passed over the catalyst at 30 °C, while the exhaust mixture was monitored with an automated GC to evaluate the progress of the catalytic reaction. The results revealed that the catalytic activity of the materials was highly dependent on the thickness of the shell of the core–shell nanomaterial.

4.1.6. Hydrogenation of alkenes by SiO₂/Pd/SiO₂ type core–shell–shell microspheres

Asefa and co-workers have reported the synthesis of stable catalytic core–shell type microreactors, which comprise SiO₂ microsphere-supported metal NPs embedded in multicores of hollow and nanoporous ZrO₂ shell.³²¹ The catalyst, SiO₂/Pd/h-ZrO₂, was synthesized in three main

steps (Fig. 26 A). In the first step, silica microspheres were prepared by the Stöber method, the surfaces of the silica microspheres were then modified by using 3-aminopropyltrimethoxysilane (APTMS) to form aminopropyl-terminated SiO₂ microspheres, and finally Pd NPs were supported on the aminopropyl-terminated silica microspheres by reducing an aqueous solution of Pd salt with citric acid. In the second step, the SiO₂/Pd core microspheres were coated with a silica shell, thus producing SiO₂/Pd/SiO₂ core-shell-shell microspheres, which were further coated by a surfactant/ZrO₂ shell. The ZrO₂ shell was prepared by mixing SiO₂/Pd/SiO₂ core-shell-shell microspheres in an aqueous solution containing polyethylene glycol dodecyl ether (Brij[®] 30) surfactant and zirconium butoxide [Zr(OBu)₄], and aging the solution for 12 h. The ensuing solid product was calcined at 1073 K for 2 h to afford the SiO₂/Pd/SiO₂/h-ZrO₂ core-shell-shell microspheres. Finally, the controlled etching of the silica shell with an aqueous NaOH solution generated the hollow SiO₂/Pd/h-ZrO₂ core-shell-shell microspheres (or core-shell microsphere catalysts). The formation of the hollow shell was closely monitored by taking TEM images (Fig. 27, B) of samples collected from solutions during etching of the inner silica shells of SiO₂/Pd/SiO₂/ZrO₂, which gradually produced yolk-shell-type SiO₂/Pd/h-ZrO₂ microspheres. The images showed that SiO₂ microsphere-supported Pd NPs were encapsulated within a hollow and nanoporous ZrO₂ shell (yolk-shell type catalytic microreactors). The hollow and nanoporous ZrO₂ shell was permeable enough to allow reactants to reach the Pd-anchored-SiO₂ cores, while at the same time robust enough to keep the Pd NPs intact and give high conversion and recyclability for the hydrogenation of olefins.

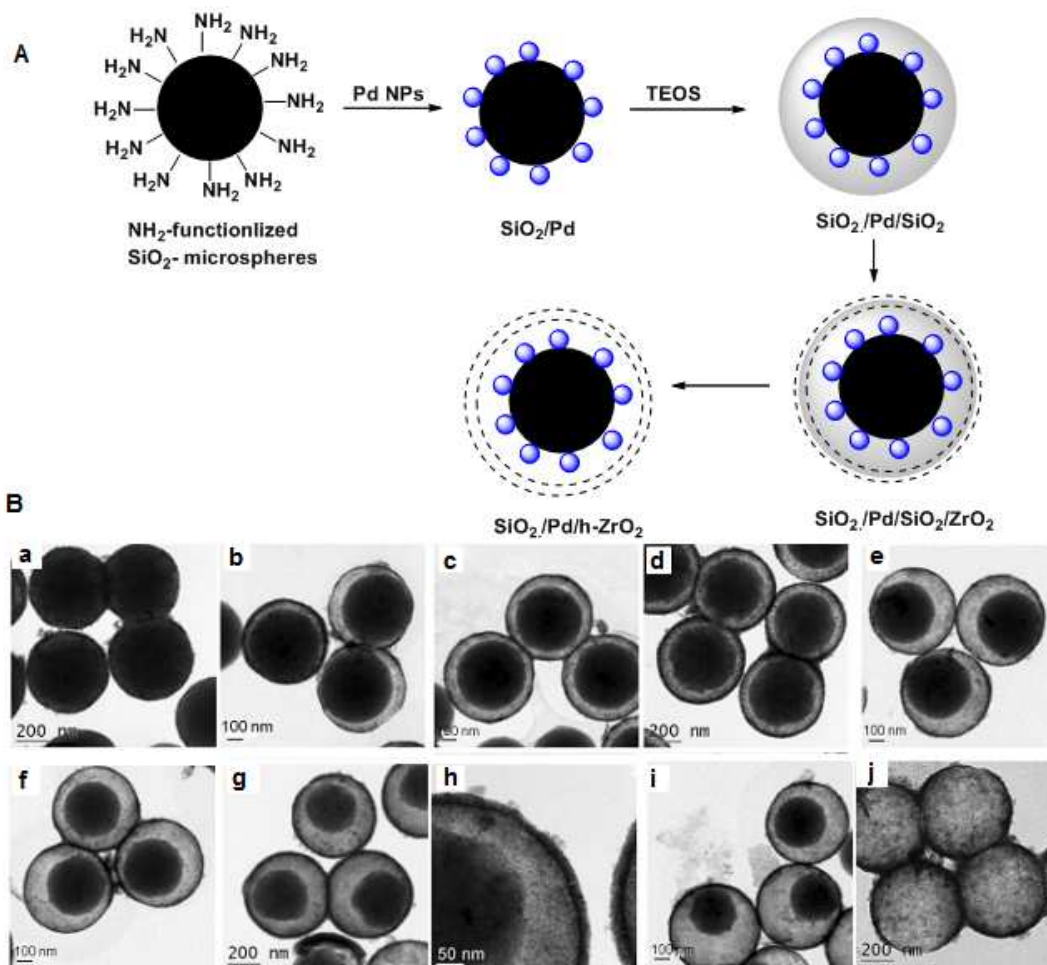
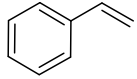
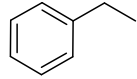
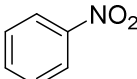
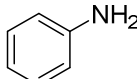
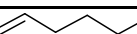



Fig. 26 (A) Schematic of the synthesis of $\text{SiO}_2/\text{Pd}/\text{h-ZrO}_2$ core-shell-shell microspheres or microsphere catalysts. (B) TEM images showing the structural evolution of $\text{SiO}_2/\text{Pd}/\text{SiO}_2/\text{ZrO}_2$ core-shell-shell-shell microspheres after etching with dilute NaOH solution for different etching times: a) 2 h, b) 6 h, c) 9 h, d) 12 h, e) 15 h, f) 20 h, g,h) 24 h, i) 27 h, and j) 48 h. Reprinted with permission from ref. ³²¹. Copyright 2012 WILEY-VCH Verlag GmbH & Co. KGaA, Weinheim.

The catalytic activity of the generated core-shell microspheres was then investigated toward the hydrogenation of styrene as a model reaction. The reaction proceeded at room temperature and under 2 MPa H_2 pressure, giving high yield in 30 min. The versatility of the catalysts was exemplified for various styrenes and recycling experiments (Table 2).

Table 2. Hydrogenation of various substrates by SiO₂/Pd/h-ZrO₂ core-shell-shell microsphere catalysts.

No.	Substrate	Product	Time (h)	Conversion (%)	Selectivity (%)	TOF (h ⁻¹)
1			0.3	~100	~100	5145
2			1.5	93	~100	1187
3			3	94	~100	492

Reaction conditions: substrate (1 mL); methanol (20 mL); catalyst (10 mg, 5.42 wt. % Pd in the SiO₂/Pd/h-ZrO₂ core-shell-shell microspheres); reaction temperature (25 °C); and reactor pressure (2 MPa H₂ pressure).

The same group reported the synthesis of CSNs containing dendrimers in the structures; core-shell microspheres containing SiO₂ cores and dendrimer-encapsulated ultra-small Pd were assembled, producing SiO₂@Pd-PAMAM microspheres.²⁶⁶ In the synthesis, SiO₂ microspheres were first prepared by the Stöber method and then functionalized with vinyl groups by grafting their surfaces with vinyltriethoxysilane (VTS). Afterwards, the vinyl groups were converted into epoxides by using *m*-chloroperoxybenzoic acid. Upon treatment with amine terminated G4 poly(amidoamine) (PAMAM) dendrimers, the SiO₂-supported epoxides underwent ring-opening and afforded SiO₂@PAMAM core-shell microspheres. Pd NPs within the cores of the SiO₂-supported PAMAM dendrimers were generated by reducing Pd(II) ions in the cores of the dendrimers with NaBH₄. TEM images and size distribution of the resulting SiO₂@PAMAM core-shell microspheres are shown in Fig. 27.

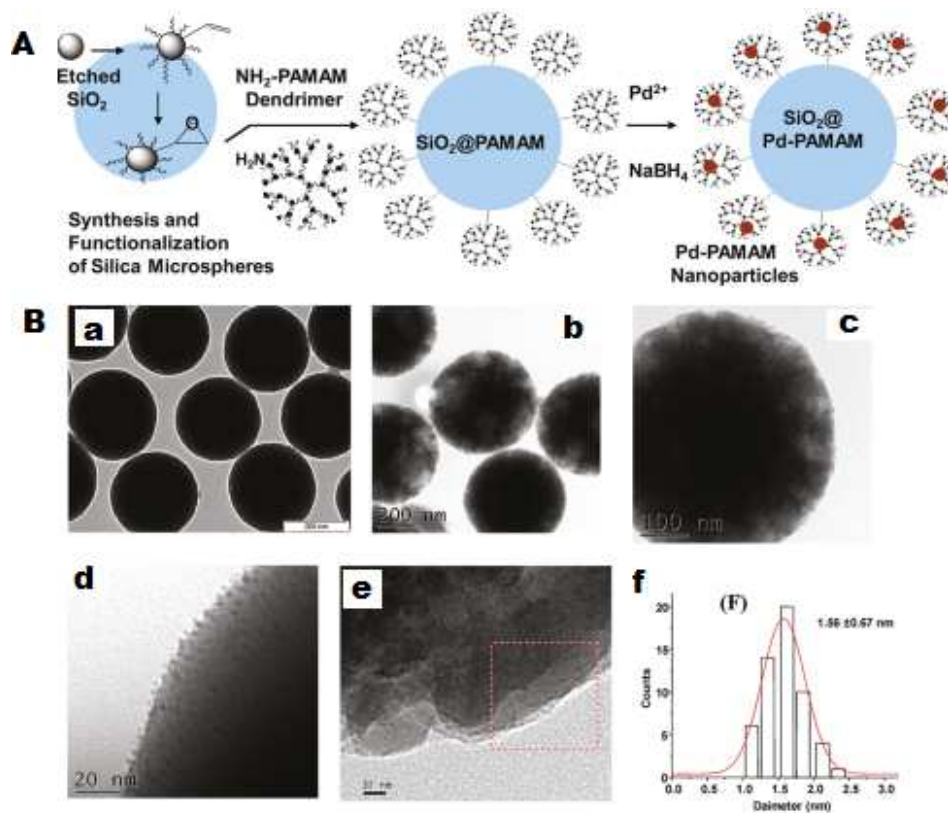


Fig. 27 (A) Schematic of the synthesis of $\text{SiO}_2@$ Pd-PAMAM dendrimer type core-shell microspheres or nanocatalysts. (B) (a, b) Low magnification and (c) high magnification TEM images of etched SiO_2 microspheres. (d, e) Enlarged TEM images of $\text{SiO}_2@$ Pd-PAMAM core-shell microspheres. (f) Size distribution of Pd NPs in $\text{SiO}_2@$ Pd-PAMAM core-shell microspheres. Reprinted with permission from ref. ²⁶⁶. Copyright 2013 American Chemical Society.

The $\text{SiO}_2@$ Pd-PAMAM core-shell microspheres were evaluated for hydrogenation (or reduction) reactions toward various functional groups under 10 bar hydrogen pressure at room temperature (RT) (Fig. 28). The SiO_2 microspheres supported the permeable core-shell structures and the ultrasmall Pd NPs embedded in the attached dendrimer contributed to high catalytic activities. The catalysts showed excellent recyclability without loss of catalytic activity. These CSNs microspheres retained their catalytic activity better than in control samples, including $\text{SiO}_2@$ Pd core-shell microspheres that contained no dendrimers or contained a commercially available Pd/C (1 wt.%) catalyst.

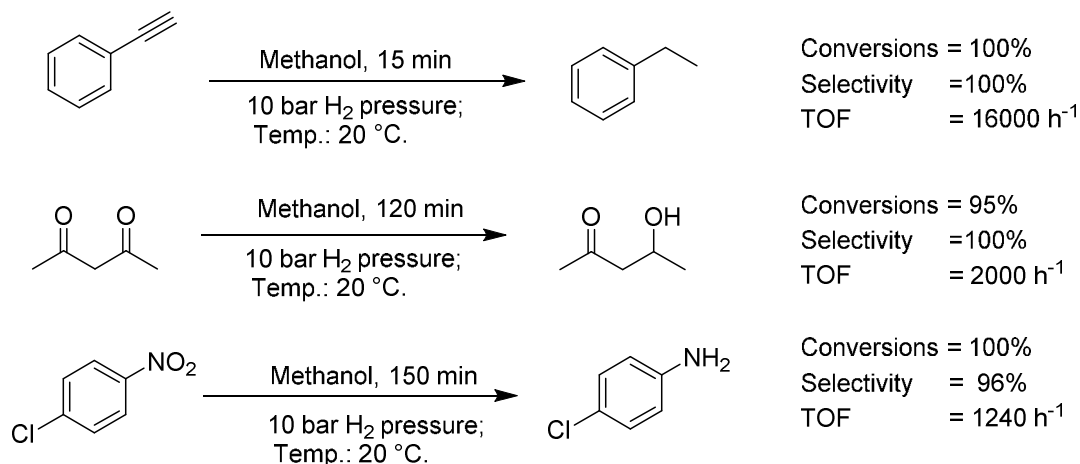


Fig. 28. SiO₂@Pd-PAMAM core-shell microspheres catalyze hydrogenation reactions of various functional groups.

4.1.7. Magnetic core-shell Au nanocatalyst for the reduction of 4-nitrophenol

Zhu and co-workers have reported a magnetic core-shell Au nanocatalyst for the reduction of 4-nitrophenol under benign reaction conditions.²⁹² The as-synthesized Au-Fe₃O₄@metal-organic framework (MOF) nanocatalyst had a magnetic Au-Fe₃O₄ core and a porous MOF shell. The nanocatalyst was synthesized by a versatile layer-by-layer assembly protocol, and the shell thickness in the CSNs was controlled by adjusting the number of cycles employed for the self-assembly. The ensuing Au (3–5 nm) NPs were located between the magnetite core and MOF shell and were evenly dispersed on the surface of the magnetite NPs (Fig. 29).

Further, the Au-Fe₃O₄@MOF nanocatalyst was shown to be the best candidate among other reported Au-based catalysts toward the reduction of 4-nitrophenol as it could be recycled for several runs due to the magnetic Fe₃O₄ core.²⁹² Such type of nanocatalyst can be employed in large-scale synthesis of various compounds in industry, where isolation, separation and reusability are essential to reduce the total synthetic cost.

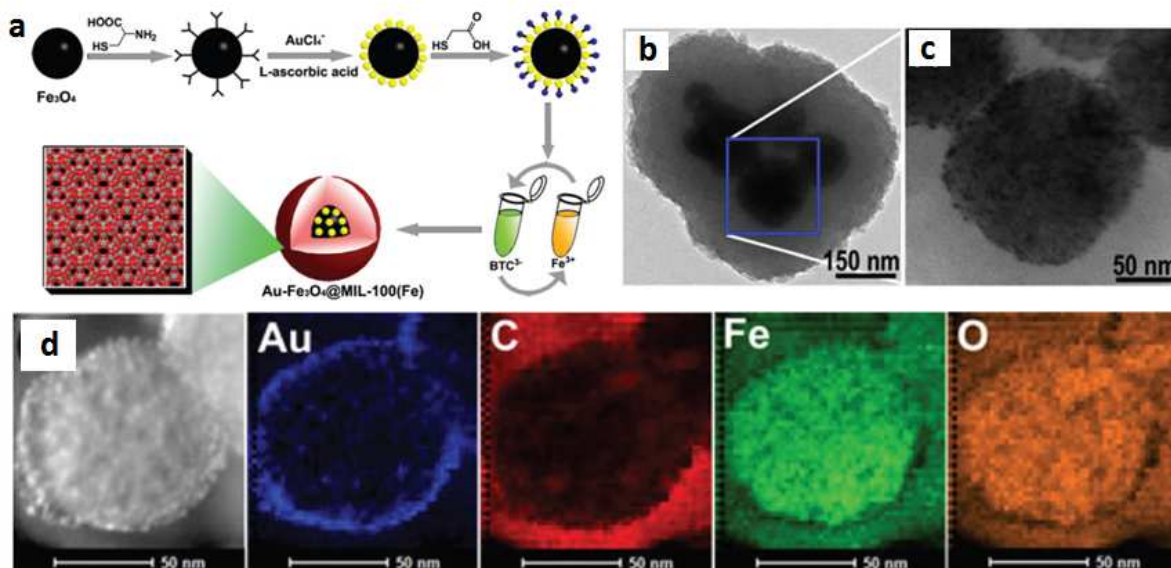


Fig. 29 (a) Synthesis of magnetic core-shell Au-Fe₃O₄@MOF nanocatalyst, (b) TEM images of Au-Fe₃O₄, (c) Single particle of core-shell Au-Fe₃O₄ showing mappings for Au, C, Fe and O elements. Reprinted with permission from ref.²⁹². Copyright 2015 The Royal Society of Chemistry.

5

Recently, bimetallic CSNs have been developed where chemical reactions occurring on the shell and core metal can distinctly modify the performance of the whole core-shell nanocatalysts. Smart design of such core-shell materials by varying the reaction conditions can control their physicochemical properties and catalytic activity.³²²⁻³²⁴ For example, Xu and co-workers synthesized Au@Ag CSNs decorated on a metal-organic framework (MOF) by a sequential deposition reduction method.²⁹⁵ In a typical synthesis of Au-Ag core-shell catalysts, Au-Ag NPs were stabilized on a representative MOF (ZIF-8) (Au-Ag-ZIF-8). The 3D scaffold of ZIF-8 (Zn(MeIM)₂, MeIM = 2-methylimidazole) provides high thermal and chemical stability with pore size and surface area conducive for depositing metal NPs.³²⁵ The size of Au@AgNPs was successfully controlled at 2-6 nm without the need for surfactant by a sequential deposition reduction approach (Fig. 30). Changing the Au/Ag ratio altered the composition; whereas reversing the Au/Ag deposition order changed the structure of the Au-Ag NPs. Applying a post treatment procedure converted the core-shell structure to an Au-Ag alloy. The Au-Ag-ZIF-8 core-shell nanocatalyst was employed for the catalytic reduction of 4-nitrophenol (4-NPh) using NaBH₄ as reductant in water. The reduction kinetics were followed by UV-vis absorption spectroscopy after the addition of the catalyst,²⁹⁵ the absorption peak of 4-nitrophenolate at 400 nm decreased along with a concomitant increase of the ~ 300 nm peak corresponding to 4-aminophenol.

As shown in Fig. 30b, the reaction did not occur over an Au (I₂₀) catalyst and proceeded only sluggishly with an “induction period” over a Ag (II₀₂) catalyst.²⁹⁵ However, the catalytic activity was significantly improved by applying the Au-Ag core-shell catalysts. Among all these synthesized catalysts,²⁹⁵ I₂₂ displayed the highest activity with a rate constant estimated to be 4.97 x

10^{-3} s^{-1} , suggesting that it is the most promising candidate among Au- and Ag-based catalysts.³²⁶⁻³²⁹ Au-Ag core-shell catalysts have also been shown to be highly reusable and stable,³³⁰ as confirmed in the latter case by TEM/ HAADF-STEM analysis after catalysis.²⁹⁵

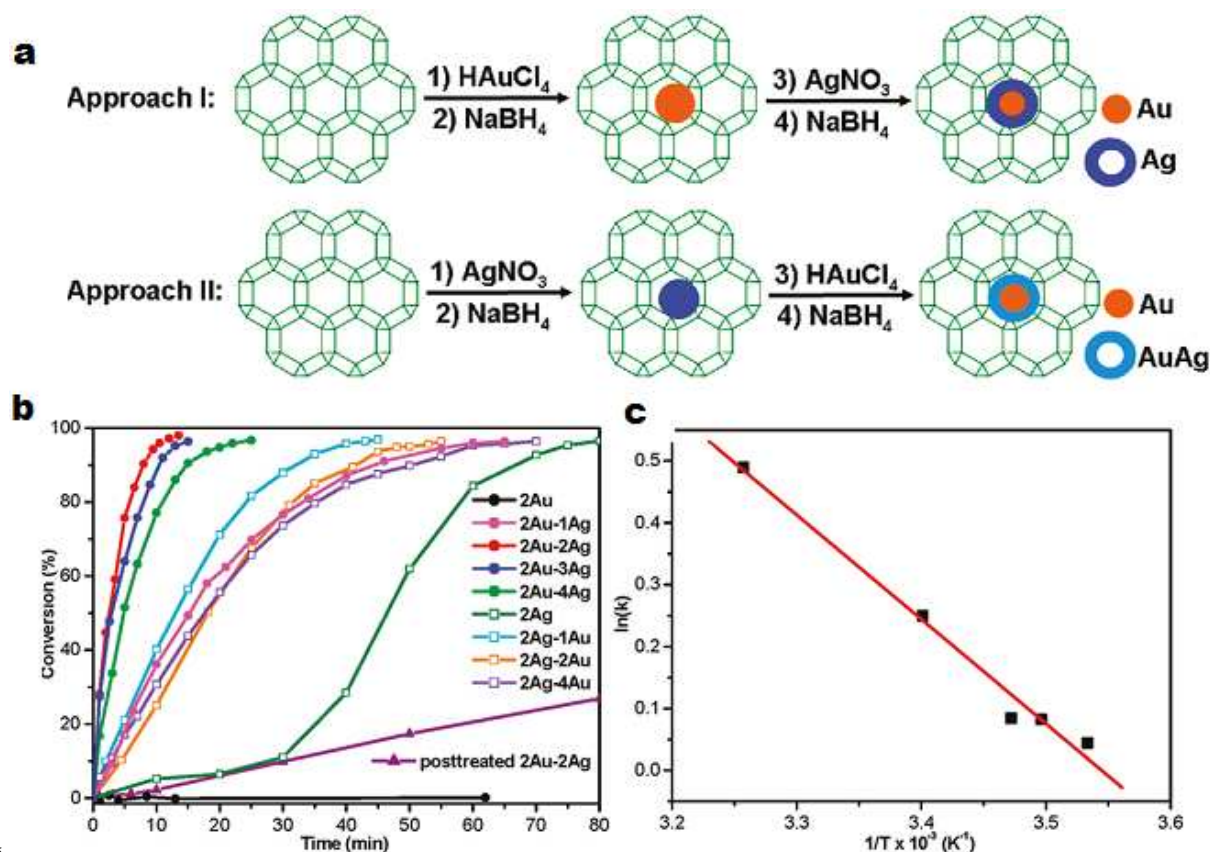


Fig. 30 (a) Schematic illustration of the preparation methods used for Au-Ag core-shell nanocatalysts. (b) Catalytic conversion of 4-NPh over ZIF-8 stabilized catalysts: 2Au (I_{20}), 2Au-1Ag (I_{21}), 2Au-2Ag (I_{22}), 2Au-3Ag (I_{23}), 2Au-4Ag (I_{24}), 2Ag (II_{02}), 2Ag-1Au (II_{12}), 2Ag-2Au (II_{22}), 2Ag-4Au (II_{42}), and post treated I_{22} . (c) Arrhenius plot of the rate constant for the reduction of 4-NPh over I_{22} . Reprinted with permission from ref. ²⁹⁵. Copyright 2011 American Chemical Society.

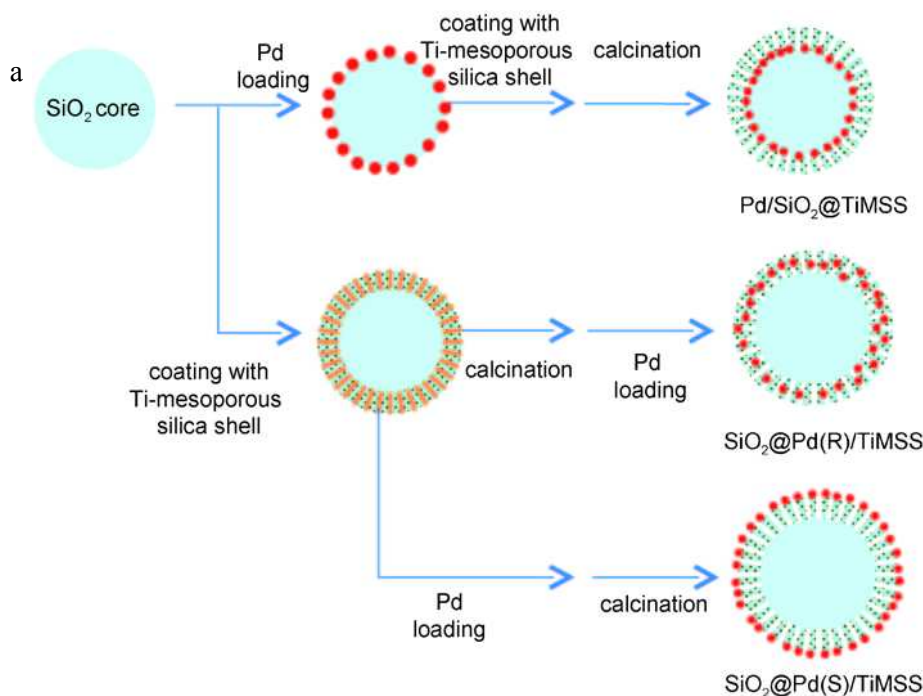
This section described various important chemoselective reductions performed by core-shell nanocomposite, AgNPs@BM, as it forms both polar and nonpolar hydrogen species on respective Ag and BM, in a protocol that precludes the use of traditional bases such as NaOH and KOH. The Pd@MPSO/SiO₂ core-shell catalyst, deployed for semihydrogenation of terminal alkynes, uses expensive Pd, which could be replaced by other transition metal such as Ni, Cu etc.; core-shell recyclable catalysts Ag@Ni, employed for nitro and carbonyl group reduction reactions, is a good example of cost-effective and sustainable process. Catalysts such as Cp*RhTSDPEN-CSSDMSS and Au-Rh core-shell provide ideal examples for asymmetric reduction of ketones and vapor-phase cyclohexene hydrogenation, respectively.

4.2. Oxidation reactions

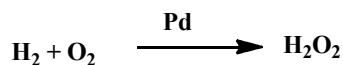
Catalytic oxidations of alcohols, aldehydes and sulfides are among the most important and common reactions in organic synthesis as they can be used to produce a range of valuable raw materials for the fine chemical and pharmaceutical industry.^{36, 331-333} Various CSNs have been employed as catalysts for oxidation transformations,^{334, 335} as shown below.

4.2.1. One-pot oxidation of sulfides by Pd/SiO₂@TiMS core-shell nanocatalyst

Yamashita and co-workers synthesized Pd NPs supported on SiO₂ nanosphere core coated with a Ti-containing mesoporous silica shell (Pd/SiO₂@TiMSS)³³⁶ for one-pot oxidation of sulfide to sulfoxide. To make the nanocatalysts, colloidal SiO₂ nanospheres, prepared *via* Stöber method were first functionalized with Pd NPs³³⁷⁻³³⁹ followed by a coating of Ti-containing mesoporous silica shell (Fig. 31a).³⁴⁰



b Effect of catalysts on the conc of H₂O₂



Catalysts = (H₂O₂ conc. mM)

SiO₂@Pd(S)TiMSS = 3.8

Pd/SiO₂@TiMSS = 3.0

SiO₂@Pd(R)TiMSS = 3.9

c Oxidation of methyl sulfide using in-situ generated H₂O₂

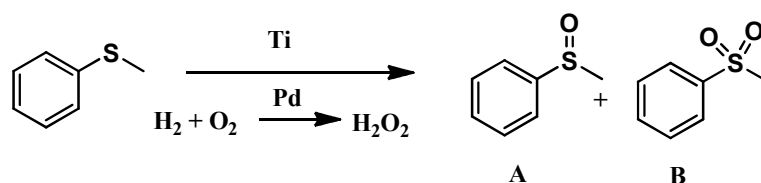


Fig. 31 (a) Schematic of the procedure used to prepare Pd/SiO₂@TiMSS, SiO₂@Pd(R)/TiMSS and SiO₂@Pd(S)/TiMSS. (b) Effect of the catalysts on the concentration of H₂O₂. (c) Oxidation of methyl phenyl sulfide using *in-situ* generated H₂O₂. Reprinted with permission from ref. ³³⁶.

5 Copyright 2011 WILEY-VCH Verlag GmbH & Co. KGaA, Weinheim.

For catalytic studies, SiO₂@Pd(R)/TiMSS and SiO₂@Pd(S)/TiMSS (where (R) denotes random and (S) designates the surface) were investigated for one-pot generation of hydrogen peroxide (H₂O₂); the concentration of H₂O₂ in the reaction medium is almost independent of the
10 catalysts used (Fig. 31b). The catalytic activity of the nanomaterials were then evaluated for the

one-pot oxidation of methyl phenyl sulfide into methyl phenyl sulfoxide (A) (Fig. 31c) using *in-situ* generated H_2O_2 , where $\text{Pd}/\text{SiO}_2@\text{TiMSS}$ was found to be the best catalyst.

4.2.2. Oxidation of alcohols on $\text{Fe}_3\text{O}_4@\text{MgAl-LDH}@Au$ core-shell catalyst

5 Facile synthesis of hierarchical core-shell $\text{Fe}_3\text{O}_4@\text{MgAl-LDH}@Au$ (LDH = Layered-Double-Hydroxides) nanomaterials as magnetically recyclable catalysts for catalytic oxidation of alcohols was reported by Zhang and co-workers.³⁴¹ Briefly, the nanomaterials were synthesized by making $\text{Fe}_3\text{O}_4@\text{MgAl-LDH}$ nanospheres and then supporting Au NPs on the surfaces of the MgAl-LDH of $\text{Fe}_3\text{O}_4@\text{MgAl-LDH}$ ^{342, 343} (Fig. 32 A). Figure 32 B (b) shows SEM/TEM images of
10 $\text{Fe}_3\text{O}_4@\text{MgAl-LDH}@Au$ nanocatalyst and its precursors. The images show that the Fe_3O_4 NPs had a smooth surface and mean diameter of 450 nm with a narrow size distribution. After coating the nanospheres with carbonate-MgAl-LDH, the materials showed honeycomb like morphology with many voids of about 100–200 nm in size.

15

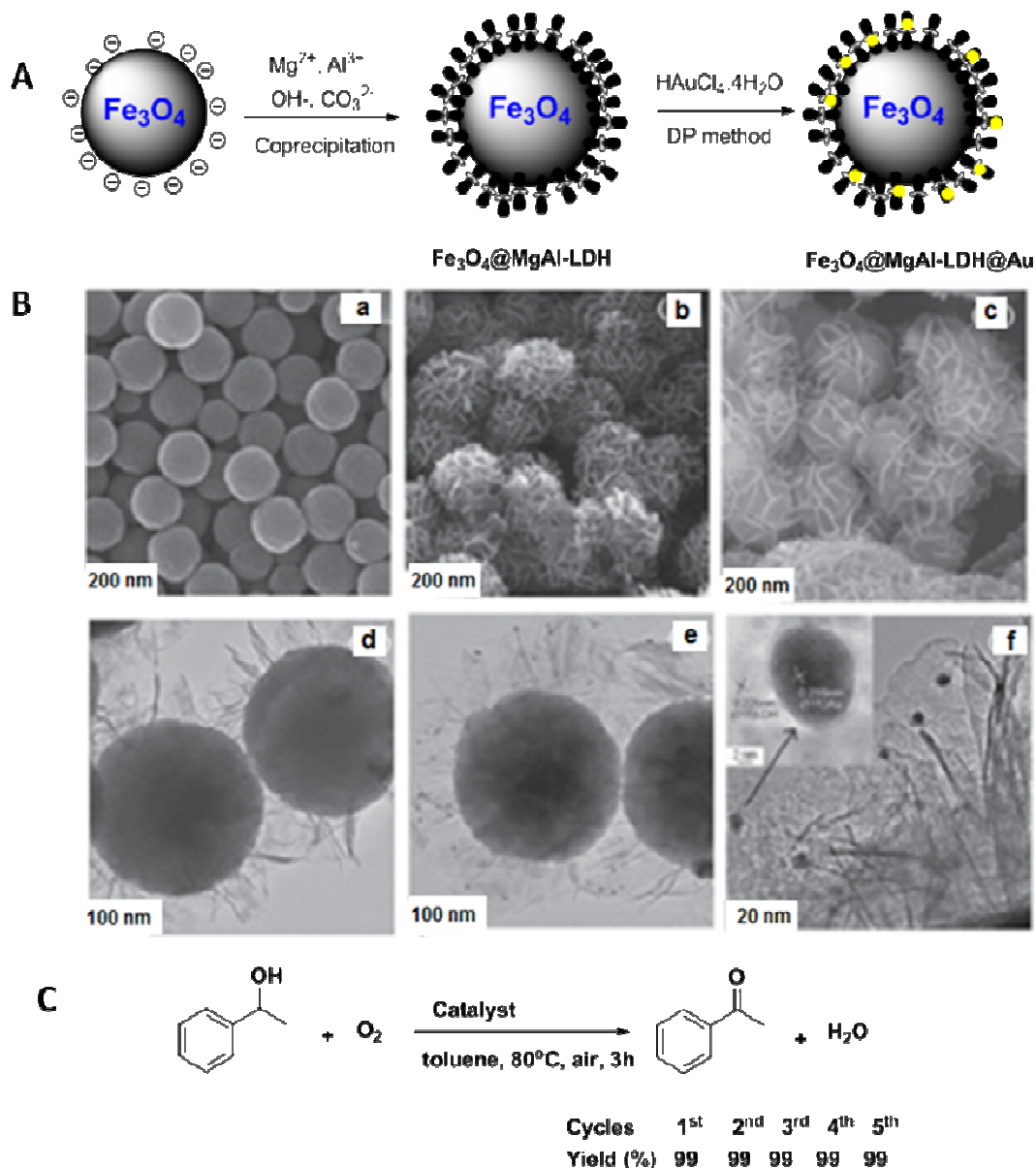


Fig. 32 (A) Synthesis of core-shell $\text{Fe}_3\text{O}_4@\text{MgAl-LDH@Au}$ NPs. (B) SEM (a, b and c), TEM (d and e), and HRTEM (f) images of Fe_3O_4 (a), $\text{Fe}_3\text{O}_4@\text{MgAl-LDH}$ (b and d), and $\text{Fe}_3\text{O}_4@\text{MgAl-LDH@Au}$ (c, e, and f). (C) Catalytic oxidation of 1-phenylethanol. Reprinted with permission from ref. ³⁴¹. Copyright 2013 Royal Society of Chemistry.

The catalytic oxidation of 1-phenylethanol was then performed by using the magnetic $\text{Fe}_3\text{O}_4@\text{MgAl-LDH@Au}$ (7.0 nm Au) NPs as catalyst, affording acetophenone (99%) with excellent yield and high turnover frequency (TOF) of 66 h^{-1} ; the catalytic activity was comparable to that, reported previously for Au/MgAl-LDH (TOF, 74 h^{-1}) containing Au NPs with average size of 2.7 nm at $40 \text{ }^\circ\text{C}$.³⁴⁴ The magnetic property of the $\text{Fe}_3\text{O}_4@\text{MgAl-LDH@Au}$ nanospheres was successfully utilized to easily separate the nanocatalysts from the reaction mixture after the reactions (Fig. 32 C).

4.2.3. Oxidation of benzyl alcohol by gold–palladium core–shell nanocrystals

Tilley and co-workers developed Au-Pd core-shell NCs with optimized size, shape and facets for catalytic applications.³⁴⁵ In their study, icosahedral Au-Pd core-shell NCs were synthesized by a seed-mediated approach, in which nucleation and growth stages were independently controlled. To grow the Pd shell around the Au seeds, palladium acetylacetonate and hexadecylamine in toluene in a 2:1 molar ratio of Pd to Au were added into the solution (Fig. 33). The CSN catalysts were then supported on activated carbon with a loading of 1 wt.% metal NPs. The catalytic activity of the resulting series of Au-Pd core-shell NCs with varied shell thickness (0.4, 0.8, 1.5, 2.2, and 3.2 nm) was evaluated toward the oxidation of benzyl alcohol to benzaldehyde. Typically, in the presence of 25 mg of these Au-Pd/C NPs, benzyl alcohol (40 mL) was converted into benzaldehyde in an autoclave under 10 bar oxygen at 140 °C under solvent-free conditions. The NCs with shell thickness of 2.2 nm (*ca.* 12 atomic layers of Pd) were found to give the highest (TOF) and selectivity in the reaction.

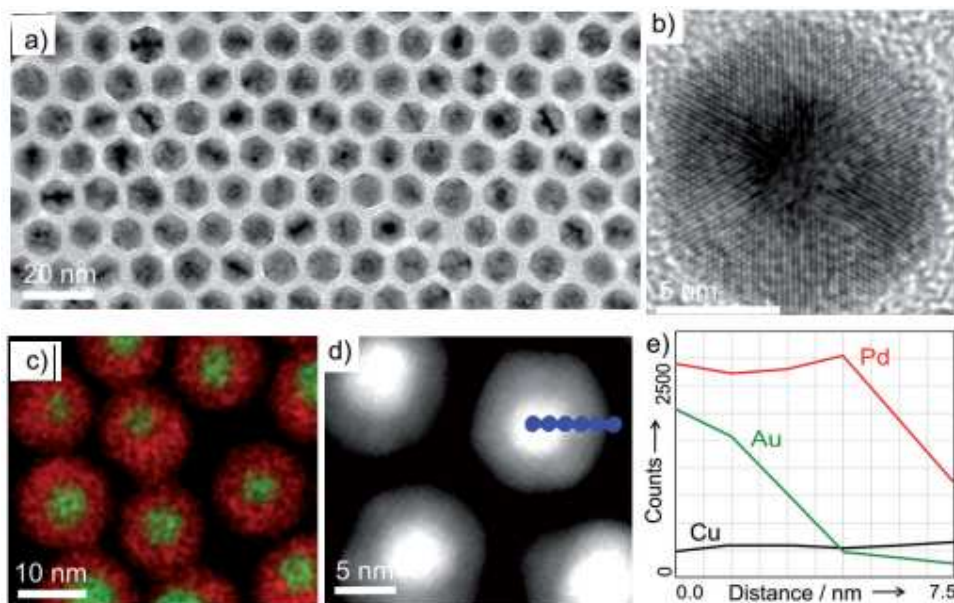


Fig. 33 Micrograph images of Au-Pd core-shell NCs: (a) bright-field TEM, (b) high-resolution TEM, (c) STEM-EDX map shown as an overlay of gold and palladium signals, and (d) HAADF-STEM image showing a contrast difference between the gold core (bright) and palladium shell (dark). Dotted blue line represents the EDX line scan shown in (e) with Pd shown in red, Au in green and Cu in black. Reprinted with permission from ref. ³⁴⁵. Copyright 2013 WILEY-VCH Verlag GmbH & Co. KGaA, Weinheim.

4.2.4. Lab-in-a-shell approach for selective catalysis

Dai and Zhang co-workers have reported a “lab-in-a-shell” approach for the synthesis of multifunctional CSNs with metal clusters as a core and microporous silica as shell.³³⁴ Noble metals such as Pd and Pt were incorporated in the void space mediated by the capture of polymer dots inside the silica shell (Fig. 34). TEM images of the Pd cluster@silica core-shell nanospheres revealed that the Pd NPs were implanted inside the silica hollow shell and most of the core clusters were attached to the interior wall of the silica shell (Fig. 34b).

The Pd-cluster embedded in the hybrid core-shell nanocatalysts displayed excellent size-selective catalysis for the allylic oxidation of cyclohexene moieties with different molecular size (e.g., 0.5 nm cyclohexene, 1.91 nm cholesteryl acetate (CA)). Whereas a Pd/silica nanocatalyst successively oxidized cyclohexene and CA to the corresponding 2-cyclohexene-1-one, 2-cyclohexenol, cyclohexene oxide and 7-ketocholesteryl acetate as main products with conversions of 23.1% (cyclohexene) and 9.8% (CA), for the Pd cluster@silica catalysts, a 4 times higher cyclohexene conversion (93.7%) was achieved with high selectivity for the dehydrogenation product (97.7%). The selective oxidation of organic compounds such as hydrocarbons or alcohols is an important reaction in industrial organic synthesis.³⁴⁶ Furthermore, Pd/silica (Pd loading 0.9%) CSNs have been employed for the solvent-free oxidation of hydrocarbons and alcohols in an O₂ atmosphere to give corresponding products with excellent conversions.

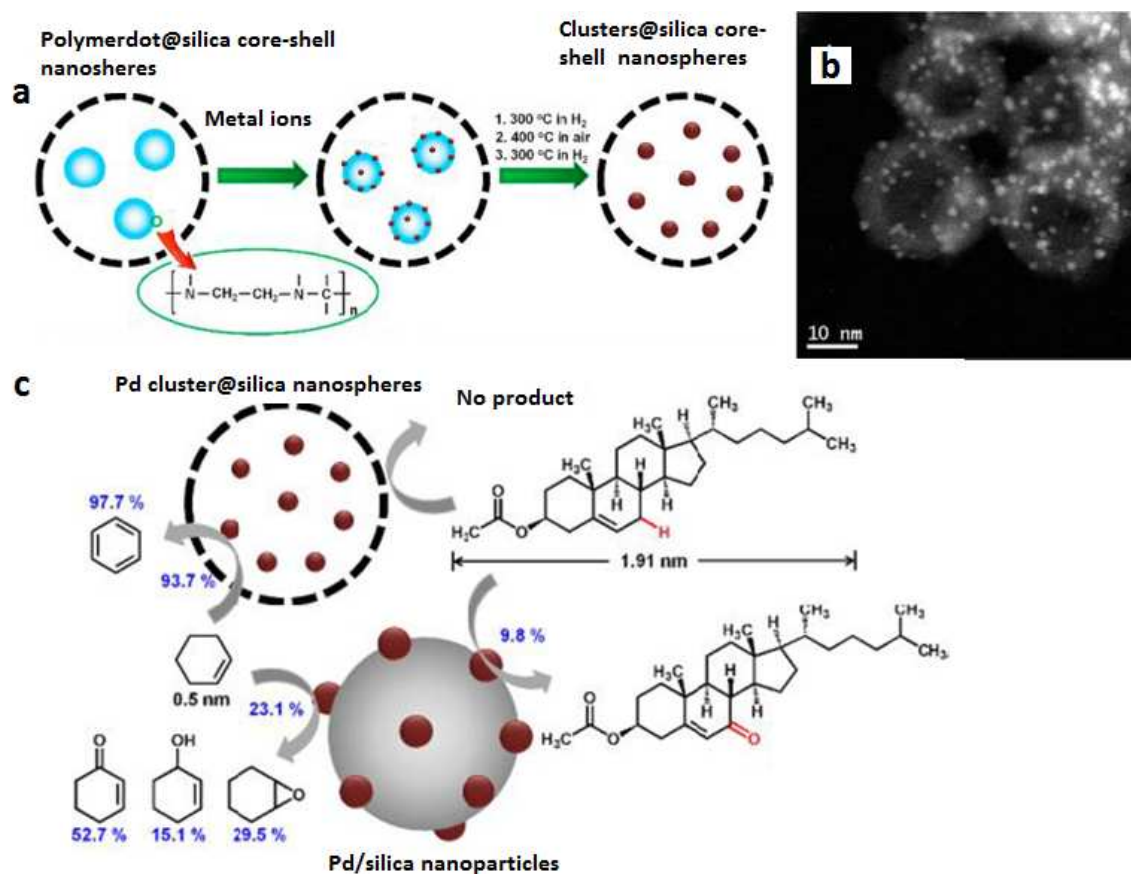


Fig. 34 (a) Schematic of the synthesis of metal cluster@silica core-shell nanospheres. (b) TEM image of Pd cluster@silica core-shell nanospheres. (c) Size-selective catalysis of Pd cluster@silica core-shell nanospheres. Reprinted with permission from ref. ³³⁴. Copyright 2011 American Chemical Society.

5

4.2.5. CO oxidation with core-shell nanoparticles

Chen *et al.* have reported a simple synthetic strategy for making core-shell microspheres consisting of CuO NPs dispersed on the surface of Al₂O₃ for CO oxidation.³⁴⁷ The obtained Al₂O₃@CuO core-shell submicrospheres displayed uniform core-shell structures, with shells composed of small CuO NPs (without the formation of CuAl₂O₄ passivation layer between CuO and Al₂O₃). Notably, when these Al₂O₃@CuO submicrospheres were used as a catalyst for CO oxidation, a significantly improved activity was observed compared to conventional supported CuO/Al₂O₃³⁴⁸ (prepared by impregnation and calcination processes) catalysts in a continuous-flow fixed-bed reactor with feed gas containing 1.0 vol. % CO, 1.6 vol. % O₂, and 97.4% He (balance gas) at a total flow rate of 50 mL.min⁻¹, which corresponds to a gas hourly space velocity (GHSV) of 30,000 mL.h⁻¹.g_{cat}⁻¹. A maximum conversion was obtained at 160 °C for the reaction.

Bao and co-workers developed a synthetic method for generating FeO-on-Cu@Pt-oxide-on-NM (noble metal) type nanomaterials³⁴⁹ for catalytic CO oxidation (Fig. 35). The Cu@Pt CSNs were synthesized by a sequential polyol process. In the synthesis, PtCl₂ was first added to a “freshly prepared” colloidal solution of Cu/EG at 130 °C under an Ar atmosphere. The resulting Cu@Pt and Pt NPs were further decorated with FeO through a reductive deposition-precipitation (RDP) process and their catalytic activity was evaluated for PROX (PReferential OXidation). The particles showed significantly improved catalytic activity for the catalytic oxidation of CO, especially after the Cu@Pt NPs had been decorated with FeO patches. Moreover, even though they contained much less Pt, they exhibited a similar catalytic activity to that of Pt NPs covered with surface FeO patches.

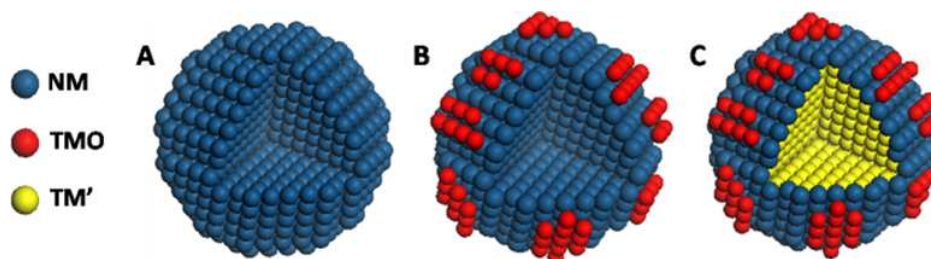


Fig. 35 Various structural configurations of supported NPs catalysts: (A) noble metal NPs, (B) “TMO-on-NM” (Transition metal oxide = TMO) NPs consisting of a noble metal NPs decorated with surface TM oxide, and (C) “TMO-on-NM Shell” NPs with TM oxide decorating the surface of

a core-shell NP. Reprinted with permission from ref. ³⁴⁹. Copyright 2012 American Chemical Society.

4.2.6. CO oxidation on sinter-resistant Au-mesoporous-silica core-shell nanoparticles

Yin and co-workers and Kresge et al. synthesized sub-5 nm nanosized Au NPs@mesoporous-silica (m-SiO₂) nanospheres *via* a soft-templating method and investigated their catalytic activity for CO oxidation (Fig. 36).^{350, 351} The BET surface area and total pore volume of the resulting material, as analyzed by the nitrogen physisorption, were found to be 736 m²/g and 0.92 cm³/g, respectively. Besides their excellent catalytic activity for CO oxidation, the Au@m-SiO₂ core-shell nanospheres displayed robustness, showing good sinter-resistant properties even at 750 °C. The SiO₂ shell not only prohibited Au NPs from migrating but also restricted its growth. Such silica-based catalytic systems could possibly be extended to other important metals and high temperature and pressure organic reactions.

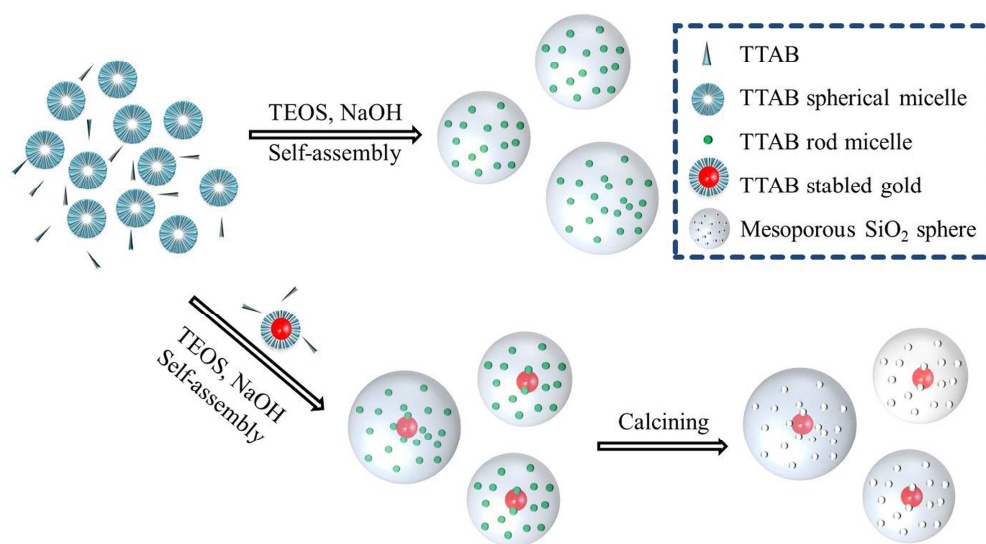


Fig. 36 Schematic of the formation procedures used for mesoporous silica nanospheres with or without Au NPs. Adapted from ref. ³⁴⁴

Significant reactions exemplified by the selective oxidation of methyl phenyl sulfide to methyl phenyl sulfoxide using SiO₂/@Pd(R)/TiMSS and SiO₂/@Pd(S)/TiMSS catalysts are highlighted wherein in-situ generated H₂O₂, avoids external addition of an oxidant. Magnetically separable core-shell Fe₃O₄@MgAl-LDH@Au catalyst accomplishes oxidation using air as an oxidant in a clean, sustainable and benign protocol.

4.3. Coupling reactions

Coupling reactions are an integral part of the synthesis of many drug intermediates and pharmaceutical precursors.³⁵²⁻³⁵⁵ The most important coupling reactions include the Heck reaction, Suzuki-Miyaura reaction and Sonogashira reaction, which often involve precious metals, such as Pd, Au, *etc.*, and are deployed in countless synthetic processes.³⁵⁶ The following section describes examples of these reactions that can be effectively catalyzed by a variety of CSNs containing metals.

4.3.1. Au–Pd core–shell catalyzed Suzuki–Miyaura reaction

Amatore and co-workers have reported the synthesis and catalytic activity of Au–Pd CSNs toward the Suzuki–Miyaura cross-coupling reaction between 4-bromoanisole and phenyl boronic acid in aqueous medium with base K_2CO_3 at room temperature (Fig. 37).³⁵⁷ The coupling products were obtained in excellent yield (95%) and also at a faster rate than other reported catalysts.^{358, 359} The Au@Pd CSNs were found to have unique structural features, in which a shell of one or several Pd(0) monolayer(s) (MLs) was precisely wrapped around a Au (0) nanocore (Fig. 37 A,a). Two to five monolayers of Pd were found to be responsible for the NPs' optimum catalytic conversion rate (Fig. 38 A,b).

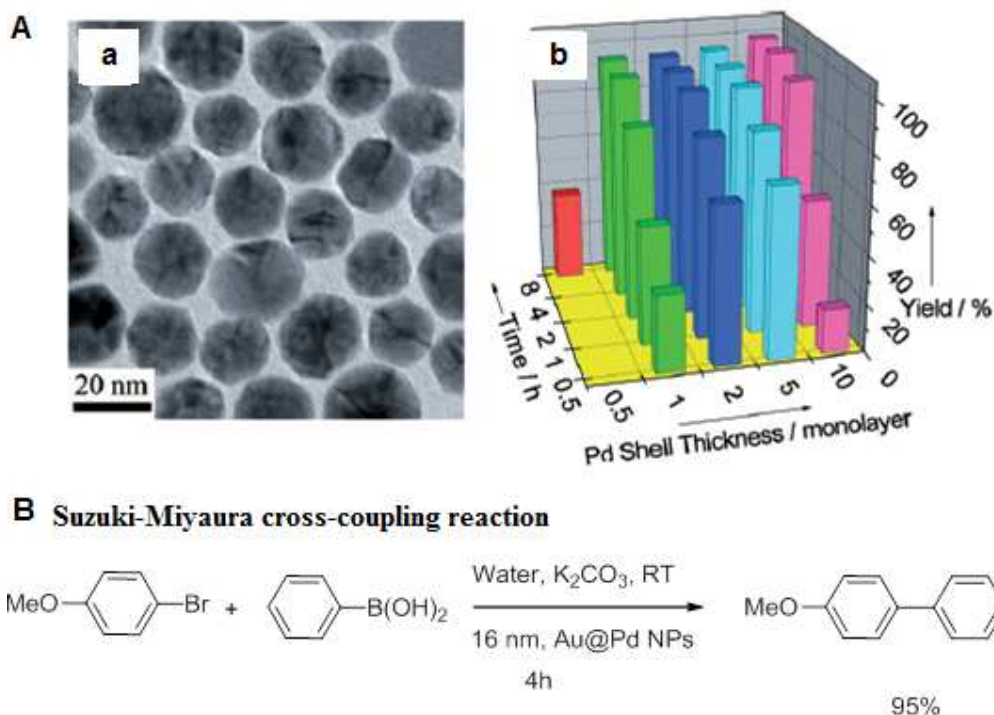


Fig. 37 (A), (a) Transmission electron microscopy (TEM) image of 16 nm Au@Pd NPs with two monolayers of Pd. (b) Plot of yield vs. Pd shell thickness as a function of reaction time for the cross-coupling between 4-bromoanisole with phenylboronic acid. (B) Suzuki-Miyaura cross-

coupling reaction. Reprinted with permission from ref. ³⁵⁷. Copyright 2011 WILEY-VCH Verlag GmbH & Co. KGaA, Weinheim.

4.3.2. Suzuki–Miyaura reaction catalyzed by Ni/Pd core–shell nanoparticles

Metin and co-workers synthesized Ni-Pd CSNs supported on graphene (G) by a sequential reduction method for the Suzuki–Miyaura reaction.³⁶⁰ The catalyst showed a narrow size distribution with mean particle size of ~10 nm and standard deviation of 5% with respect to the particle diameter. Phenyl boronic acid and 4-chloro-4-fluorophenylboronic acid were successfully coupled with aryl iodides, bromides and even chlorides in a mixture of dimethylformamide (DMF)/water in the presence of base at 110 °C. To compare the effect of the NPs' structural features on the catalytic activity, three different Ni/Pd NPs with different Ni/Pd molar ratio, namely 2/3, 7/3 and 3/2, were synthesized. The resulting Ni/Pd CSNs supported on graphene were then employed as catalysts for the Suzuki–Miyaura cross-coupling reactions, all delivering excellent yields of the corresponding products (Fig. 38). Among the three Ni/Pd NPs investigated, the one with Ni/Pd ratio of 3/2 was found to be the most active catalyst for the reaction. Moreover, the G–Ni/Pd nanocatalysts remained stable under the reaction condition and were easily recyclable, affording 98% conversion after five catalytic cycles without any noticeable Ni/Pd compositional change.

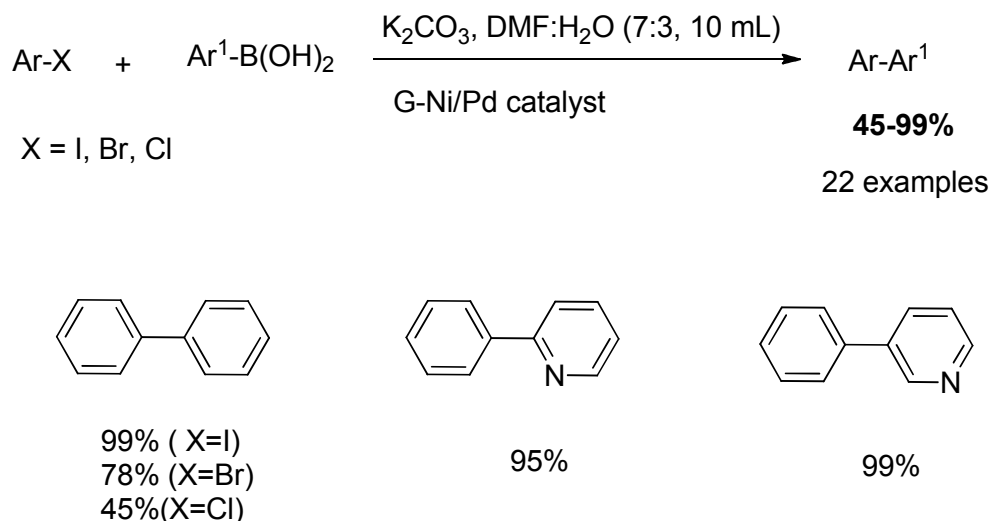
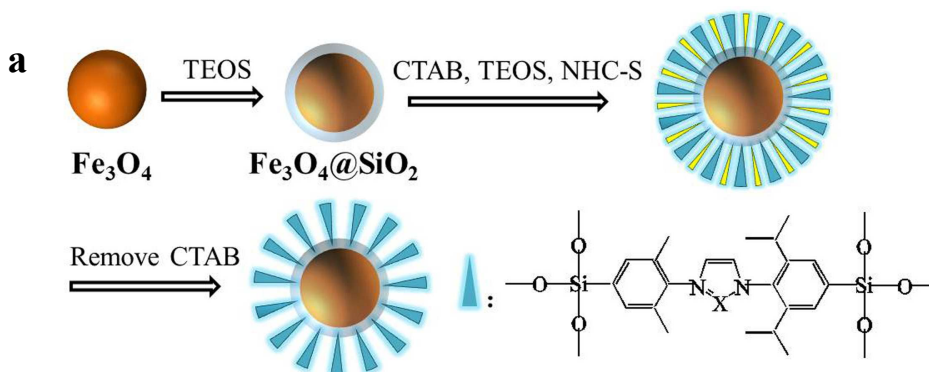


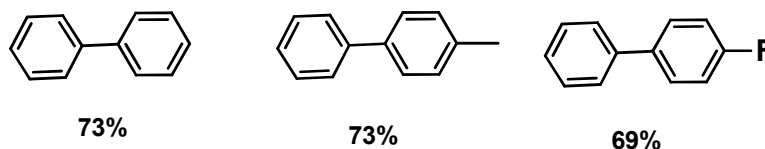
Fig. 38 Suzuki coupling reaction catalyzed by G-Ni/Pd CSNs.

Yang *et al.* have reported the synthesis of nanoporous organosilica microspheres consisting of a magnetic Fe₃O₄ core and an organosilica shell with built-in *N*-heterocyclic carbene (NHC) moiety (Pd-coordinated Fe₃O₄@mSiO₂-NHC) (Fig. 39a).³⁶¹ The Fe₃O₄ microspheres were coated with a thin layer of SiO₂ on which a NHC-functionalized nanoporous organosilica shell was created surrounding silica-coated Fe₃O₄ cores *via* a sol–gel process in the presence of CTAB templates.

After removing the CTAB templates, magnetic core-shell nanoporous organosilica microspheres with built-in NHC moieties were formed. By gradually reducing the amount of siliceous precursors added in the third step, three different materials could be obtained with decreasing shell thickness. The corresponding Pd-coordinated $\text{Fe}_3\text{O}_4@m\text{SiO}_2\text{-NHC}$ was finally obtained by dispersing the nanospheres in dry 1,4-dioxane containing $\text{Pd}(\text{acac})_2$ (acac = acetylacetonate) and mixing the dispersion at 100 °C for 30 h under N_2 atmosphere.



b The Suzuki–Miyaura couplings of various phenylboronic acids and chlorobenzene over the Pd-coordinated $\text{Fe}_3\text{O}_4@m\text{SiO}_2\text{-NHC}$



c The C-C coupling reaction of benzylic chloride with various arylboronic acids

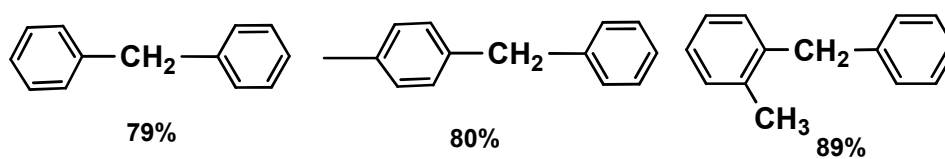


Fig. 39 (a) Schematic of the synthesis of $\text{Fe}_3\text{O}_4@m\text{SiO}_2\text{-NHC}(x)$, HNC-S $\frac{1}{4}$ 1,3-bis(4-triethoxysilyl-2,6-diisopropylphenyl)-imidazol-3-ium-trifluoro-methane sulfonate (NHC-bridged organosilane). (b) Suzuki-Miyaura coupling between various arylboronic acids with chlorobenzene over Pd-coordinated $\text{Fe}_3\text{O}_4@m\text{SiO}_2\text{-NHC}$. (c) C-C coupling reaction of benzylic chloride with various arylboronic acids over Pd-coordinated $\text{Fe}_3\text{O}_4@m\text{SiO}_2\text{-NHC}$. Adapted from ref. ³⁶¹

The catalytic activity of the resulting Pd-coordinated $\text{Fe}_3\text{O}_4@m\text{SiO}_2\text{-NHC}$ was evaluated for Suzuki–Miyaura coupling of chlorobenzene and phenylboronic acid in isopropyl alcohol at 80 °C under N_2 atmosphere (Fig. 39 b). Many other substrates, including moderately sterically demanding

arylboronic acids, were found to be smoothly converted to the corresponding coupling products in 70–86% yields with the aid of NPs as catalyst. Using phenylboronic acid as substrate, the Pd-coordinated $\text{Fe}_3\text{O}_4@\text{mSiO}_2\text{-NHC}$ gave diphenylmethane in a yield up to 79% (Fig. 39 c). Both electron-rich and electron-poor arylboronic acids afforded various diarylmethanes in 71–89% yields.

4.3.3. Sonogashira coupling reaction catalyzed by inside-out type core–shell nanoparticles

The Sonogashira reaction is typically a C–C bond forming reaction, which enables the coupling of a terminal sp hybridized carbon from an alkyne with a sp^2 carbon of an aryl or vinyl halide (or triflate).³⁶² There are many examples in the literatures of this class of reaction, catalyzed by various metal-containing nanomaterials, including CSNs.^{363, 364}

Recently, Varma and co-workers reported the use of inside-out core–shell architectures ($\text{Cu}_2\text{O}@\text{Cu}$) with a Cu_2O core and Cu shell as catalyst for the Sonogashira coupling reaction.^{365, 366} Their facile solution-phase synthetic strategy generated Cu on the outside, producing $\text{Cu}_2\text{O}@\text{Cu}$ type CSNs (*cf.*, the more commonly reported material is $\text{Cu}@\text{Cu}_2\text{O}$) (Fig. 40).³⁶⁶

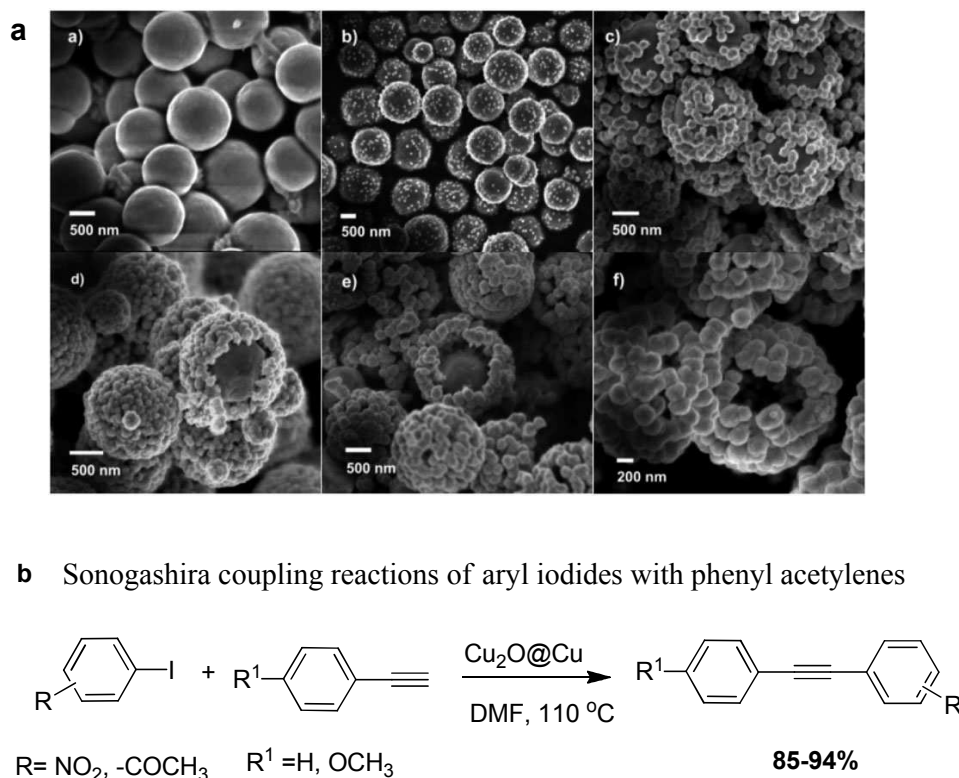


Fig. 40 (a) SEM images of inside-out core–shell architectures ($\text{Cu}_2\text{O}@\text{Cu}$). (b) Sonogashira coupling reactions of aryl iodides with phenyl acetylenes catalyzed by $\text{Cu}_2\text{O}@\text{Cu}$ NPs. Reprinted with permission from ref. ³⁶⁶. Copyright 2012 Royal Society of Chemistry.

The $\text{Cu}_2\text{O}@Cu$ CSNs were found to successfully catalyze Sonogashira coupling reactions between aryl iodides and phenylacetylenes to afford the corresponding biarylacetylenes in excellent yields (85–94%) (Fig. 40 b). Notably, the reaction does not proceed with either Cu_2O or Cu alone but only with the porous core–shell catalyst. Thus, $\text{Cu}_2\text{O}@Cu$ offers a good substitute for expensive Pd in this type of coupling. The recovered $\text{Cu}_2\text{O}@Cu$ CSNs after the catalytic reactions retained their core–shell nanostructures and remained stable without significantly losing their catalytic activity even after multiple runs.

Common coupling reactions such as Suzuki–Miyaura, Heck reaction, and Sonogashira reaction are well studied using various types of heterogeneous catalysts. A variety of core-shell NPs namely Au–Pd , Ni/Pd and Pd -coordinated $\text{Fe}_3\text{O}_4@m\text{SiO}_2\text{-NHC}$ core-shell NPs are used for Suzuki–Miyaura coupling reactions in benign media. The noble and rare metals, Pd , and Au could be replaced by other inexpensive base metals such as copper. Chiral NHC could be incorporated in core-shell NPs synthesis for application in asymmetric reactions. The inside-out core–shell architectures ($\text{Cu}_2\text{O}@Cu$) used for the Sonogashira reaction is an example of a benign protocol where coinage metal replaces a noble metal.

4.4. Ammonia decomposition reaction with iron-based core–shell nanoparticles

Ammonia synthesis, which was invented by Fritz Haber almost one-hundred years ago, is a key reaction in various industrial processes.³⁶⁷ In recent years, the reverse protocol that entails the decomposition of ammonia into hydrogen and nitrogen has come into the limelight, particularly in the context of alternative fuel-resources. This approach has enabled the development of ammonia-based hydrogen production, in addition to ammonia fuel cells (as sources of ‘clean’ energy).³⁶⁸

In the hydrogen production process, ammonia decomposition requires temperatures above 400 °C for thermodynamic reasons, and therefore most direct ammonia fuel cells typically function at temperatures between 500 and 700 °C. In this context, high temperature stability coupled with long lifetime is the most important requirement for potential catalysts. Core–shell nanocatalysts address this problem, as exemplified by Lu and co-workers, who synthesized high-temperature stable iron-based core–shell nanocatalysts for ammonia decomposition (Fig. 41).³⁶⁹

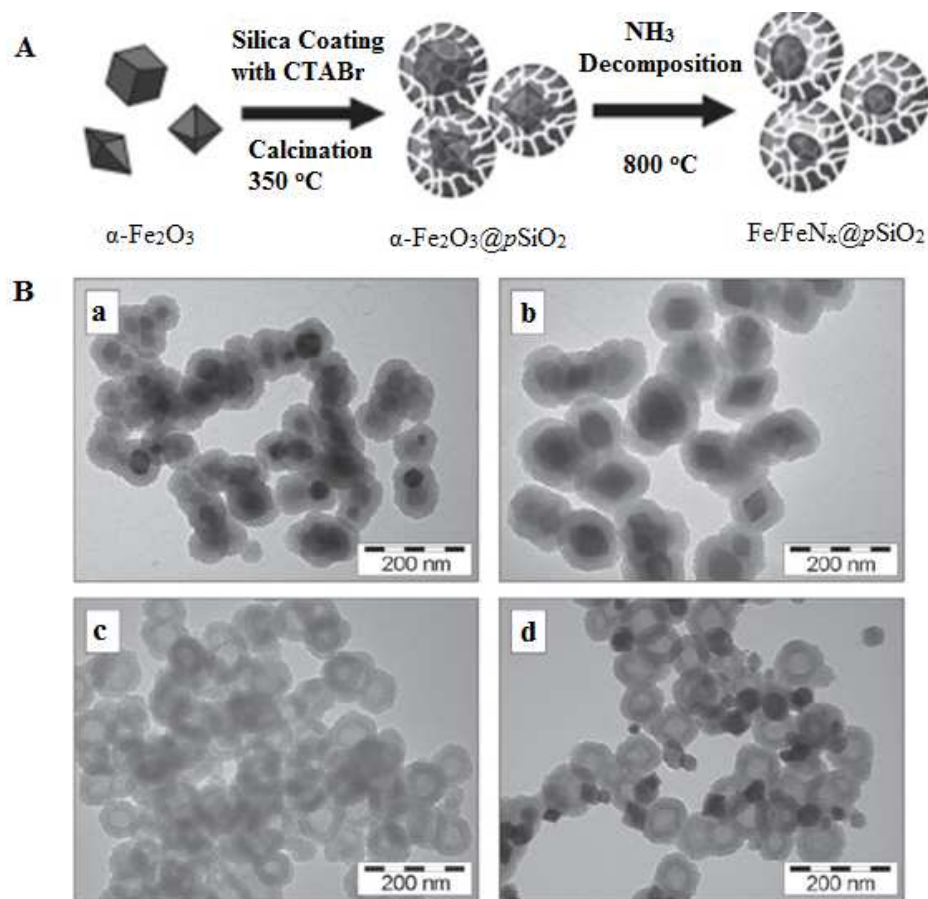


Fig. 41 (A) Schematic pathway for the synthesis and application of high temperature-stable NH_3 decomposition catalysts based on hematite NPs in a porous silica shell. (B) TEM images of (a) $\alpha\text{-Fe}_2\text{O}_3\text{-}35@p\text{SiO}_2$, (b) $\alpha\text{-Fe}_2\text{O}_3\text{-}75@p\text{SiO}_2$, (c) $@p\text{SiO}_2$, and (d) $\alpha\text{-Fe}_2\text{O}_3\text{-}50 + @p\text{SiO}_2$ after calcination, respectively. Reprinted with permission from ref. ³⁶⁹. Copyright 2011 WILEY-VCH Verlag GmbH & Co. KGaA, Weinheim.

The catalysts were found to be highly stable at $750\text{ }^\circ\text{C}$ with a space velocity of $120,000\text{ cm}^3\text{g}_{\text{cat}}^{-1}\text{h}^{-1}$ and maintained conversions of around 80% for the test period of 33 h. Furthermore, the particle size had only a limited effect on the catalytic activity for the diameter range 35–75 nm (Fig. 41). Moreover, it was noted that the cooling rate after reaction has a strong influence on the observed iron and iron nitride phases.

4.5. Tandem deprotection-Knoevenagel and Henry reaction by core–shell nanocatalysts

In addition to stabilizing catalytic groups and increasing catalyst shelf-life, some CSNs can serve as multifunctional catalyst for tandem reactions. Catalytically-active organo-functional groups can be grafted onto CSNs, as exemplified by Song and co-workers,³⁷⁰ who designed a core-shell structured mesoporous silica nanosphere with acid and basic groups in isolation from one other (Fig. 42).

The detailed synthetic method is illustrated in Fig. 42. Tetraethylorthosilicate (TEOS) and 3-mercaptopropyltrimethoxysilane (MPTMS) were self-assembled with surfactant (CTAB) templates, followed by oxidation of the thiol groups to sulfonic acid functionalities to produce acid-functionalized mesostructured silica (MS-A). The resulting material was further coated with an amino group functionalized mesoporous silica shell using TEOS and APTMS. Final removal of surfactant by an extraction procedure delivered the desired acid-base bifunctional core-shell catalyst (MS-A@MS-B) (Fig. 42A). In two cascade reaction sequences, this catalyst showed superb activity and selectivity, giving nearly quantitative yields of the desired product with no intermediate species (Fig. 42B). In addition, the bifunctional MS-A@MS-B catalyst was successfully used for performing one-pot tandem deprotection-Knoevenagel and Henry reactions (Fig. 42C).

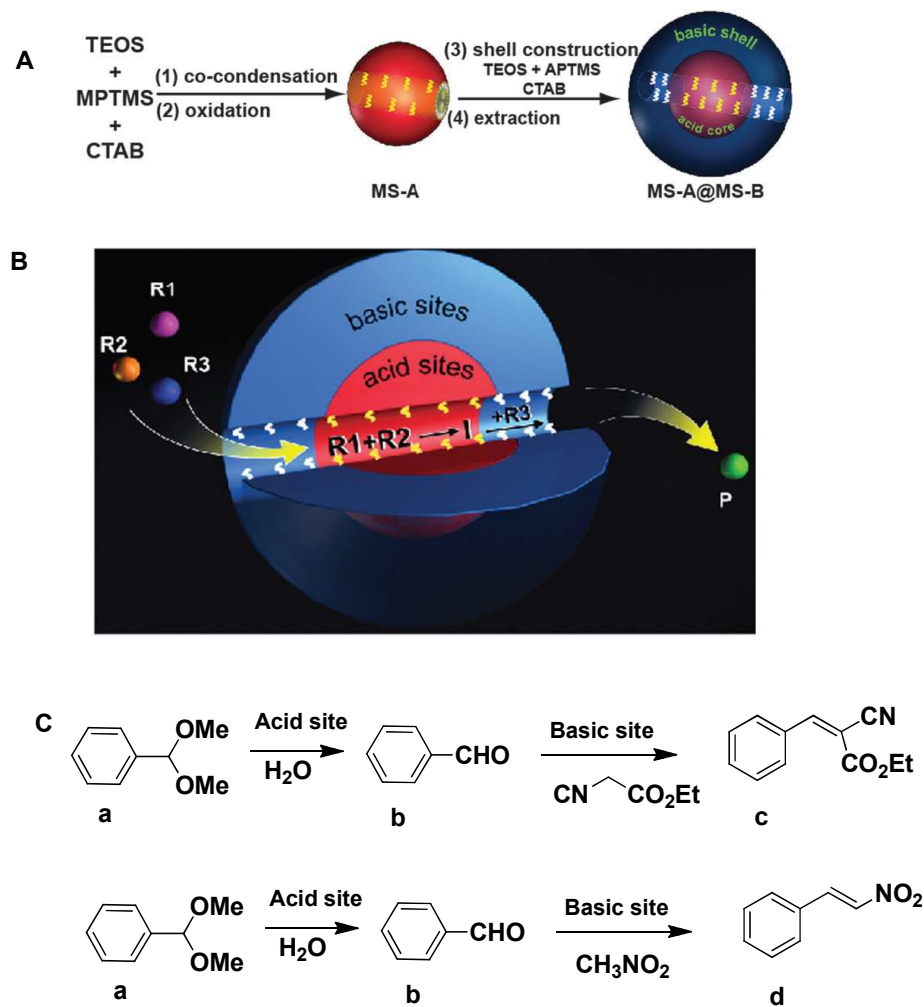


Fig. 42 (A) Synthesis procedure for acid–base bifunctional core–shell structured catalyst (yellow helix = $-\text{SO}_3\text{H}$, white helix = $-\text{NH}_2$). (B) Schematic reaction flow of the two-step cascade reaction sequences on the core–shell structured bifunctional catalyst MS-A@MS-B. (C) One-pot tandem deprotection-Knoevenagel and Henry reaction successfully catalyzed by acid–base containing MS-A@MS-B core–shell type nanocatalyst. Reprinted with permission from ref. ³⁷⁰. Copyright 2012 Royal Society of Chemistry.

4.6. CO adsorption on Pd- and Pt-based core-shell nanocatalysts

Remarkable advances in the field of CSNs have enabled nanocatalysts to be designed with unique properties, such as nanoarchitecture, composition and particle size, which can be easily adjusted in a controllable way to tune their optical, electrical, magnetic and catalytic properties.^{288, 371, 372} All-metal core-shell colloids, especially Au-, Pd-, and Pt-based core-shell colloids, with controlled shapes are attractive due to their excellent optical and catalytic activities. Among these, Au@Pd, Au@Pt, Pt@Pd, and Pd@Pt CSNs have been shown to exhibit superior catalytic properties generally not attainable by their monometallic counterparts.^{122, 373, 374}

Gorte and co-workers have reported a synthetic procedure involving self-assembly for generating novel CSN catalysts for CO chemisorption with optimized Pt and Pd cores and CeO₂, ZrO₂, and TiO₂ shells and showing excellent dispersity in organic solvent medium (Figure 43a).³⁷⁵ Previously, the same group prepared dispersible Pd@CeO₂ NPs, by reaction of a cerium alkoxide with Pd NPs stabilized by 11-mercaptoundecanoic acid, in which Ce species self-assembled on the surface of the particles.³⁷⁶

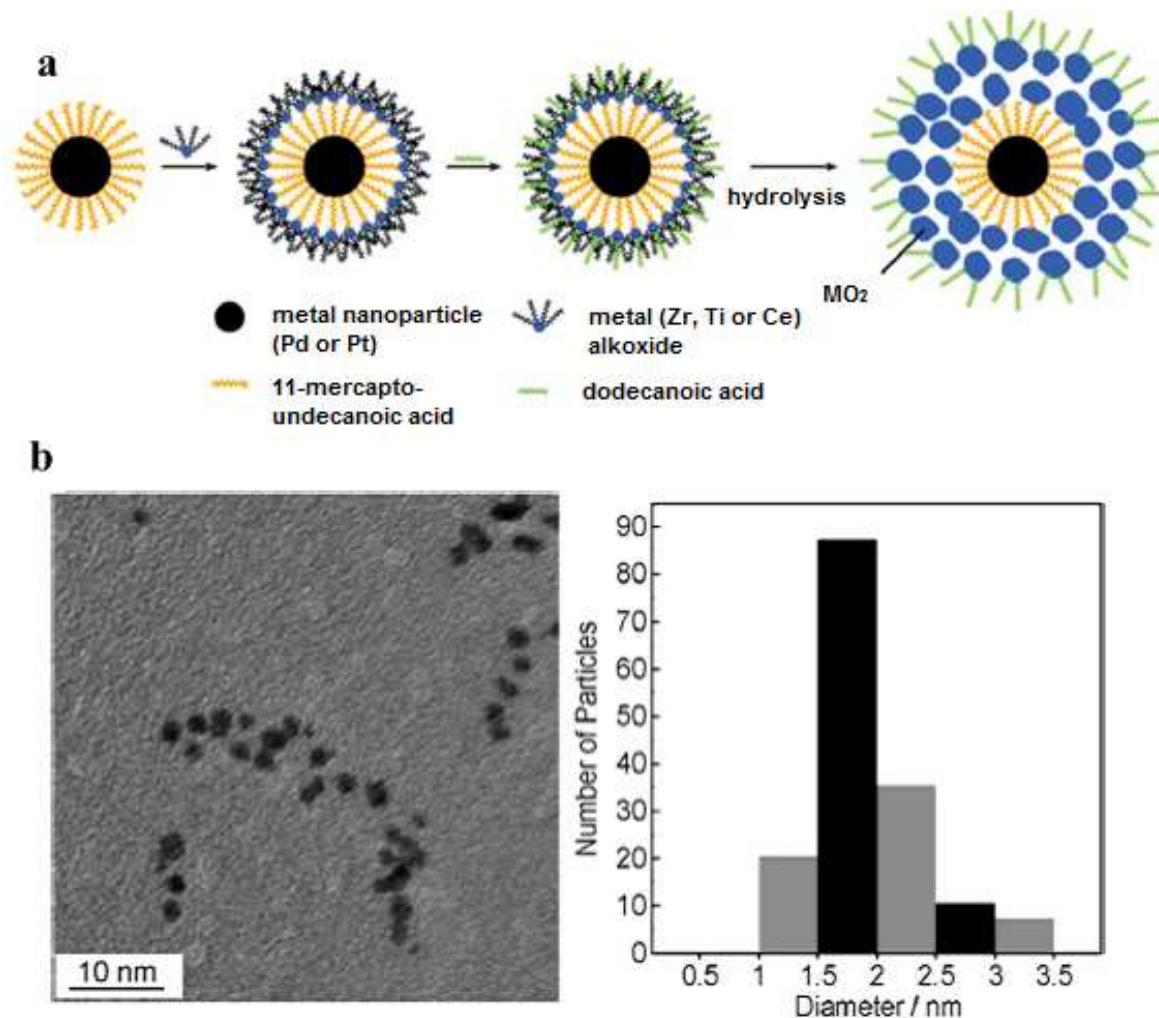


Fig. 43 (a) Schematic of the procedure used for synthesizing M@oxide nanostructures. (b) Representative TEM image of dodecylamine-protected Pt NPs (left), along with a histogram indicating particle size distribution (right). Reprinted with permission from ref. ³⁷⁵. Copyright 2012 WILEY-VCH Verlag GmbH & Co. KGaA, Weinheim.

5

TEM study revealed that the core of the NPs was approximately 2 nm in diameter and decorated by amorphous oxide shells (Fig. 43b);³⁷⁵ these particles adsorbed onto inert supports and served as heterogeneous nanocatalysts. The interaction between the different metals and the reducible shells was undoubtedly the key factor affecting the activity as well as stability of the core-shell catalysts. The adsorption of CO uptake was quantitatively performed by volumetric adsorption measurements on samples after they had been oxidized and reduced under conditions identical to those employed in the diffuse reflectance infrared Fourier transform spectroscopy (DRIFTS) experiments (Table 3).

Table 3. CO chemisorption promoted by CSNs containing Pd/Pt NPs.

Sample	Pd/Pt dispersion (%)
1 wt% Pd/Al ₂ O ₃	32
1 wt%Pd@9 wt % CeO ₂ /Al ₂ O ₃	10
1 wt%Pd@9 wt % TiO ₂ /Al ₂ O ₃	16
1 wt%Pd@9 wt % ZrO ₂ /Al ₂ O ₃	17
1 wt%Pt@9 wt % CeO ₂ /Al ₂ O ₃	6
1 wt%Pt@9 wt % TiO ₂ /Al ₂ O ₃	17
1 wt%Pt@9 wt % ZrO ₂ /Al ₂ O ₃	18

The CO adsorption uptake was measured on Pt@CeO₂/Al₂O₃ and Pd@CeO₂/Al₂O₃ CSNs after raising the reduction temperature to 673 K prior to chemisorption of CO at room temperature. After raising the reduction temperature from 423 to 673 K, dispersion of the Pd@CeO₂/Al₂O₃ core-shell nanocatalysts decreased considerably from 12 to 5% (Table 4). Re-oxidation of the Pd@CeO₂/Al₂O₃ CSNs and subsequent reduction at 423 K again decreased the dispersion considerably to 10%, signifying that the oxidizing treatment partially restored the initial dispersion. In contrast, for Pt@CeO₂/Al₂O₃, there was no loss in CO uptake upon increasing the reduction temperature. Rather, the calculated dispersion actually increased slightly from 6 to 8%. Oxidizing the Pt@CeO₂/Al₂O₃ core-shell nanocatalysts, followed by subsequent reduction at 423 K restored the initial metal dispersion, suggesting that Pt@CeO₂/Al₂O₃ is considerably less susceptible towards deactivation following the reduction-oxidation process. The interaction between the reducible shells and different metals certainly appears to be an overbearing factor affecting the stability of these core-shell nanocatalysts.

Table 4. Metal dispersion based on CO uptake at RT.

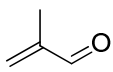
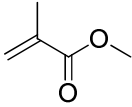
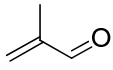
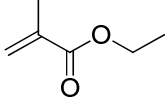
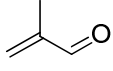
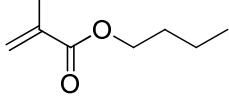
Sample	1st Reduction at 423 K	2nd Reduction at 423 K	3rd Reduction at 423 K
1 wt%Pd@9 wt % CeO ₂ /Al ₂ O ₃	12	5	10
1 wt%Pt@9 wt % CeO ₂ /Al ₂ O ₃	6	8	6
1 wt%Pd@9 wt % ZrO ₂ /Al ₂ O ₃	18	11	17
1 wt%Pt@9 wt % ZrO ₂ /Al ₂ O ₃	18	14	19

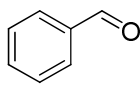
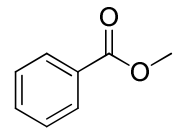
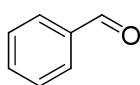
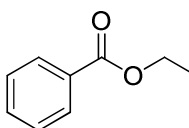
4.7. Aerobic oxidative esterification by AuNiO_x/SiO₂-Al₂O₃-MgO catalysts

Esterification is one of the most common transformations in organic synthesis.³⁷⁷ The oxidative esterification of aldehydes with alcohols is a useful route for the synthesis of esters because aldehydes as raw materials are readily available on a commercial scale.

Suzuki and co-workers have investigated AuNiO_x core-shell nanostructures for oxidative esterification, in which the surface of a Au NP core was covered by NiO_x.³⁷⁸ The oxidative esterification of methacrolein with methanol to form methyl methacrylate was performed on supported gold-nickel oxide (AuNiO_x) NPs as the catalyst and molecular oxygen as the terminal oxidant. Various types of supports, such as SiO₂-Al₂O₃ and SiO₂-TiO₂, were explored for the esterification of aldehydes by alcohols, and the best yield was obtained for AuNiO_x/SiO₂-Al₂O₃-MgO catalysts.³⁷⁸ The reaction scope was studied using different aldehydes and alcohols under optimized conditions (Table 5).

Table 5. AuNiO_x-catalyzed aerobic oxidative esterification of aldehydes with alcohols with AuNiO_x/SiO₂-Al₂O₃-MgO catalysts.^a

Entry	Aldehyde	Alcohol	Product	Conversion/Selectivity (%) ^b
1		Methanol		62/98
2		Ethanol		11/97
3		n-butanol		15/97

4		Methanol		61/97
5		Ethanol		10/97

^aReaction conditions: aldehyde (15 mmol), AuNiO_x/SiO₂-Al₂O₃-MgO (Au: 0.1 mol%) in alcohol (10 mL), O₂/N₂ (7:93 (v/v), 3 MPa) at 80 °C for 1 h. ^bDetermined by GC.

The distribution of AuNiO_x NPs was precisely controlled to avoid any loss of metal during these reactions. The AuNiO_x layer was sharply localized to a region 10 μm deep from the catalyst surface layer (Fig. 44).

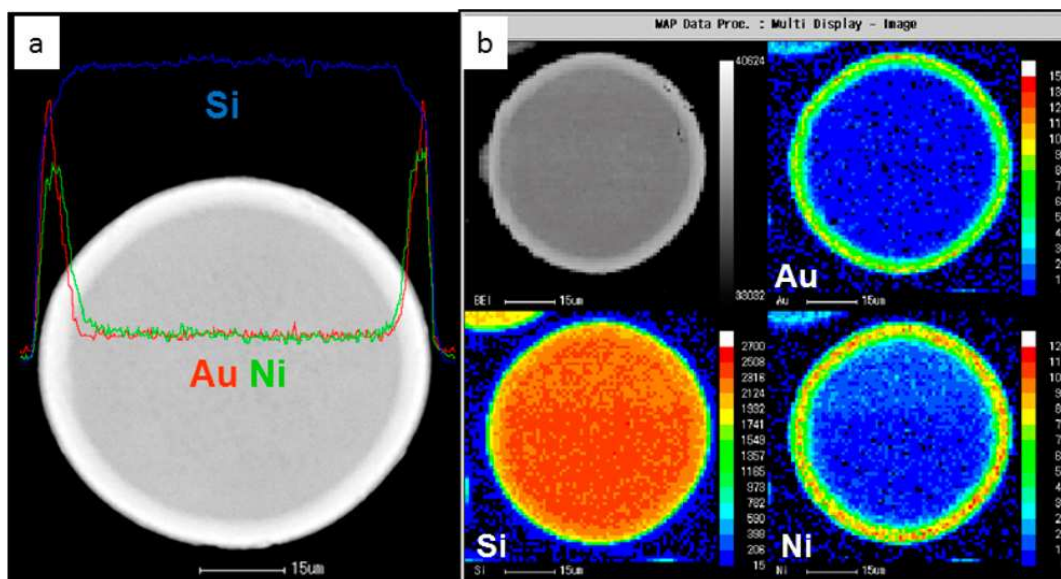


Fig. 44 Electron-probe microanalysis spectra of a single particle of AuNiO_x/SiO₂-Al₂O₃-MgO. (a) Secondary electron image and line analysis. (b) Color mapping display corresponding to the concentration of the element distribution. Reprinted with permission from ref. ³⁷⁸. Copyright 2013 American Chemical Society.

4.8. Catalytic applications of Al₂O₃@Fe₂O₃ CSNs for the synthesis of adipic acid

Adipic acid is one of the most widely used dicarboxylic acids in the chemical industry.³⁷⁹ The most common industrial process for its synthesis involves nitric acid oxidation of cyclohexanol or cyclohexanol-cyclohexanone mixtures.³⁸⁰ However, in this process, production of nitrous oxide (N₂O) as an unavoidable chemical waste contributes significantly to global warming. Bhaumik and co-workers have reported mesoporous, crystalline Al₂O₃@Fe₂O₃ CSNs *via* a new synthetic approach in aqueous medium³⁸¹ utilizing the negative charges on the surface of γ-Al₂O₃ for the

formation of the CSNs. TEM images and the BET surface area analysis support the mesoporosity in the materials (Fig. 45). These $\text{Al}_2\text{O}_3@\text{Fe}_2\text{O}_3$ CSNs acted as a Fenton catalyst in the presence of hydrogen peroxide, and displayed high catalytic activity for the one-step conversion of cyclohexanone to adipic acid in an environmentally greener aqueous reaction medium.

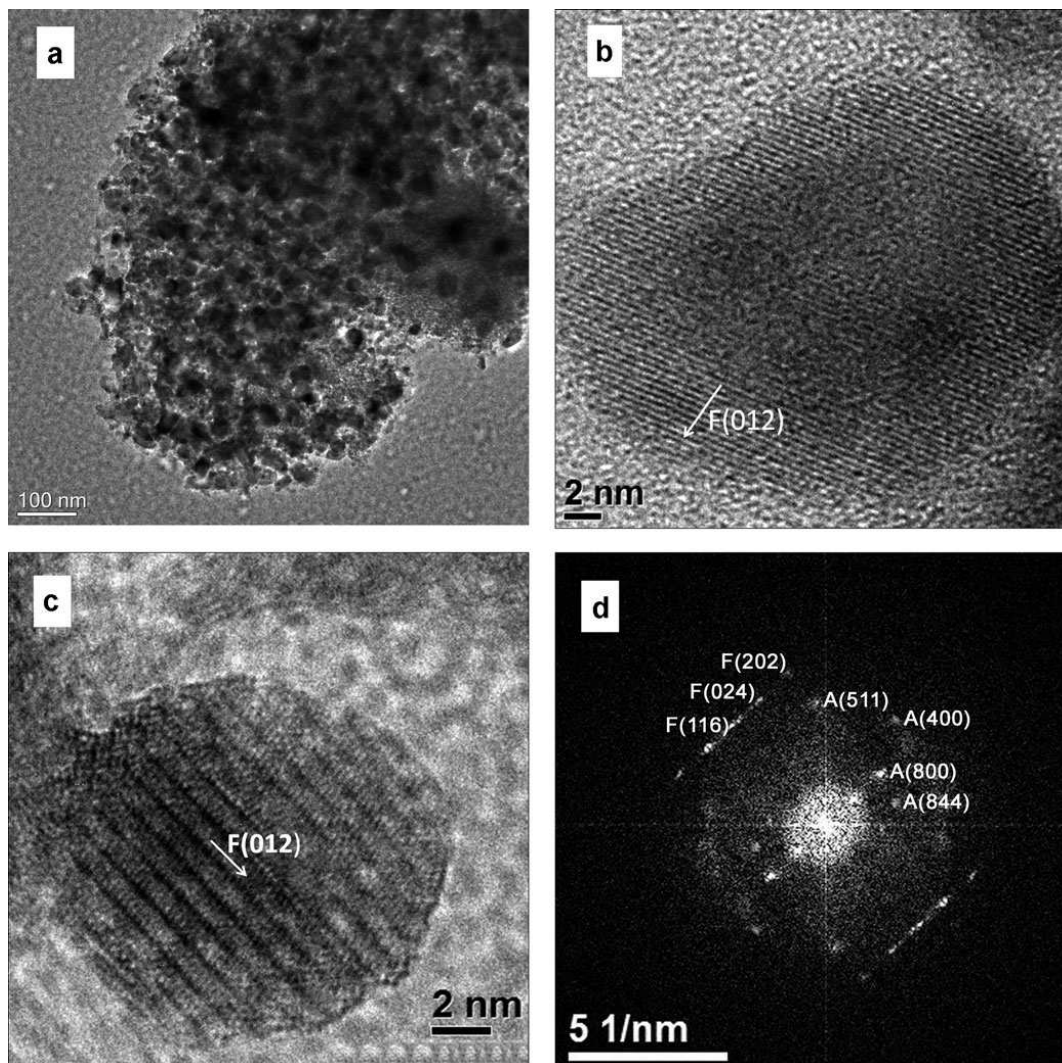


Fig. 45 TEM images of (a) self-assembled $\text{Al}_2\text{O}_3@\text{Fe}_2\text{O}_3$ CSNs, and (b), (c) single particles. In (b), a peripheral $\alpha\text{-Fe}_2\text{O}_3$ layer and (012) lattice fringes are clearly seen. The FFT pattern of (c) is shown in (d). Reprinted with permission from ref. ³⁸¹. Copyright 2013 WILEY-VCH Verlag GmbH & Co. KGaA, Weinheim.

5

4.9. Heterogeneously exposed core-shell $\text{Pt}@\text{TiO}_2$ catalysts

A simple method for the synthesis of heterogeneous exposed core-shell catalyst array has been reported using the space specificity of an embodied micelle.³⁸² The particular chemical sources for the core and shell were deposited selectively at specific regions on the embodied
 15 micelles with the help of chemical treatment (Fig. 46).

The catalyst was prepared by spin coating 0.5% micelle solution (polystyrene-block-poly(4-vinylpyridine) (PS-b-P4VP) in toluene on a silicon wafer, followed by immersing the silicon wafer in methanol at room temperature for 10 h, which generated embodied micelles with distinct core and shell regions. This arrangement allowed the catalyst to act as photocatalyst for water splitting; micelles are commonly used materials for thin film processes³⁸³ and they allow NPs to be produced with varied compositions^{384, 385} that can be deposited on various substrates.³⁸⁶ Additionally, a heterogeneous Pt–TiO₂ catalyst array was also developed to permit facile fabrication of a catalyst for efficient hydrogen generation through photocatalytic water decomposition.

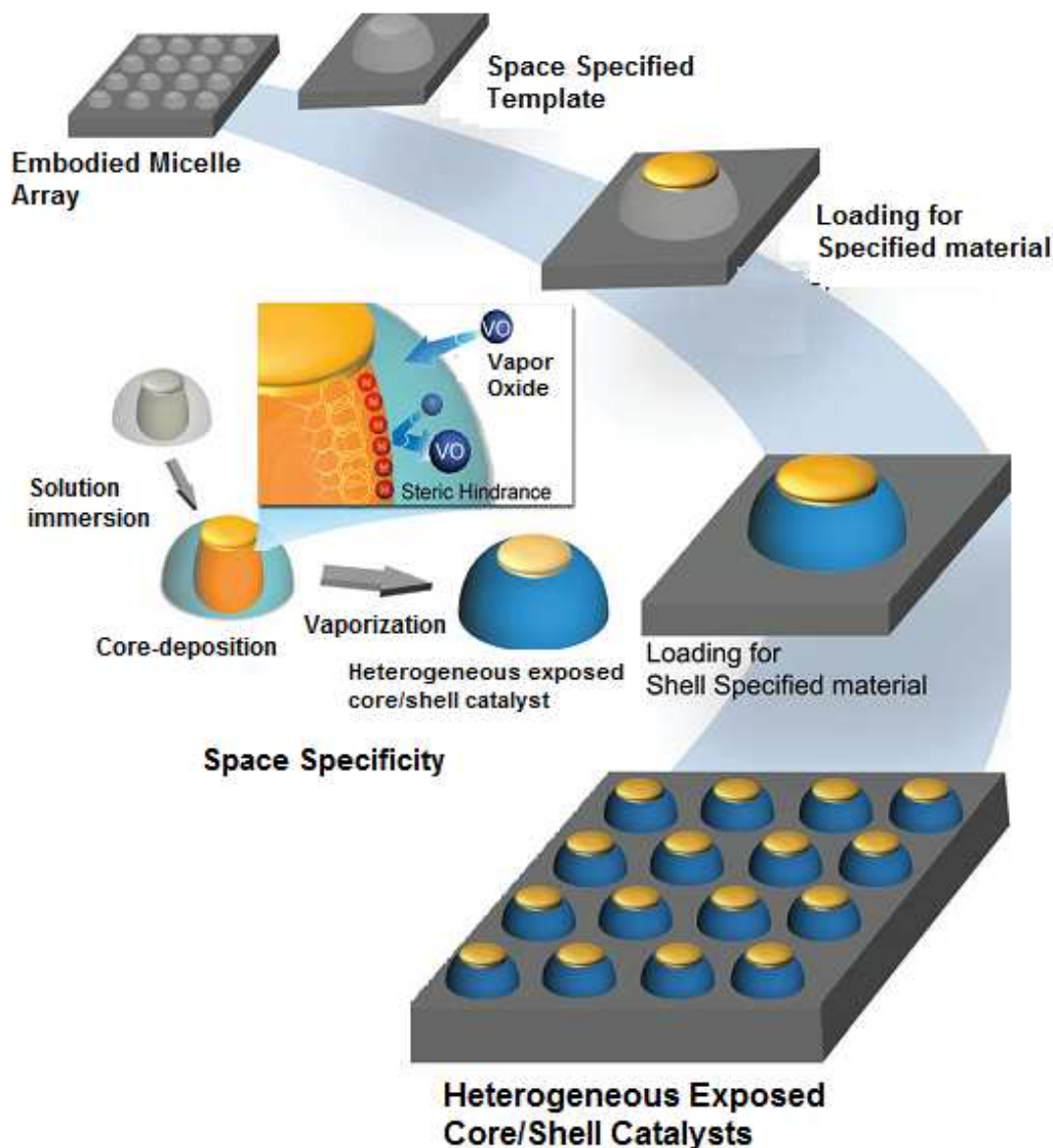


Fig. 46 Schematic of the synthesis of heterogeneous exposed core–shell catalysts using space specificity. The inset diagram shows the principle of space specificity. Reprinted with permission from ref. ³⁸². Copyright 2013 Royal Society of Chemistry.

5. Electrocatalysis by core–shell nanocatalysts

Noble metal-based catalysts are widely employed for various electrochemical transformations and energy conversion, enabling technologies such as water electrolyzers, fuel cells and metal–air batteries to be developed.^{387,388} As mentioned earlier, some of the main synthetic methodologies employed for the synthesis of core–shell materials include dendrimer encapsulation,³⁸⁹ sol-gel synthesis,³⁹⁰ as well as colloidal and reverse micelle methods.³⁹¹ Energy conversion using electrocatalysts plays an important role in the design and improvement of cost-effective benign technologies that alleviate global warming and over-dependence on fossil fuels. In this regard, polymer electrolyte membranes containing fuel cells (electrochemical energy-conversion devices) can act as convenient power sources in the transportation sector, one of the principal consumers of fossil fuels and emitters of greenhouse gases.

The optimum catalytic activity of these materials can be tuned by controlling their size, structure, and composition for a specific catalytic reaction.^{392, 393} The electrocatalytic activity of such catalyst depends on its synergistic interactions between the core and shell, primarily involving (a) ligand effects, which affect charge transfer between the components, (b) ensemble effects, which govern the material's adsorption due to the presence of distinct atomic groups, and finally (c) geometric effects, which depend on three dimensional structural characteristics.³⁹⁴ Based on the type, core–shell catalysts have been used in many areas of electrocatalysis, such as ORR (oxygen reduction reaction), OER (oxygen evolution reactions), alcohol oxidation, *etc.*;^{287, 395-416} some recent examples of core–shell based catalysts are discussed below.

Platinum metal is the single best metal catalyst for the ORR at low temperature in polymer electrolyte membrane (PEM) fuel cells in both, alkaline and acid electrolytes.⁴¹⁷⁻⁴¹⁹ To increase the reaction rate, several bimetallic electrocatalysts composed of Pt and 3d-transition metals (Fe, Co, Ni,) have been examined.^{401, 420-425} Adzic and co-workers have investigated PtNiN core–shell catalysts with a low Pt content shell and inexpensive NiN core and showed that they displayed excellent electrocatalytic activity and stability for the ORR.⁴²⁶ The catalysts were synthesized by chemical reduction and subsequent thermal annealing in N₂, wherein NH₃ was used as a nitrogen precursor at ambient pressure. High angle annular dark-field (HAADF) images of the materials revealed the core–shell structure of the NPs (Fig. 47). By overlapping the two-dimensional mapping of Pt and Ni in EELS signals from a single NP, as shown in Fig.47a (dotted lines), the core–shell structure of the materials was confirmed. The EELS line scan profile defined the distribution of Pt and Ni components in a representative single NP, enabling the Pt shell thickness to be directly measured (Fig. 47c).

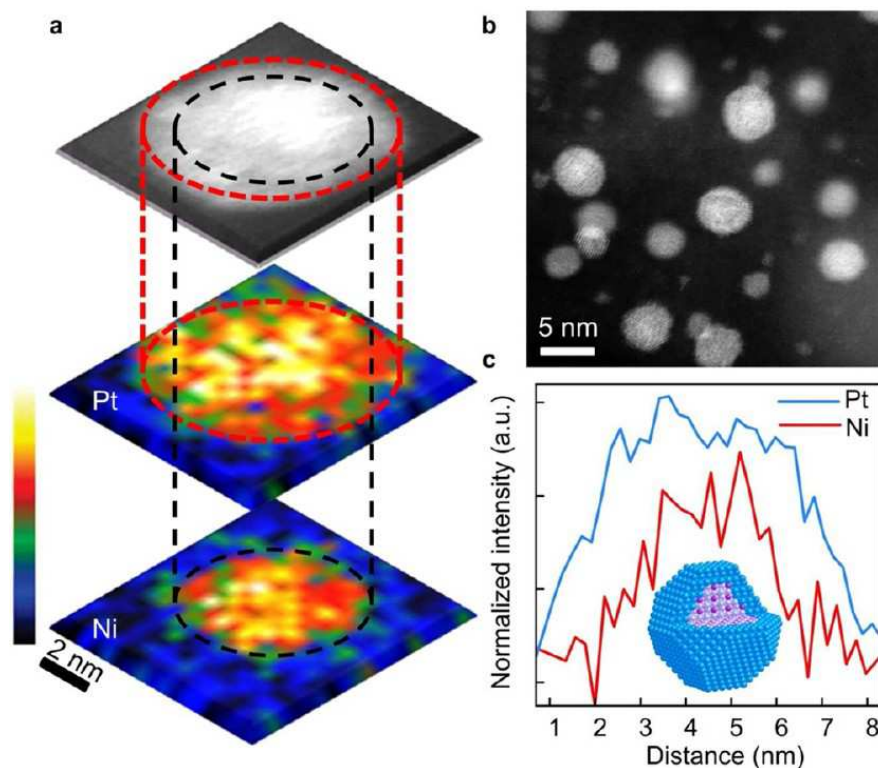


Fig. 47 (a) HAADF-STEM image of a PtNiN CSN with corresponding two-dimensional EELS mapping of Pt M and Ni L signals (dotted lines for visualization purposes only). (b) STEM image of PtNiN CSNs. (c) EELS linescan profiles of Pt and Ni and schematic of a single PtNiN NP (blue, Pt; gray, Ni; purple, N). Reprinted with permission from ref. ⁴²⁶. Copyright 2012 American Chemical Society.

The presence of N atoms in the core allowed facile diffusion of interacted Pt from the inner shells to the surface, filling the vacancy sites (geometric effect), resulting in augmented durability of the catalysts (Fig. 48).

10

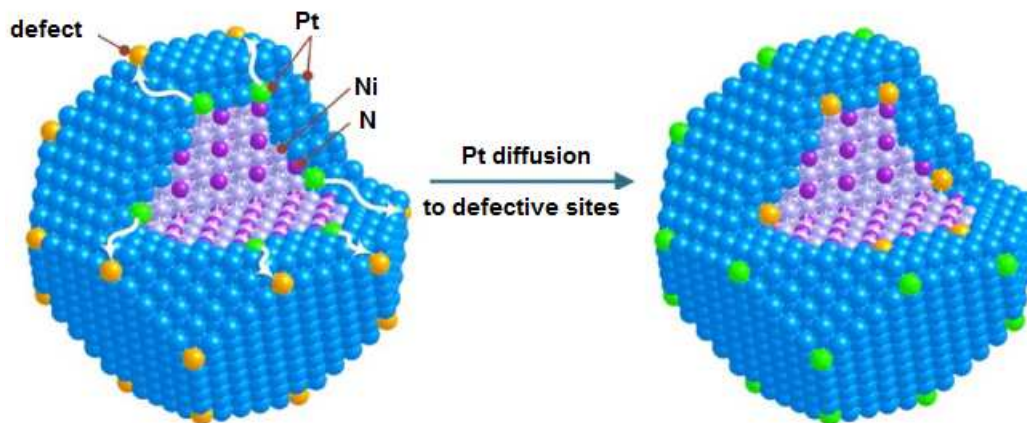


Fig. 48 Schematic of the inner Pt diffusion process to the defective sites at the vertex during cycling in electrolyte. For clarity, the inner Pt atoms involved in diffusion are shown in green, whereas defects are in yellow. Reprinted with permission from ref. ⁴²⁶. Copyright 2012 American Chemical Society.

5 Electrochemistry and DFT methods revealed that the high ORR activity and durability of the PtNiN catalyst can be attributed to the Ni nitride core, which influences the behavior of the Pt shell by inducing both geometric and electronic effects, thus controlling the catalytic activity.⁴²⁶ The same group used a surfactant-free, ethanol-aided, wet chemical synthetic approach to coat Pd NPs with uniform Pt atomic layers on a carbon support.⁴²⁷ The monolayer deposition was carried
10 out during the oxidation of ethanol catalyzed by the core NPs. Subsequent reduction of $[\text{PtCl}_6]^{2-}$ ions to Pt atoms allowed the formation of atomic Pt layers; the reducing power of ethanol was tunable by adjusting the temperature, H_2O , and pH. Table 6 summarizes the ORR activities for Pd@Pt_{ML} and Pd@Pt_{2ML} samples fabricated *via* the ethanol-based approach as compared with those for Pd@Pt_{ML} fabricated *via* Cu under potential deposition. The smooth Pt surface obtained at 70 °C
15 was responsible for a smaller electrochemical surface area (ECSA) than that obtained at room temperature owing to high coordination sites on smooth terraces (less reactive to H adsorption/desorption) rather than low coordination sites on a roughened surface with edges and defects.

20 **Table 6.** Mass activities (MA) and specific activities (SA) for PtML samples synthesized by either ethanol-based approach or by Cu underpotential deposition (UPD), derived from the ORR kinetic currents at 0.9 V *vs* reversible hydrogen electrode (RHE).⁴²⁷

Samples	Pd@Pt _{ML} Cu UPD	Pd@Pt _{ML} ethanol	Pd@Pt _{2ML} ethanol
Pt/(Pt + Pd) (at. %)	26.9	27.3	33.3
Pt (wt. %)	16.5	17.1	18.1
Pd (wt. %)	24.5	24.9	19.7
MA _{Pt} (A mg ⁻¹) ^a	0.62	0.64	0.62
MA _{PGM} (A mg ⁻¹) ^b	0.25	0.26	0.30
SA (mA cm ⁻²) ^c	0.25	0.58	0.70
ECSA (m ² g ⁻¹) ^d	191	110	89

^a MA_{Pt}, mass activity normalized by the mass of Pt. ^b MA_{PGM}, mass activity normalized by the
25 mass of Pt-group metals (PGM). ^c SA, specific activity normalized by the ECSA. ^d ECSA, electrochemical surface area.

Ge *et al.* have synthesized composition-controlled bimetallic catalysts containing Pt as a shell and Cu as a core by electrochemically dealloying a bulk Pt₁₅-Cu₈₅ (at. %) binary alloy using a potential-controlled approach.⁴²⁸ Dealloying at 0.4, 0.5, 0.6 and 0.7 V yielded bimetallic Pt-Cu catalysts with chemical compositions of Pt₄₈Cu₅₂, Pt₅₅Cu₄₅, Pt₆₇Cu₃₃ and Pt₁₀₀Cu₀, respectively. The Pt/Cu ratio of the dealloyed nanoporous catalyst could readily be adjusted over a wide composition range by simply controlling the dealloying potential. The thickness of the Pt shell was dependent on the potential cycles. The prepared catalyst was well characterized by aberration corrected scanning transmission electron microscopy (STEM) equipped with electron energy-loss spectroscopy (EELS), the results of which are shown in Fig. 49. The resulting material was used as an electrocatalyst for the electrochemical oxidation of formic acid and its catalytic activity was compared with a commercial Pt/C catalyst in 0.1 M HClO₄ solution media. The dealloyed Pt-Cu sample containing ≈ 67.2% Pt exhibited voltammetric behavior very similar to that of the Pt/C catalyst, *i.e.*, hydrogen adsorption/desorption at 0.03–0.4 V, the electrochemical double layer at 0.4–0.6 V and the formation of Pt oxides and their reduction at 0.6–1.2 V vs RHE.

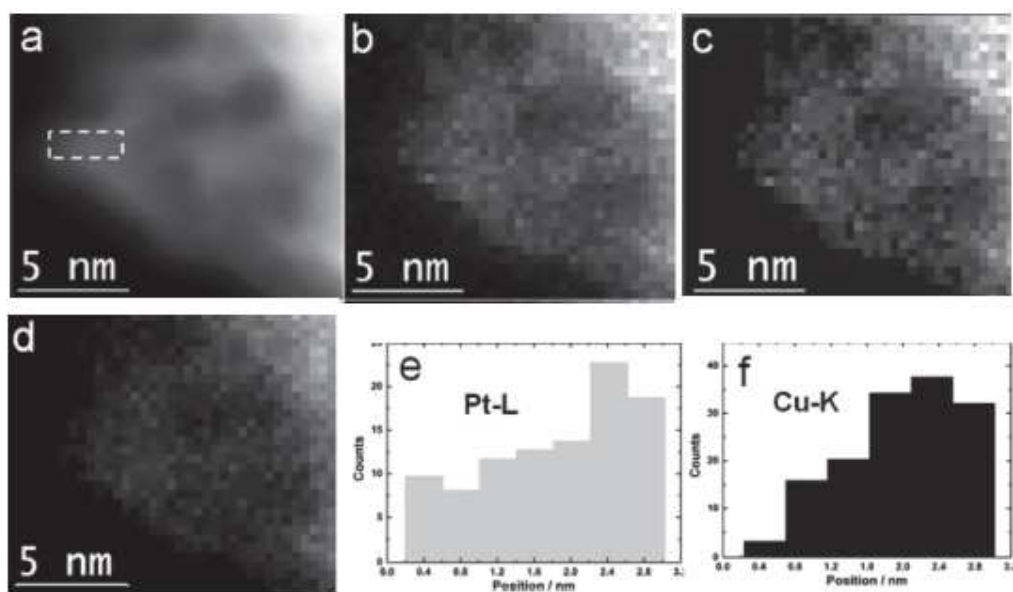


Fig. 49 STEM image and EDS elemental maps of the dealloyed Pt-Cu ligament: (a) HAADF-STEM image of the nanoporous structure; (b) mixed STEM-EDS elemental mappings of Pt-L & Cu-K; (c) elemental mapping of Pt-L; and (d) elemental mapping of Cu-K. The composition intensity profile of (e) Pt and (f) Cu were taken from the labeled region in (a). Reprinted with permission from ref. ⁴²⁸. Copyright 2013 WILEY-VCH Verlag GmbH & Co. KGaA, Weinheim.

Bimetallic IrCu NPs have been synthesized and used as a core for a Pt monolayer electrocatalyst.⁴²⁹ The CSNs were prepared by dissolving IrCu alloy, which ultimately resulted in a relatively Ir-rich shell. Partial removal of the surface Cu by dealloying greatly increased the mass activity and specific activity of the catalyst. It was suggested that these IrCu particles may have a controlled Pt monolayer, leading to a downshift of the d-band center with respect to the Fermi level. The altered electronic and geometric effects due to the IrCu core were compared to pure Ir enhanced ORR activities and an augmented stability for the Pt_{ML}IrCu core-shell electrocatalyst was obtained.

IrNi@IrO_x NPs were also prepared in an analogous manner, using IrNi_x as precursor alloy by selective surface dealloying of Ni and controlled surface oxidation of Ir. These metal-oxide hybrid (M₁M₂@M₁O_x) core@shell NPs were used as an electrocatalyst for the OER; a 3-fold higher catalytic activity was observed for the electrochemical OER over benchmark catalysts (IrNi@IrO_x metal oxide core-shell). Furthermore, the noble-metal content of the catalysts could be lowered without compromising the catalytic activity of the materials⁴¹¹ and the general synthetic approach could be adapted to make a range of other noble metal NPs for catalysis.

In another recent report, a Au@Co₃O₄ core-shell nanocatalyst with uniform overall particle size and shell thickness was synthesized by adjusting the amount of OAm and OA ligands (Fig. 50). The resulting material showed a very strong synergistic effect between the core and shell. Specifically, the Co₃O₄ shell in Au@Co₃O₄ displayed strong binding to oxygen due to its Co atoms, which are known active centers for the OER. The nanocatalyst was shown to catalyze the OER, giving an overpotential value of 0.35 V. The Au@Co₃O₄ NCs gave a 7 times higher current density in the OER than a Au and Co₃O₄ NC mixture or Co₃O₄ NCs alone and 55 times higher than Au NCs alone (Fig. 51). A stable overpotential of only 0.31 V was needed for Au@Co₃O₄ to achieve a current density of 10 A g_{catalyst}⁻¹.⁴³⁰

25

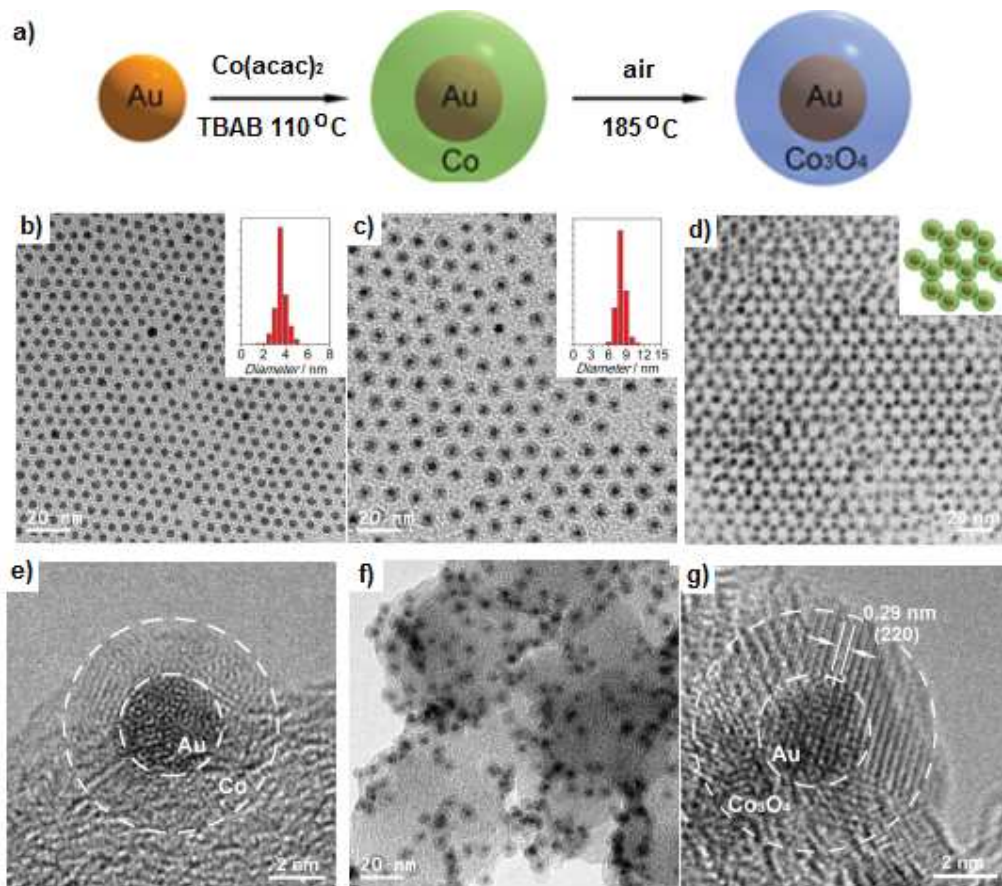


Fig. 50 (a) Scheme showing the synthetic route for Au@Co₃O₄ core-shell NCs. (b) TEM image of Au NCs (inset: histogram of the size distribution). (c) TEM image of Au@Co NCs (inset: histogram of the size distribution). (d) TEM image of a two-layer array of the Au@Co NCs (inset: modeled projection of the two-layer NC assembly). (e) HRTEM image of a single Au@Co NC. (f) TEM image of Au@Co₃O₄ NCs supported on carbon. (g) HRTEM image of a single Au@Co₃O₄ NC. Reprinted with permission from ref. ⁴³⁰. Copyright 2009 WILEY-VCH Verlag GmbH & Co. KGaA, Weinheim.

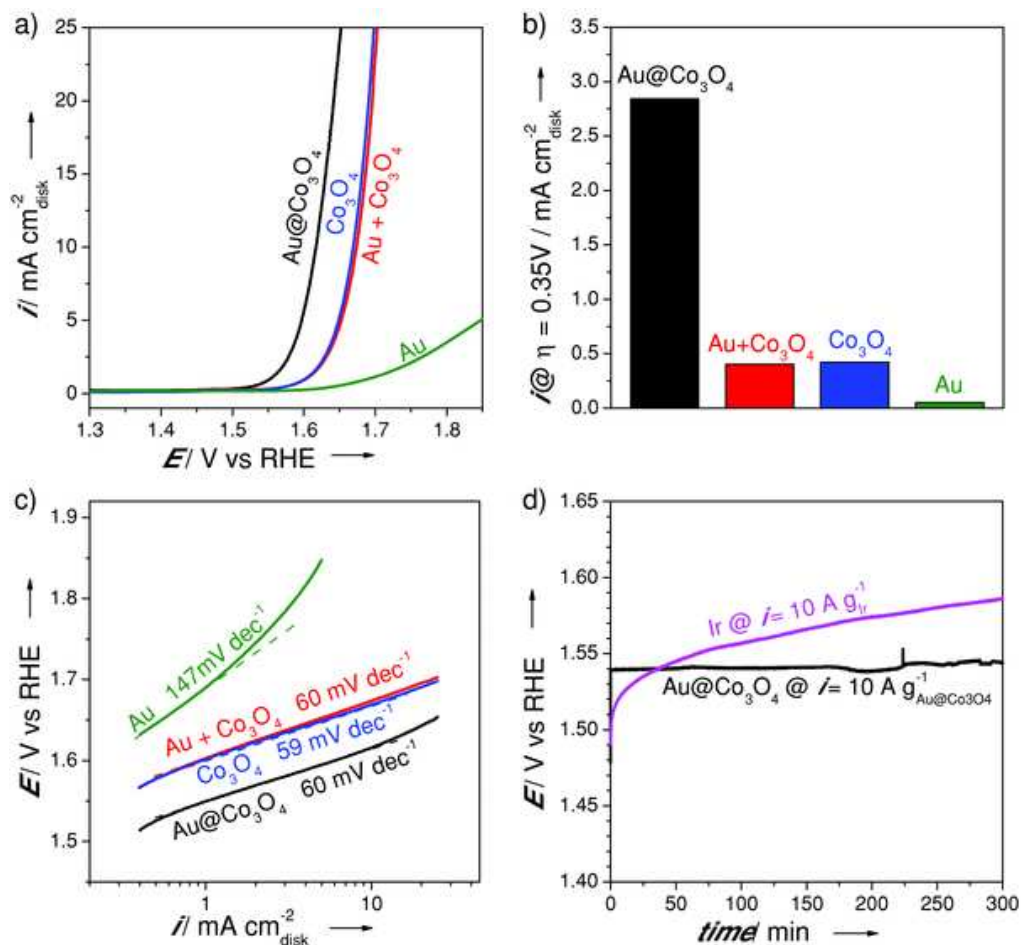


Fig. 51 (a) iR -corrected polarization curves of $\text{Au@Co}_3\text{O}_4/\text{C}$ ($64 \mu\text{g}_{\text{Au@Co}_3\text{O}_4} \text{cm}^{-2}$, in which the Au loading was $24 \mu\text{g}_{\text{Au}} \text{cm}^{-2}$ and Co_3O_4 loading was $40 \mu\text{g}_{\text{Co}_3\text{O}_4} \text{cm}^{-2}$), $(\text{Au}+\text{Co}_3\text{O}_4)/\text{C}$ ($24 \mu\text{g}_{\text{Au}} \text{cm}^{-2}$ and $40 \mu\text{g}_{\text{Co}_3\text{O}_4} \text{cm}^{-2}$), $\text{Co}_3\text{O}_4/\text{C}$ ($40 \mu\text{g}_{\text{Co}_3\text{O}_4} \text{cm}^{-2}$), and Au/C ($24 \mu\text{g}_{\text{Au}} \text{cm}^{-2}$) catalysts recorded in O_2 -saturated 0.1 M KOH at a scan rate of 5 mV s^{-1} and continuous electrode rotating speed of 2500 rpm . (b) Activity of the catalysts at an overpotential of 0.35 V . (c) Tafel plots of catalysts. (d) Chronopotentiometry curves of $\text{Au@Co}_3\text{O}_4/\text{C}$ and Ir/C ($40 \mu\text{g}_{\text{Ir}} \text{cm}^{-2}$) under a current density of $10 \text{ A g}_{\text{Au@Co}_3\text{O}_4}^{-1}$ or $10 \text{ A g}_{\text{Ir}}^{-1}$ in O_2 -saturated 0.1 M KOH . Reprinted with permission from ref. ⁴³⁰. Copyright 2009 WILEY-VCH Verlag GmbH & Co. KGaA, Weinheim.

10

Wang *et al.* have investigated the effect of synthetic parameters on a Pd-Pt core-shell catalyst by STEM analysis and their electrocatalytic activity for the ORR;⁴³¹ effects of the thickness of the Pt shell, lattice mismatch and particle size on the specific and mass activities originating from changes in the effective surface area were discussed. The prepared core-shell structure was characterized at an atomic level using Z -contrast scanning transmission electron microscopy coupled with element-sensitive electron energy loss spectroscopy (Fig. 52a-f). The total number of

atoms in the column, the square of their average atomic number (Z^2), was determined based on brightness reflecting into enhanced HAADF intensity. Coupling element-sensitive EELS with HAADF images offered an alternate means for determining the thickness and uniformity of the Pt shells (Fig. 52g-h). The enhanced catalytic activity was attributed to the effect of nanosize-induced surface contraction on the facet-dependent oxygen binding energy.

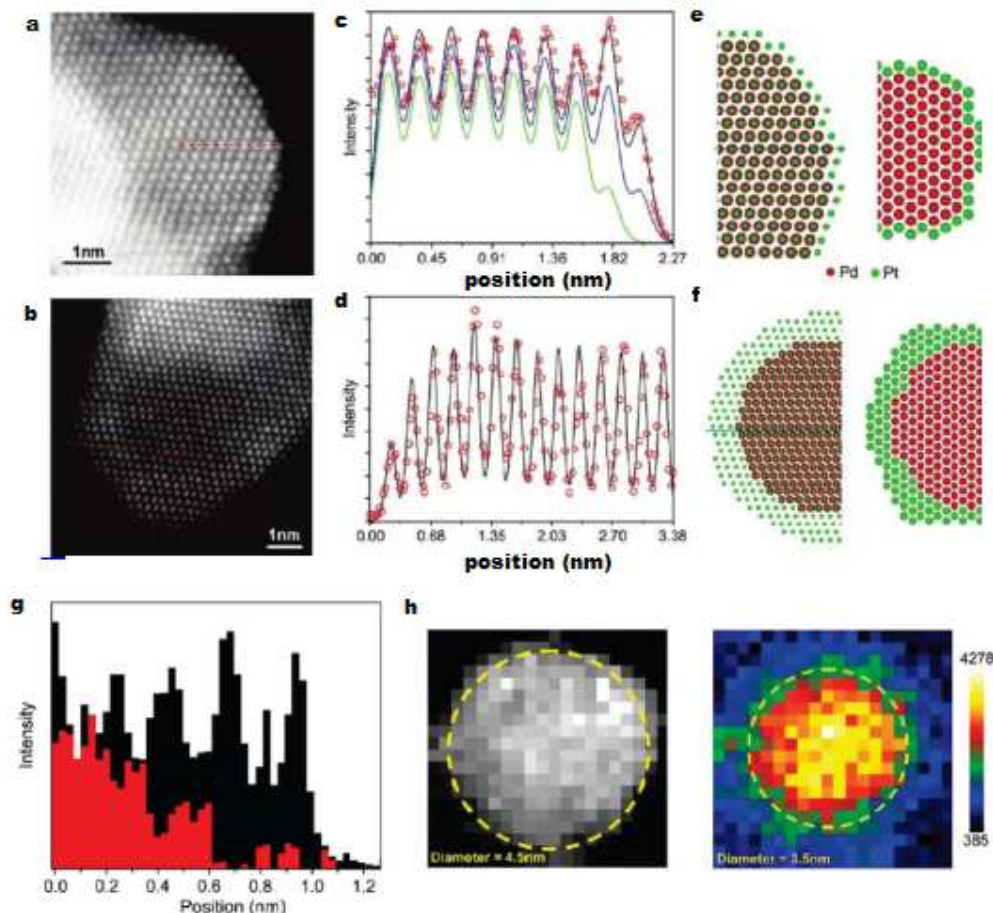


Fig. 52 (a,b) HAADF-STEM images of the Pd(core)-Pt(shell) NPs obtained for the PdCPT₁ and PdCPT₄ samples, respectively. NPs overlap on the left side in (a) and at the top in (b). (c,d) Intensity profiles (O) from the scan lines (the left ends are defined to be zero on the x -axes and the intensity at the nearby vacuum set the zero for y -axes) in (a) and (b), and the best fits (black lines), based on the structure models shown in (e) and (f) for Pd particles with 1 and 3-4 Pt surface layers, respectively. (f) Projection of the structure model with 4 Pt layers on the STEM image plane (left) and the arrangements of atoms in the vertical columns along the scan line (right); HAADF and Pd EELS intensity profiles for a PdCPT₂ sample. (g) Comparison of HAADF (black) and Pd EELS (red) intensity profiles in a line scan. (h) Two-dimensional mapping of HAADF intensity (left) and Pd EELS signal (right) obtained with 0.27 nm/pixel resolution. Reprinted with permission from ref. ⁴³¹. Copyright 2009 American Chemical Society.

Sun *et al.* have reported a facile synthetic method for making monodisperse, sub-5 nm core/shell Au/PtCu NPs by reducing platinum- and copper-acetylacetonate in the presence of 5 nm Au NP seeds and 1,2-hexadecanediol (HDD), oleylamine (OAm) and oleic acid (OA) as capping agent at 200 °C (Fig. 53a-d).⁴³² The Au core provided suitable nucleation sites for CuPt alloy formation. The interaction between the core and shell made these Au/CuPt NPs useful for ORR and methanol oxidation reaction in 0.1 M HClO₄ solution. Their specific (mass) reduction and oxidation activities reached 2.72 mA/cm² (1500 mA/mg Pt) at 0.9 V and 0.755 mA/cm² (441 mA/mg Pt) at 0.8 V (*vs* RHE), respectively (Fig. 53e and f). The existence of the Au NPs at the core suppressing the Pt usage as well as the stability of the Au/CuPt catalyst for fuel cell reactions was demonstrated.

10 The core/shell design was found to be effective for optimizing the NP catalysis.

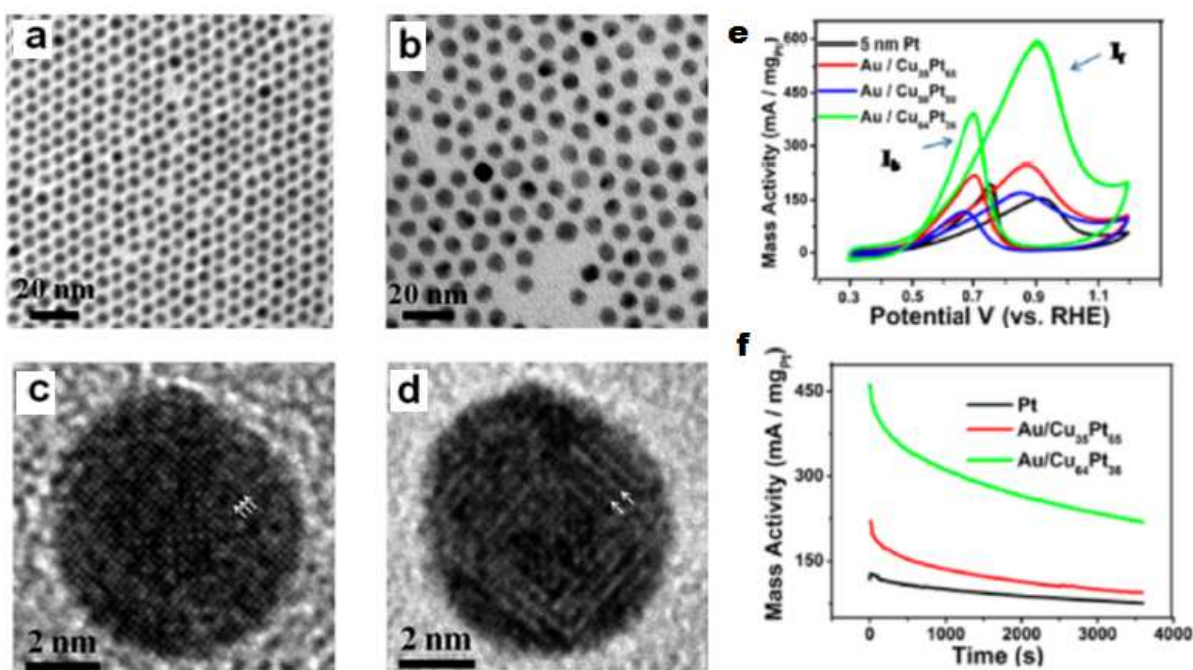


Fig. 53 TEM images of (a) 5 nm Au NPs and (b) 7.5 nm Au/Cu₃₅Pt₆₅ NPs. (c, d) HRTEM images of a single Au/Cu₃₅Pt₆₅ NP acquired at a different focus condition. Reprinted with permission from ref.⁴³². Copyright 2014 American Chemical Society.

15

A one-pot solvothermal method has been used for the preparation of reduced graphene oxide (RGO) supported hollow Ag@Pt core-shell nanospheres (hAg@Pt), using ethylene glycol (EG) as a reducing agent and sodium dodecyl sulfate (SDS) as a soft template. Control experiments showed that the molar ratios of the Pt-Ag precursors, amount of SDS, presence of RGO and reaction temperature were critical for achieving the best catalytic activity (Fig. 54). The electrocatalytic activity and durability toward ethylene glycol oxidation was enhanced using hAg@Pt-RGO, which could offer a promising potential electrocatalyst for direct alcohol fuel cells. Certain defects in RGO were suggested to be responsible for better adsorption of the OH(ads)

20

species generated from water dissociation during the electrochemical measurements. Compared to metallic nanostructures, hAg@Pt–RGO showed a higher catalytic activity for water dissociation as more OH(ads) could be adsorbed on the catalyst. Meanwhile, the well-dispersed hAg@Pt on the RGO increased the surface area and improved the electrical conductivity of the nanocomposites, providing more active sites available for EG molecules.⁴³³

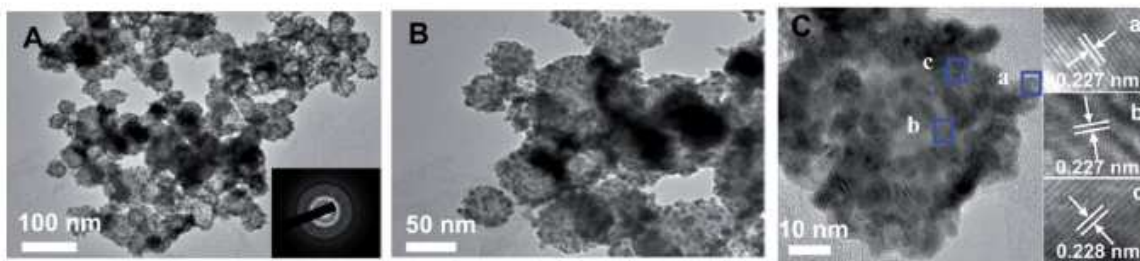


Fig. 54 (A and B) TEM and (C) HRTEM images of hAg@Pt–RGO. The inset in image (A) shows the corresponding SAED pattern. Reprinted with permission from ref. ⁴³³. Copyright 2014 Royal Society of Chemistry.

10

In another study, monodispersed core/shell Ni/FePt NPs were prepared by seed-mediated growth and subsequently converted to Ni/Pt NPs. The aforementioned NPs were washed by acetic acid to obtain active Ni/Pt catalysts and employed in the ORR. The specific activity and mass activity of 4.2/0.8 nm core/shell Ni/FePt after an acetic acid wash reached 1.95 mA/cm² and 490 mA/mgPt at 0.9 V (vs RHE). These results were much better than those obtained with a benchmark commercial Pt catalyst (0.34 mA/cm² and 92 mA/mg of Pt at 0.9 V). Cu@CuPt core@shell NWs with 1D nanostructure were also synthesized using Cu NWs as templates in organic solvent medium and they were shown to have efficient electrocatalytic activity toward the ORR.⁴³⁴

Well-defined Pt-Pd@Pd core-shell nanospheres (PtPd@Pd NSs) have been synthesized for electrocatalytic oxidation using a simple one-pot solution approach; *N*-methylimidazole and poly(vinyl pyrrolidone) (PVP) were used as directing and capping agents without application of any seed, template or organic solvent.⁴³⁵ The ORR mass activity and specific activity over the PtCu NWs were 0.216 A mg⁻¹ and 0.404 mA cm⁻² at 0.9 V, respectively, which were found to be 3.1 and 3.7 times larger than values obtained for a commercial Pt/C catalyst, respectively.⁴³⁵ According to theoretical calculations, the electronic effect of the Cu substrate on the Pt monolayer was responsible for the higher activity of PtCu NWs compared to the commercial Pt/C catalyst. Further, the PtCu NWs showed much better durability and stability compared to the commercial Pt/C.

Recently, Yung and co-workers have synthesized Pt nanostructures from submonolayer to monolayer by ion adsorption–*in situ* electrochemical reduction on Au NPs supported on multiwall carbon nanotubes (MWCNTs).⁴³⁶ The coverage of Pt on the Au surface was controlled by varying

30

the concentration of Pt(II) or by repeating the ion adsorption and electrochemical reduction process; the as-prepared Au@Pt/CNTs catalysts displayed coverage-specific electrocatalysis. Au@Pt/CNTs with low Pt coverage were shown to be inactive towards methanol oxidation but oxidized formic acid effectively through a direct pathway with mass specific activity 90 times higher than that of a commercial Pt/C catalyst. Owing to the catalyst's inertness to methanol, it showed high performance in the ORR with high methanol tolerance. However, simply increasing the Pt coverage to above 40% caused the formic acid oxidation process to proceed by both direct and indirect catalytic pathways, resulting in high methanol oxidation activity (Fig. 55). A strong relationship between the surface Pt coverage of the as-prepared Au@Pt/CNTs material and its electrocatalytic activity towards formic acid, methanol and oxygen was reported.

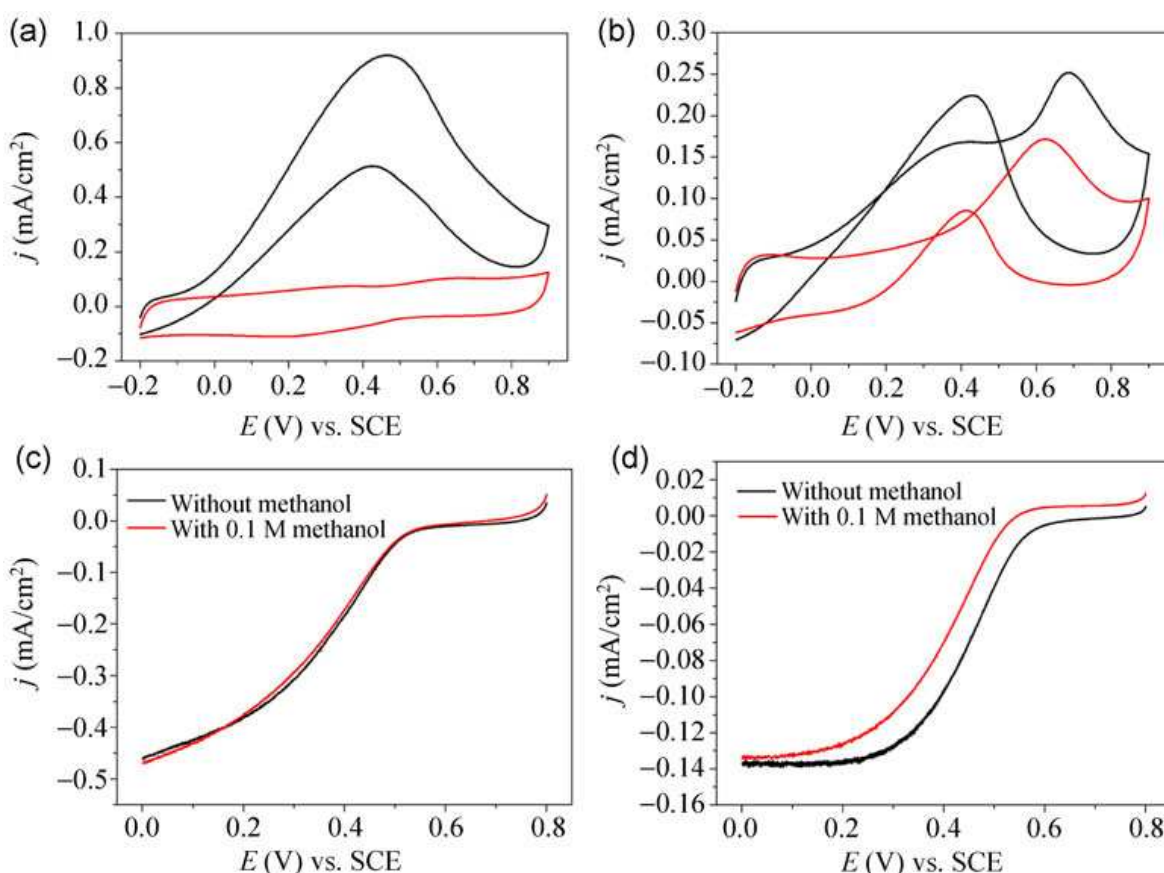


Fig. 55 (a) Cyclic Voltammograms (CVs) of Au@Pt/CNTs with 27.9% Pt coverage in 0.1 M H₂SO₄ + 0.025 M HCOOH (black line) and 0.1 M H₂SO₄ + 0.1 M methanol (red line), both recorded at 50 mV/s. (b) CVs of Au@Pt/CNTs with 57.6% Pt coverage in 0.1 M H₂SO₄ + 0.025 M HCOOH (black line) and 0.1 M H₂SO₄ + 0.1 M methanol (red line), both recorded at 50 mV/s. (c) LSVs (linear sweep voltammograms) of Au@Pt/CNTs with 27.9% Pt coverage in 0.5 M H₂SO₄ with and without 0.1 M methanol, 10 mV/s, 1600 rpm. (d) Linear Sweep Voltammetry (LSV) results of Pt/C in 0.5 M H₂SO₄ with and without 0.1 M methanol, 10 mV/s, 1600 rpm. Reprinted with permission from ref. ⁴³⁶. Copyright 2013 Springer.

Kim *et al.* have reported Pd@Pt core-shell NCs⁴³⁷ synthesized by an aqueous one-pot synthetic method comprising sequential formation of the Pd core followed by the Pt shell as a result of the inherently slower reduction of Pt precursors used in the synthesis. The Pt shell thickness of the Pd@Pt NCs could readily be manipulated by controlling the molar ratio of Pt and Pd precursors in the growth solutions (Fig. 56). The electrocatalytic activity of the prepared Pd@Pt catalyst was tested for MOR activity and shown to be highly dependent on the Pt shell thickness due to different interactions between the Pt and Pd. The Pd1@Pt1 catalyst was found to exhibit the highest catalytic activity.

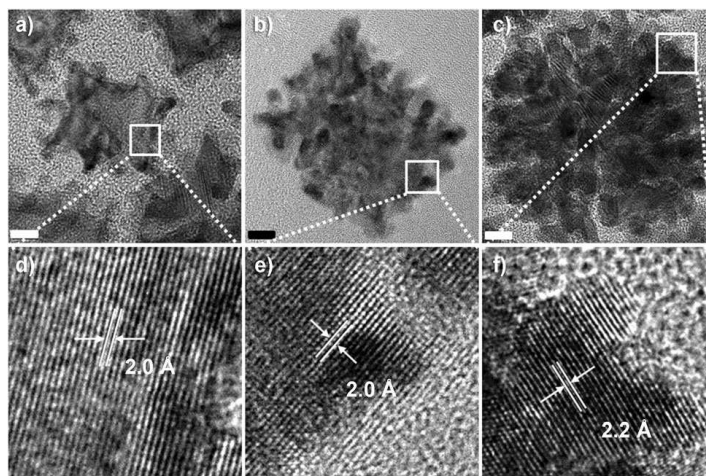


Fig. 56 Low (a–c) and high magnification (d–f) HRTEM images of Pd3@Pt1 (a,d), Pd1@Pt1 (b,e), and Pd1@Pt3 (c,f) NCs. Scale bars indicate 5 nm. Reprinted with permission from ref. ⁴³⁷. Copyright 2014 American Chemical Society.

Nogami and co-workers synthesized Pt-Pd core-shell nanoparticles using a modified polyol method and have described the details of their formation and growth mechanism.^{70, 438-440} In their procedures, in order to control the morphology of the Pt-NP core, AgNO₃ acts as a structure-modifying agent; ensuing Pt-NP core serve as seeds for Pd-shell materials. Well-characterized materials by HRTEM and EDS have revealed the information regarding the morphology and the size of the core and shell (Fig. 57), which have allowed them to provide the possible growth mechanism. The materials were successfully applied as electrocatalyst in proton exchange membrane fuel cells (PEMFCs) and in direct methanol fuel cells (DMFCs). Their electrochemical study revealed that the Pt-Pd nanocatalysts showed better electrocatalytic activity and stabilization than the parent and Pt nanocatalysts and the activity is more dependent on the nanostructuring effect than the size of materials. This is one of the examples, where a direct synergistic effect of Pt-Pd nanocatalysts was demonstrated, which aided the materials to achieve higher catalytic activity than their individual components.

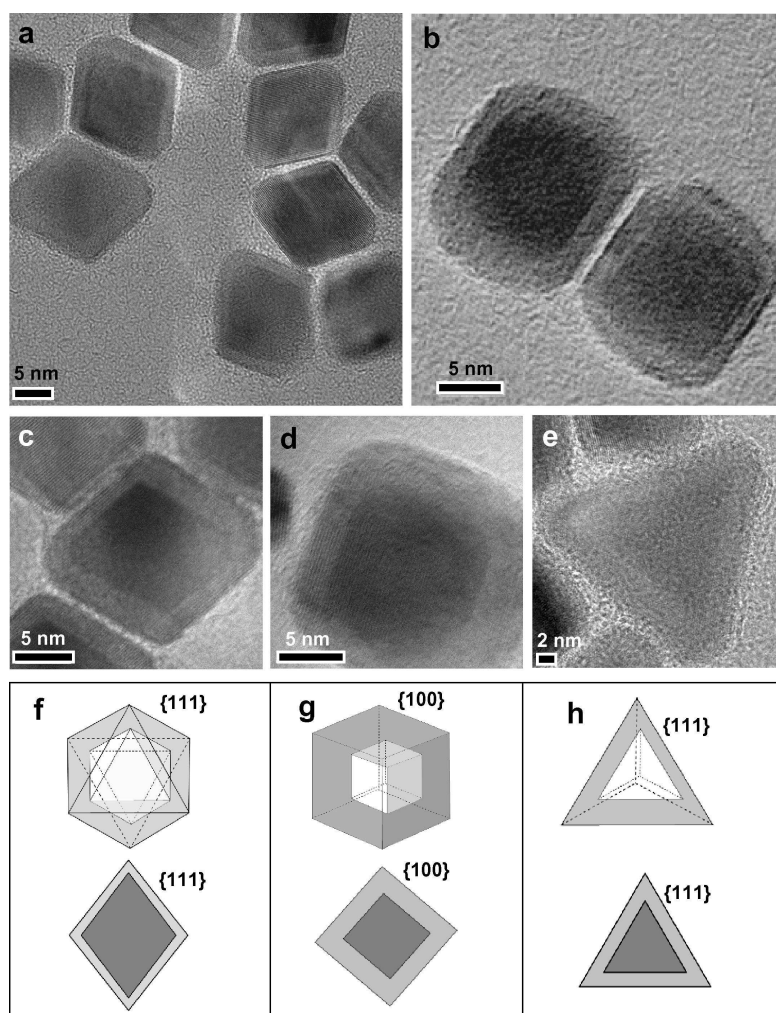


Fig. 57 (a–e) HRTEM images of Pt–Pd core–shell nanoparticles. (f–h) Models of octahedral, cubic and tetrahedral Pt–Pd core–shell nanoparticles. Scale bars: (a–d) 5 nm and (e) 2 nm. Reprinted with permission from ref. ⁴³⁹. Copyright 2011 Elsevier Ltd.

The size-dependent activity of Pt-based alloys consisting of Pt and late transition metals (TM) elements in the 3d series, typically Pt₃Fe, Pt₃Co and Pt₃Ni, were studied for the ORR in fuel cells. The electrocatalytic results were supported by DFT calculations. The activity of core–shell Al₁₃@Pt₄₂ catalyst was found to depend on the formation of alloy with Al with the cluster; the covalent Pt–Al bonding effectively activated the Pt atoms at the edge sites, which enabled a high utility to be achieved of up to 70% (Fig. 58).⁴⁴¹

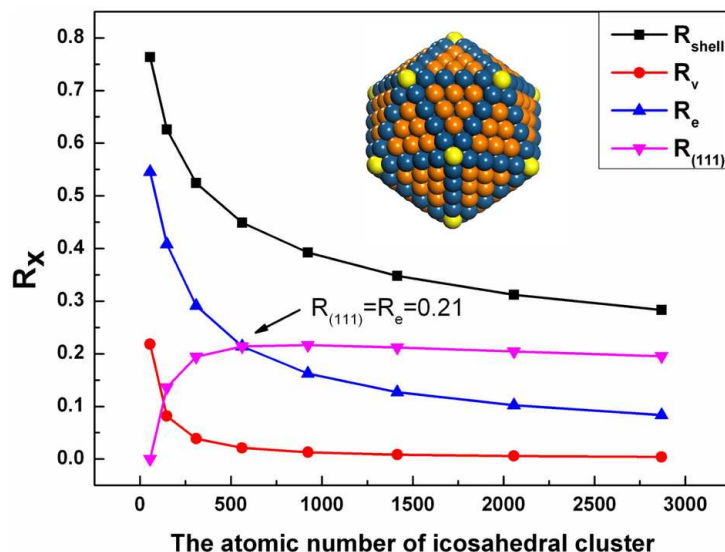


Fig. 58 Size-dependent percentage of atoms on the (111) plane, edge and vertex, represented by $R_{(111)}$, R_e and R_v , respectively. R_{shell} denotes the percentage of atoms on the shell, where $R_{shell} = R_{(111)} + R_e + R_v$. Atoms in yellow, blue and orange denote Pt_v , Pt_e and $Pt_{(111)}$ atoms. Inset is the structure of Pt_{561} where $R_e = R_{(111)}$. Reprinted with permission from ref. ⁴⁴¹. Copyright 2014 Nature Publishing Group.

Guo *et al.* used a seed-mediated growth method to prepare core/shell FePtM/FePt (M = Pd, Au) NWs.⁴⁴² They adapted a method of controlled decomposition of $Fe(CO)_5$ and reduction of $Pt(acac)_2$ in the presence of 2.5 nm wide FePtM NW seeds and were able to deposit ~0.3-1.3 nm thick FePt shell on the FePtM core. These FePtM/FePt NWs were used for the ORR and displayed activity that was dependent on shell thickness and core composition as well as significant stability under the ORR conditions.

Generally, bimetallic and multimetallic NPs display better catalytic activity compared to their monometallic counterparts. It is quite tricky to optimize activity on the basis of composition and structure, as metal migration causes the control of geometric, electronic, and ensemble effects to change over time. Bimetallic nanoparticles endure metal migration under specific reaction conditions, caused by surface energy discrepancy and oxidizing or reducing agents in the system. This has gained tremendous interest in nanocatalysis research.³²² For instance, in well-designed core-shell structure, the core metal could have lower surface energy than the shell metal, so when sufficient energy provided, the core metal would transfer to the particle surface in order to lower the overall surface energy.

Brodsky *et al.* have synthesized Au@Pd core-shell octahedral NPs with tunable thicknesses for electrocatalytic applications.⁴⁴³ Under electrochemical conditions, Au metal migrated from the core to shell, and the extent of migration was shown to depend on the type and pH of the

electrolyte, as well as the potential range employed (Fig. 59). TEM images revealed Au seeds and thin and thick shell Au-Pd octahedra (Fig. 59b), as well as continual lattice fringes from the Au core to Pd shell phases, indicating epitaxial growth (Fig. 59c).

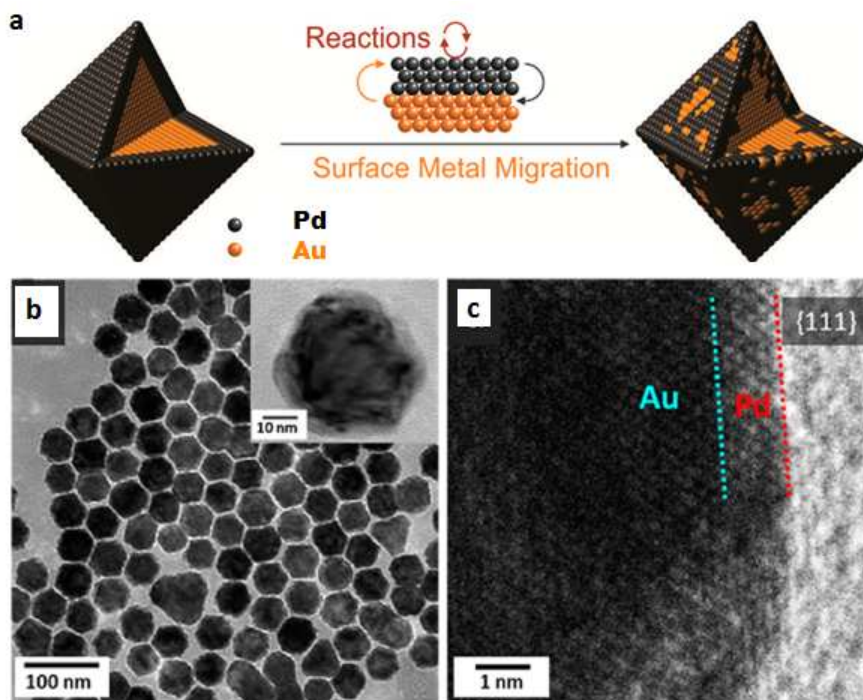


Fig. 59. (a) Surface metal migration of CSNs. (b) Thick shell Au-Pd nanooctahedra, and (c) HR-TEM image of a thin shell octahedron's Au-Pd interface, showing epitaxial growth. Reprinted with permission from ref. ⁴⁴³. Copyright 2014 American Chemical Society.

Both particle types had well-defined structures and good monodispersity, which enabled a thorough electrochemical evaluation. The Au@Pd core-shell nanocatalyst was employed for its electrocatalytic activity, including metal relocation by cyclic voltammetry and the ethanol oxidation reaction (EOR).⁴⁴³ In the EOR, it was observed that migration was more prevalent in the thin shell particles, at first promoting EOR activity by strain effects, but then inhibiting activity by ligand and ensemble effects. The thick octahedral shell prevented relocation but inhibited Au-induced strain effects, resulting in overall low catalytic activity. Migration of metals during catalytic ethanol oxidation was found to alter the particle's surface composition and electronic structure, thus improving the core-shell particles' activity (Fig. 60).

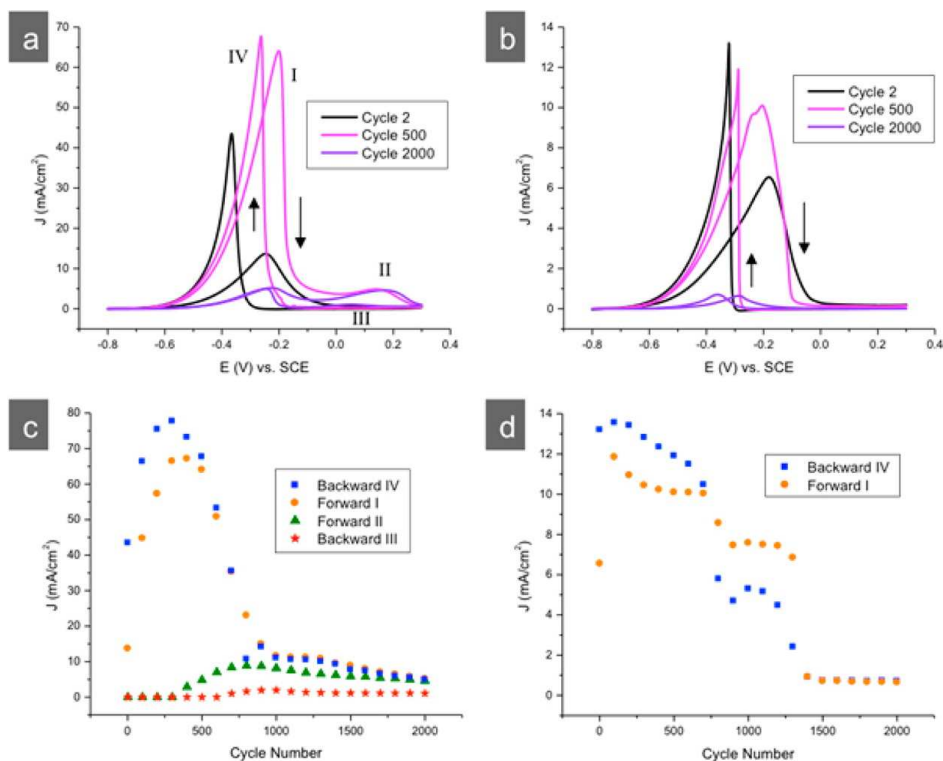
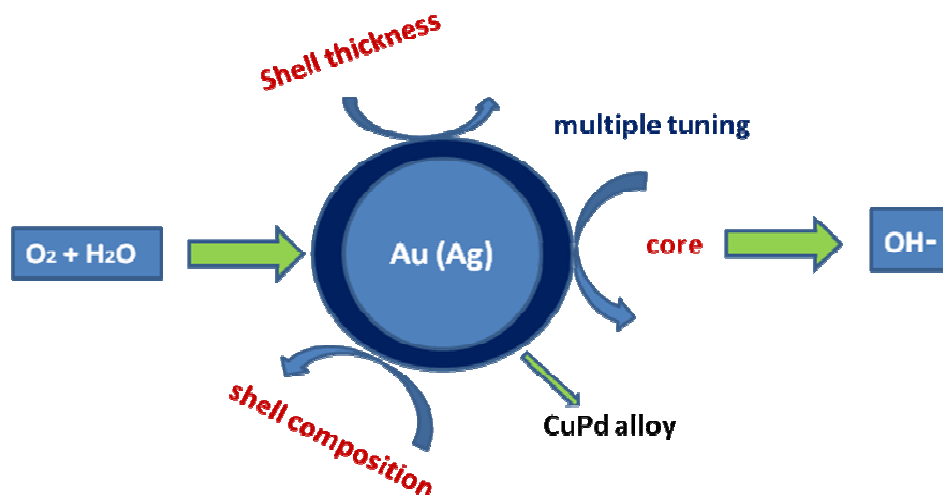


Fig. 60 (a, b) EOR performed on thin and thick shell Au-Pd core-shell octahedra, respectively, in 1 M KOH and 1 M ethanol. (c, d) Plots of EOR current density vs. cycle number for thin and thick shell octahedra, respectively, for peaks I-IV as labeled in (a). Reprinted with permission from ref. ⁴⁴³. Copyright 2014 American Chemical Society.

Sun and Lu have reported⁴⁴⁴ monodispersed M/CuPd NPs by using palladium- and copper-acetylacetonate in the presence of Ag (or Au) NPs with well-ordered shell thicknesses (0.4, 0.75, and 1.1 nm) and CuPd compositions for use in the ORR (Fig. 61).



10

Fig. 61 Monodisperse M/CuPd NPs for the ORR. Reprinted with permission from ref. ⁴⁴⁴. Copyright 2014 American Chemical Society.

Catalysts with compositions of Ag/Cu₃₇Pd₆₃ and Au/Cu₄₀Pd₆₀ having 0.75 and 1.1 nm shells, respectively, were found to be more efficient compared to a commercial Pt catalyst, exhibiting their mass activity ~ 0.20 A/mg of noble metal at -0.1 V vs Ag/AgCl (4 M KCl). Additionally, DFT-based calculations showed that Ag/CuPd and Au/CuPd NPs with 0.8 and 1.2 nm thick CuPd₂ shells have the optimal surface strain and composition to catalyze the ORR. The obtained catalysts exhibited higher stability than Pt-based catalysts, retaining 77.6% of their activity after 48000 s *i-t* test (62.9% for the Pt catalyst). Thus, these Ag (Au)/CuPd NPs offer a promising non-Pt alternative for catalyzing the ORR. This investigation focused on tuning the surface strain and composition in the core-shell structure to maximize its ORR performance, thereby identifying an advanced nanocatalyst that exhibited ORR catalysis superior to that of Pt.

Lin and co-workers have reported near-monolayer thick shell atoms for application as ORR electrocatalysts in the direct methanol fuel cell (DMFC).⁴⁴⁵ X-ray diffraction results confirmed that the crystal structure experienced compressive strain near the Pt shell region. The shell thickness of Ru@Pt CSNs was determined to be 1.5 atomic layers using a core-shell scattering model in the small-angle X-ray scattering experiment. The power density of a DMFC with Ru core-Pt shell NPs was $\sim 450\%$ (from 17.1 to 92.8 mW cm⁻² mg⁻¹), which was far superior to component Pt NPs. Overall, this proved to be one of the most inexpensive and environmentally benign DMFCs whilst showing exceptional performance (Fig. 62). The inherent strain promoted substantial valence charge donation from Pt to Ru, increased the (binding energy) E_b by 0.44 eV and lowered the valence band (VB) level by 0.31 eV. Such VB amendment increased the surface activity for the electrooxidation of methanol and chemisorption, initiated carbon monoxide oxidation and enhanced the anodic reaction kinetics of the DMFC system. The electrocatalytic results indicated that the Pt_{shell}/Ru_{core} NPs are promising candidates for the development of high-performance, inexpensive and benign DMFCs.

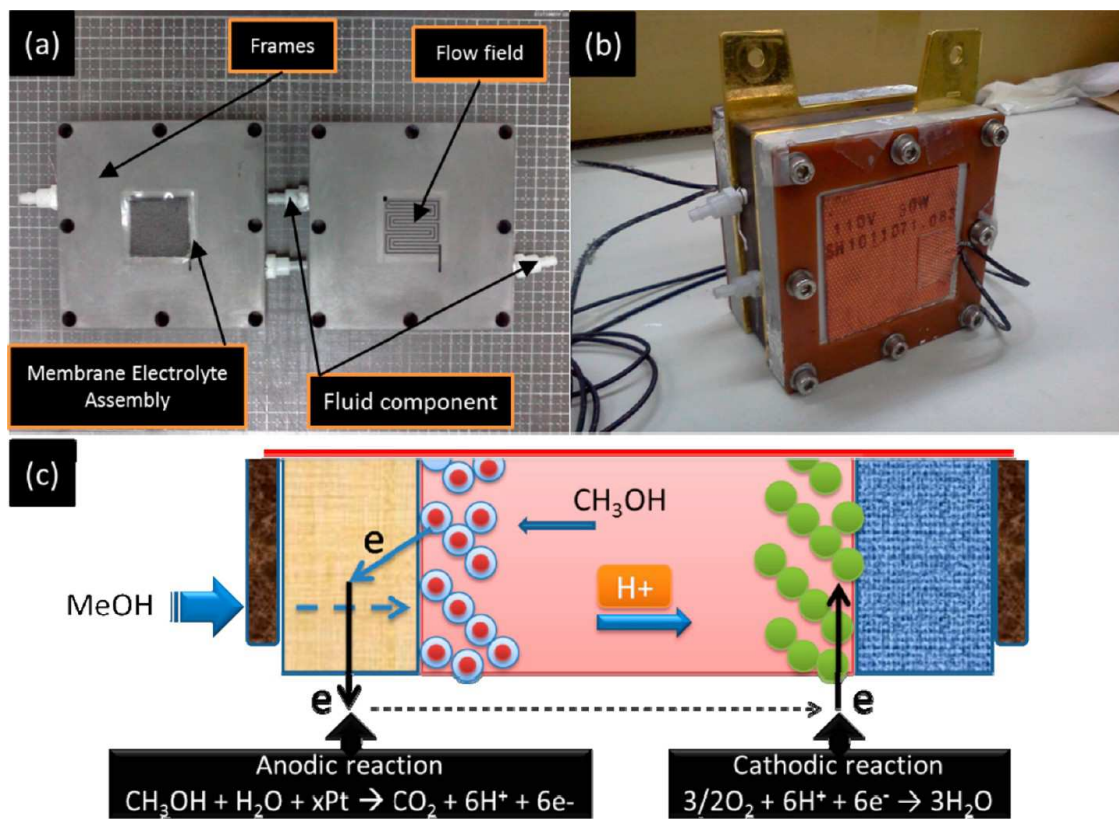


Fig. 62 Scheme for assembly of a DMFC full stack. (a) Devices of flow field, fluid components, frames and membrane electrolyte assembly (MEA). (b) Assembled full stack. (c) Details of MEA component. Reprinted with permission from ref. ⁴⁴⁵. Copyright 2014 American Chemical Society.

The noble and the non-noble elements can be tuned in the alloy precursor, such that both expansive and compressive strain can control the strengthening or weakening of surface bonds; this permits continuous alteration of the catalytic reactivity. Overall, this strain-related tuning for the ORR may offer a means for controlling the activity of other important electrocatalytic reactions that require amendment of the adsorption energy for the electrooxidation of small organic molecules, including ethanol, methanol and associated species. Strasser *et al.* have investigated the remarkable electrocatalytic activity exhibited by dealloyed Pt–Cu NPs and demonstrated how lattice strain can be employed practically to adjust the catalytic activity of dealloyed bimetallic NPs for the ORR.⁹⁵ The density of the shell changed the d-band structure of the Pt atoms, thereby weakening the adsorption energy of the reactive intermediates compared to using unstrained Pt, resulting in increased catalytic performance, as confirmed by DFT-based calculations. Energy-dispersive elemental color-map overlays for Pt and Cu were acquired using a probe-corrected scanning transmission electron microscope (STEM) for the Pt₂₅Cu₇₅ alloy precursor annealed at 800 °C and dealloyed catalyst separately (Fig. 63). A resultant EDS sketch across the diameter of characteristic (~ 4 nm) dealloyed NPs confirmed the existence of a Pt-enriched layer (~0.6 nm) on the surface of the dealloyed particles, (Fig. 63c). Figure 63d shows that the dealloyed NP catalysts synthesized at

higher annealing temperature displayed reduced activity probably because of alterations in the mean particle size. Overall, the strain-related tuning for the ORR may offer a useful route for controlling the activity of other significant electrocatalytic chemical reactions that involve amendment of the adsorption energy of reactive intermediates, including the electrooxidation of small organic molecules (*viz.* methanol, ethanol and related moieties).⁹⁵

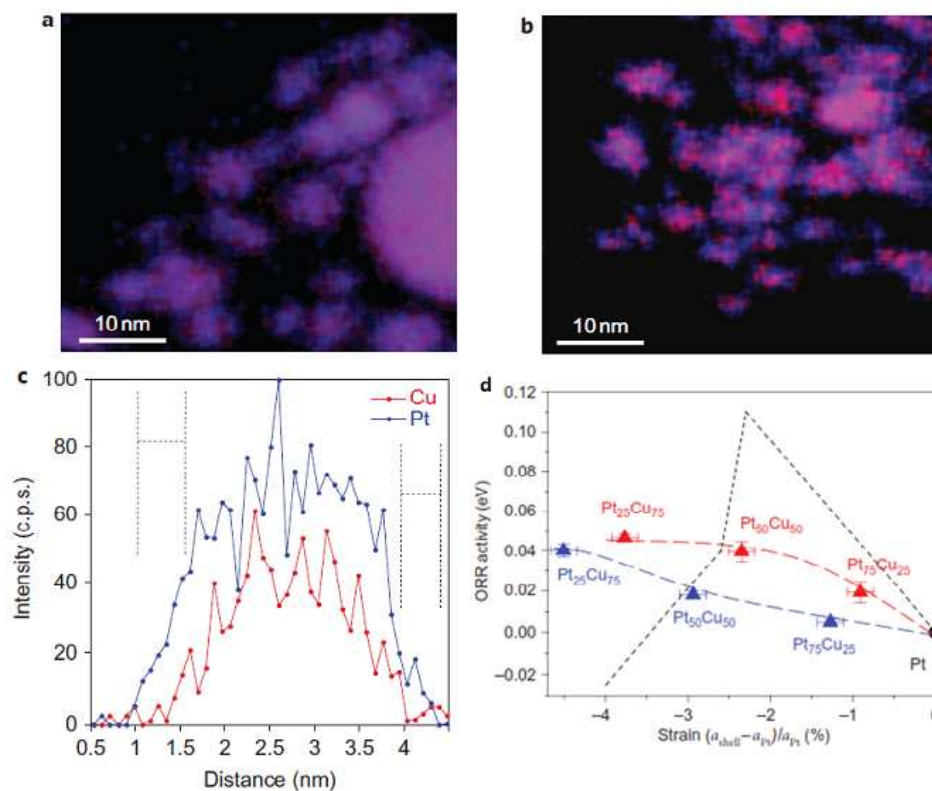


Fig. 63 Elemental maps and line profiles of Pt–Cu bimetallic NP precursors and dealloyed active catalysts. High resolution energy dispersive spectroscopy (HR-EDS) elemental maps of a Pt₂₅Cu₇₅ bimetallic NP alloy precursor (a) and the active electrocatalyst obtained after Cu dealloying from the precursor (b). Pt is shown in blue, Cu in red and pink domains indicate well-alloyed Pt–Cu domains. (c) HR-EDS line profile across an individual 4 nm diameter dealloyed Pt–Cu alloy active-catalyst particle. (d) Experimental and predicted relationships between electrocatalytic ORR activity and lattice strain. Reprinted with permission from ref. ⁹⁵. Copyright 2010 Nature Publishing Group.

The deployment of core-shell nanostructures as electrocatalyst in various applications including ORR, HER, EOR, DMFC etc. displayed many unique properties that are not exhibited by several others catalysts. The design and development of practical electrochemical processes using core-shell nanocatalysts is generally meant to overcome the great overpotentials and low current density; core-shell nanostructures provide an exceptional approach to increase the surface energy of active sites on shell surface and decrease the reactions overpotential.

The integration of various components into a hybrid nanosystem for the optimum and synergistic utilization is an effective way to design the electrocatalysts as exemplified by various hybrid strategies to enhance the electrocatalytic property of core-shell nanostructures nanoparticles for different electrocatalytic applications.

5

6. Perspectives and future prospects

Over the last decade, CSNs have been actively employed in various advanced applications, including solar cells, chemical sensing, catalysis and electrocatalysis. Some of the biggest challenges in this field include ensuring the compatibility between the core and shell and utilizing
10 the unique properties of core and shell individually. In addition, improvement of both core and shell materials for specific applications, particularly in the context of sustainable energy, has also been the focus of recent research efforts.

Various types of cores have been used, including oxides such as silica, ZrO₂, iron oxides and also metals /noble metals (*e.g.*, Ag, Cu, Pd). Among these options, earth-abundant iron oxide or
15 iron supports (magnetite and maghemite) are considered a superior class for decorating (or being decorated with) various catalytic active shells (Cu, Pt, Ni, *etc.*),^{293, 434, 446-451} mainly because they i) are inexpensive, ii) can be prepared easily, and, most importantly, iii) can be separated magnetically, which is undoubtedly a great advantage when considering sustainable chemistry. Recently, iron (Fe(0))-based CSNs have also been synthesized successfully in a variety of
20 applications,⁴⁵²⁻⁴⁵⁴ but maintaining a stable Fe(0) oxidation state has always been a topic of concern which needs to be resolved in a better and more efficient way.

As explained in the review, core-shell nanomaterials are often known to have better catalytic activity due to the presence of different effects (ligand, ensemble and geometric). Hence, it's important to identify the experimental factors that can steer the core-shell materials to have
25 such desirable effects. The understanding of the atomic arrangements and the interactions between core and shell at the interface has always been considered crucial for designing efficient nanocatalysts. However, the availability of the state-of-the-art instrumental techniques and powerful computational ability has allowed studying them so closely; high resolution aberration corrected STEM technique and theoretical-calculation-directed studies have elucidated the
30 formation mechanism and explained the stability of Pd-Pt and Pt-Pd bimetallic core-shell materials.⁴⁵⁵ In another study, the atomic arrangements of Fe/Cu and Fe/Au core-shell nanomaterials, prepared via gas-phase deposition, have been investigated using EXAFS (extended absorption fine structure)⁴⁵⁶ which revealed the structural complexity of the core materials as a function of shell materials. The synergism between the core and shell is an important factor for
35 several catalytic and electrocatalytic applications; electrocatalytic activity of Pd-Pt alloy and core-shell has been investigated for DMFCs as a function of size, shape, and compositions of the

nanocatalyst and the highest activity was discerned for core-shell nanoparticles with monolayer shell when compared to their alloys and mixed NPs.⁴⁵⁷ Such continuing progress in this area will help attain the optimum conditions to develop core-shell nanocatalysts endowed with higher efficiency.

5 Another significant challenge for core-shell synthesis is their bulk-scale preparation, as during the scaling up process, they often lose their intrinsic chemical and physical properties, which are fundamentally important for their catalytic behavior. Additionally, most of these core-shell NPs, especially the ones employed in electrocatalysts, are rather expensive, although they are quite effective for the respective applications.⁴⁵⁸⁻⁴⁶³ Hence, replacing such noble metal containing CSNs
10 by inexpensive materials for electrocatalysis and related types of applications is likely to be an active area of future research.⁴⁶⁴⁻⁴⁶⁷

Recently, “surface-protected etching” processes have been successfully employed for the fabrication of several nanostructured systems, including yolk-shell and core satellite nanocatalysts, in which mostly metal nanocatalysts are stabilized by porous shells.^{330, 468-470} Although, the
15 uniformity of the pores can often be a concern and needs thorough investigation, the porosity of the silica and titania shells, which affects the reaction rates of catalytic processes, can be well controlled during such an etching process. An advanced “surface-protected calcination” method may also be ideal for the preparation of anatase titania shells, in which added silica species can stop overgrowth of the titania grains and help maintain its porous structure and structural reliability.

20 A similar approach may also be used for materials with effective photocatalytic activity. Additional important considerations for these types of core-shell nanostructures are the availability of various metal combinations and prospects for studying the synergies between the different components of the core-shell structures to boost structural stability and catalytic activity/selectivity. This has allowed the development of highly effective and stable photocatalysts
25 featuring multilayer core-shell structures. The etching-based protocol mentioned above is easy to use, convenient in engineering the pore size and generally applicable to many oxide materials.

In terms of the synthesis, recent advances have led to the design and preparation of more complicated structures including movable cores within hollow shells and hollow movable cores within hollow shells and surface metal migration of CSNs.⁴⁴³ The unique design and characteristics
30 of these nanocatalysts offer advantages in different applications, including magnetic photocatalysts, self-assembled photonic crystals with controlled bandgaps, and magnetic toners and inks; they have good encapsulation ability, and hence the targeted release of biomolecules may also be possible.

The emerging areas of flow chemistry, MW- and sonication-assisted techniques have also recently made inroads in the nanocatalysis and electrocatalysis arena.^{471,472} However, the synthesis
35 of CSNs by MW irradiation is relatively unexplored compared to other established techniques and is often limited in terms of the controlling morphology. Hence, it would be an interesting area for

future research.⁴⁷³ Use of a flow reactor in conjunction with MW-assisted methods appears to be the best approach for preparing CSNs on a relatively large scale. Mechanochemical mixing/grinding, useful in nanomaterial synthesis, has not yet been explored for the synthesis of CSNs, probably due to inherent limitations of the technique. Recently, a trimetallic core-shell system, also known as trimetallic NPs or integrated NPs, has been employed for ORR, hydrolytic dehydrogenation, methanol electrooxidation, catalytic hydrolysis of amine borane and other applications.⁴⁷⁴⁻⁴⁷⁶ On this basis, optimal metallic cores or shells could be designed for specific applications. Considering the current state of core-shell nanocatalysts, we are hopeful that better systems than currently available ones will be found that are capable of performing more efficiently and selectively.

7. Concluding remarks

CSNs have emerged as valuable and versatile nanomaterials for catalysis because of their additive or complementarily enhanced properties compared to their one-component counterparts. The strain and ligand effect between the core and surrounding shell can be exploited for tailoring the catalytic activity and selectivity of core-shell nanocatalysts. Recent developments in the preparation of CSNs and their catalytic and electrocatalytic applications, including hydrogenation reactions, oxidation reactions, coupling reactions, cycloaddition reactions, ammonia decomposition, ORR, AOR, *etc.* have been summarized in this review article. Advanced techniques used for the characterization of core-shell nanostructures have also been briefly illustrated. The key structural factors affecting catalytic activities of nanostructured materials, namely surface charge, surface area, surface functionality, size distributions, structure, *etc.*, have particularly been emphasized. In addition, ways to unravel their structure-catalytic activity relationships and use the outcomes of studies as a guide for further development of new and improved CSNs for catalytic applications have been discussed.

In spite of their widespread application in catalysis, some aspects require further research; the interaction between the core and shell is possibly the most important among them. As an example, there have been some disagreements as to whether the ligand effect contributes to the d-band width or induces a direct charge transfer that affects d-band filling and how the thickness/properties of the shell influences the overall catalytic process.

Moreover, core-shell catalysts have become useful materials for electrocatalysis and have shown enhanced catalytic activity in various electrocatalytic reactions. These catalysts have been made from transition or non-transition metals, and their properties have been varied or tuned according to the elements they are composed of and the synthetic protocols employed to make them. Many of the synthetic methods used to make these materials have involved wet chemical

approaches, electrodeposition, electrochemical dealloying, solvothermal method, *etc.* By using one or a few of these synthetic methods, or in combination, and by varying the synthetic conditions, a wide variety of core–shell electrocatalysts with different structure and properties has been prepared. While many of the materials reported and discussed above contain noble metals, making materials entirely of non-noble metals and earth-abundant elements is of increasing interest in order to address sustainability challenges. Many of these materials and the electrochemical transformations they catalyze would also be of great interest for future renewable energy technologies, such as fuel cells, water electrolyzers and energy storage devices.

CSNs appear to offer great potential for vapor phase reactions (*e.g.*, hydrogenation, oxidation, and alkylation) involving gas phase reactors as well. Combination of two different metals (bimetallic) for the core and shell has led to the emergence of a new generation of nanocatalyst that can be explored for a number of important chemical reactions. Further, tuning the composition of the two metals may would allow selective organic transformations with ease and provide additional tools for chemists to attain the goal of sustainability. These advancements in core–shell nanocatalysts will be expected to provide a solid and stable platform for the development of heterogeneous catalysis, green chemistry, and environmentally benign protocols in the near future.

AUTHOR INFORMATION

Corresponding Authors

***Email:** manoj.gawande@upol.cz (MBG); radek.zboril@upol.cz (RZ);

Varma.Rajender@epamail.epa.gov (RSV)

BIOGRAPHIES



Manoj B. Gawande received his Ph.D. degree in Chemistry in 2008 from, Institute of Chemical Technology (formerly UDCT), Matunga, Mumbai, India. He was awarded several prestigious fellowships, including BK-21 Research fellowship, FCT Research fellowship and recently was awarded Mahatma Gandhi Pravasi Samman, by Govt. of India and NRI Welfare Society of India. After several research stints in Germany, Portugal, Singapore, England and USA, he is presently working as Senior Researcher and Head of Division of Nanocatalysis laboratory at RCPTM, Faculty of Science, Palacky University, Olomouc, Czech Republic. His research interests include core-shell/carbon/magnetic nanocatalysis. He has published nearly 65 scientific papers/reviews.



Anandarup Goswami obtained his Ph.D. in organolithium chemistry under Prof. David B. Collum (2010) and later joined Prof. Kai C. Hultsch's group at Rutgers University to work on organometallic catalysis. He has a keen interest in heterogeneous catalysis, which he explored in Prof. Tewodros (Teddy) Asefa's group, with special emphasis on silica/metal/carbon-based nanomaterials and their applications. Presently, he is working as researcher in the field of nanocatalysis at the Regional Centre of Advanced Technologies and Materials, Faculty of Science, Palacky University, Olomouc, Czech Republic, with Dr. Manoj B. Gawande and Prof. Radek Zboril.



Tewodros (Teddy) Asefa is a Professor in Departments of Chemistry and Chemical Biology & Chemical and Biochemical Engineering at Rutgers University at New Brunswick, USA. He received his MSc from SUNY-Buffalo (1998) and his PhD from University of Toronto (2002). He received fellowships to serve as Visiting Professor at Kyoto University, Japan (2014); Maringá State University, Brazil (2014-2017); and ETH Zürich, Switzerland (2015). He also received NSF CAREER award (2007-2012), NSF Special Creativity award (2011), Rutgers Board of Governors Research Fellowship (2012), and NSF's American Competitiveness Fellowship (2010). He co-edited a book on Nanocatalysis (Wiley) and wrote 120 papers/book chapters.



Ankush V. Biradar received his Ph.D. in chemistry from the National Chemical Laboratory, Pune/University of Pune under the supervision of Dr. Shubhangi Umbarkar in 2009. After graduating, he moved to Prof. Tewodros Asefa's group, first at Syracuse University and then Rutgers University in New Jersey, USA, where he worked on the synthesis and catalytic properties of multifunctional nanomaterials. In 2012, he moved back to India and joined the National Chemical Laboratory, Pune, as a Scientist. His research interests lie in the development of nanostructured catalysts, especially non-noble metal-based ones and their utilization for oxidation and hydrogenation reactions.



Radek Zboril received his Ph.D. degree from Palacky University, Olomouc. After his Ph.D. study, he underwent several foreign stays at universities in Tokyo, Delaware and Johannesburg. Currently, he is a Professor at the Department of Physical Chemistry and General Director of the Regional Centre of Advanced Technologies and Materials at Palacky University, Olomouc. He has published more than 250 papers in prestigious journals with research interests in nanomaterials area that includes iron and iron oxide based nanoparticles (NPs), silver NPs, carbon nanostructures, and magnetic NPs and their applications in biomedicine, environmental technologies, sensing and catalysis.

10



Rajender S. Varma was born in India (Ph.D., Delhi University 1976). After postdoctoral research at Robert Robinson Laboratories, Liverpool, U.K., he was a faculty member at Baylor College of Medicine and Sam Houston State University prior to joining the Sustainable Technology Division at the US Environmental Protection Agency in 1999. He has over 40 years of multidisciplinary research experience and lately engaged in greener assembly of nanomaterials and the sustainable applications of magnetically retrievable nanocatalysts. He is member of the editorial advisory board of several international journals, published over 415 scientific papers, and has been awarded 14 US Patents.

20

ACKNOWLEDGMENTS

The authors gratefully acknowledge support from the project LO1305 and the Operational Program Education for Competitiveness – European Social Fund (project CZ.1.07/2.3.00/ 30.0041) of the Ministry of Education, Youth and Sports of the Czech Republic. TA gratefully acknowledges financial support from the National Science Foundation in the USA for his groups work on core-shell nanocatalysis.

Disclaimer

30

U.S. Environmental Protection Agency (EPA), through its Office of Research and Development, partially funded and collaborated in, the research described herein. It has been subjected to the Agency's administrative review and has been approved for external publication. Any opinions expressed in this paper are those of the author(s) and do not necessarily reflect the views of the Agency, therefore, no official endorsement should be inferred. Any mention of trade names or commercial products does not constitute endorsement or recommendation for use.

References

1. M. C. Daniel and D. Astruc, *Chem. Rev.*, 2004, **104**, 293-346.
2. M. B. Gawande, V. D. B. Bonifacio, R. S. Varma, I. D. Nogueira, N. Bundaleski, C. A. A. Ghumman, O. M. N. D. Teodoro and P. S. Branco, *Green Chem.*, 2013, **15**, 1226-1231.
3. M. B. Gawande, P. S. Branco and R. S. Varma, *Chem. Soc. Rev.*, 2013, **42**, 3371-3393.
4. M. B. Gawande, A. K. Rathi, I. D. Nogueira, R. S. Varma and P. S. Branco, *Green Chem.*, 2013, **15**, 1895-1899.
5. A. H. Lu, E. L. Salabas and F. Schuth, *Angew. Chem. Int. Ed.*, 2007, **46**, 1222-1244.
6. A. K. Geim and K. S. Novoselov, *Nature Mater.*, 2007, **6**, 183-191.
7. V. Georgakilas, A. B. Bourlinos, R. Zboril, T. A. Steriotis, P. Dallas, A. K. Stubos and C. Trapalis, *Chem. Commun.*, 2010, **46**, 1766-1768.
8. V. Georgakilas, M. Otyepka, A. B. Bourlinos, V. Chandra, N. Kim, K. C. Kemp, P. Hobza, R. Zboril and K. S. Kim, *Chem. Rev.*, 2012, **112**, 6156-6214.
9. M. Pykal, K. Safarova, K. M. Siskova, P. Jurecka, A. B. Bourlinos, R. Zboril and M. Otyepka, *J. Phys. Chem. C*, 2013, **117**, 11800-11803.
10. R. Zboril, F. Karlicky, A. B. Bourlinos, T. A. Steriotis, A. K. Stubos, V. Georgakilas, K. Safarova, D. Jancik, C. Trapalis and M. Otyepka, *Small*, 2010, **6**, 2885-2891.
11. H. C. Zeng, *Acc. Chem. Res.*, 2013, **46**, 226-235.
12. A. T. Bell, *Science*, 2003, **299**, 1688-1691.
13. A. Wittstock, V. Zielasek, J. Biener, C. M. Friend and M. Baumer, *Science*, 2010, **327**, 319-322.
14. J. Pecher and S. Mecking, *Chem. Rev.*, 2010, **110**, 6260-6279.
15. R. Silva and T. Asefa, *Adv. Mater.*, 2012, **24**, 1878-1883.
16. R. Silva, J. Al-Sharab and T. Asefa, *Angew. Chem. Int. Ed.*, 2012, **51**, 7171-7175.
17. B. Baruwati, V. Polshettiwar and R. S. Varma, *Green Chem.*, 2009, **11**, 926-930.
18. B. Baruwati and R. S. Varma, *ChemSusChem*, 2009, **2**, 1041-1044.
19. G. Zoppellaro, J. Tucek, R. Herchel, K. Safarova and R. Zboril, *Inorg. Chem.*, 2013, **52**, 8144-8150.
20. M. Hu, S. Furukawa, R. Ohtani, H. Sukegawa, Y. Nemoto, J. Reboul, S. Kitagawa and Y. Yamauchi, *Angew. Chem. Int. Ed.*, 2012, **51**, 984-988.
21. M. B. Gawande, S. N. Shelke, R. Zboril and R. S. Varma, *Acc. Chem. Res.*, 2014, **47**, 1338-1348.
22. C. Burda, X. B. Chen, R. Narayanan and M. A. El-Sayed, *Chem. Rev.*, 2005, **105**, 1025-1102.
23. C. T. Duncan, A. V. Biradar, S. Rangan, R. E. Mishler and T. Asefa, *Chem. Mater.*, 2010, **22**, 4950-4963.
24. F. Zaera, *Chem. Soc. Rev.*, 2013, **42**, 2746-2762.
25. J. C. Park, A. Y. Kim, J. Y. Kim, S. Park, K. H. Park and H. Song, *Chem. Commun.*, 2012, **48**, 8484-8486.
26. M. Kim, J. C. Park, A. Kim, K. H. Park and H. Song, *Langmuir*, 2012, **28**, 6441-6447.
27. J. C. Park and H. Song, *Nano Res.*, 2011, **4**, 33-49.
28. X. Guo, P. Brault, G. Zhi, A. Caillard, G. Jin and X. Guo, *J. Phys. Chem. C*, 2011, **115**, 24164-24171.
29. M. N. Nadagouda, V. Polshettiwar and R. S. Varma, *J. Mater. Chem.*, 2009, **19**, 2026-2031.
30. M. B. Gawande, V. D. B. Bonifacio, R. Luque, P. S. Branco and R. S. Varma, *Chem. Soc. Rev.*, 2013, **42**, 5522-5551.
31. M. B. Gawande, V. D. B. Bonifacio, R. Luque, P. S. Branco and R. S. Varma, *ChemSusChem*, 2013, **7**, 24-44.
32. B. M. Trost, *Acc. Chem. Res.*, 2002, **35**, 695-705.
33. R. S. Varma, in *Green Chemical Reactions*, eds. P. Tundo and V. Esposito, 2008, pp. 155-171.
34. F. Jutz, J. M. Andanson and A. Baiker, *Chem. Rev.*, 2011, **111**, 322-353.
35. M. B. Gawande, R. K. Pandey and R. V. Jayaram, *Catal. Sci. Technol.*, 2012, **2**, 1113-1125.
36. M. B. Gawande, A. Rathi, I. D. Nogueira, C. A. A. Ghumman, N. Bundaleski, O. M. N. D. Teodoro and P. S. Branco, *ChemPlusChem*, 2012, **77**, 865-871.
37. S. S. Kahandal, S. R. Kale, M. B. Gawande, R. Zboril, R. S. Varma and R. V. Jayaram, *RSC Adv.*, 2014, **4**, 6267-6274.
38. H. Wang, L. Y. Chen, Y. H. Feng and H. Y. Chen, *Acc. Chem. Res.*, 2013, **46**, 1636-1646.
39. C. F. Hoener, K. A. Allan, A. J. Bard, A. Campion, M. A. Fox, T. E. Mallouk, S. E. Webber and J. M. White, *J. Phys. Chem.*, 1992, **96**, 3812-3817.
40. I. Honma, T. Sano and H. Komiyama, *J. Phys. Chem.*, 1993, **97**, 6692-6695.

41. H. Amouri, C. Desmarests and J. Moussa, *Chem. Rev.*, 2012, **112**, 2015-2041.
42. L. J. Lauhon, M. S. Gudiksen, D. Wang and C. M. Lieber, *Nature*, 2002, **420**, 57-61.
43. H. H. Park, K. Woo and J.-P. Ahn, *Sci. Rep.*, 2013, **3**, 1497.
44. H.-L. Jiang, T. Akita, T. Ishida, M. Haruta and Q. Xu, *J. Am. Chem. Soc.*, 2011, **133**, 1304-1306.
- 5 45. A. P. Douvalis, R. Zboril, A. B. Bourlinos, J. Tucek, S. Spyridi and T. Bakas, *J. Nanopart. Res.*, 2012, **14**, 1130.
46. D. Maity, G. Zoppellaro, V. Sedenkova, J. Tucek, K. Safarova, K. Polakova, K. Tomankova, C. Diwocky, R. Stollberger, L. Machala and R. Zboril, *Chem. Commun.*, 2012, **48**, 11398-11400.
47. X. Pang, L. Zhao, W. Han, X. Xin and Z. Lin, *Nat. Nano*, 2013, **8**, 426-431.
48. D. Wang and Y. Li, *Adv. Mater.*, 2011, **23**, 1044-1060.
- 10 49. J. Kitchin, J. Nørskov, M. Barteau and J. Chen, *Phys. Rev. Lett.*, 2004, **93**, 156801.
50. W. Cha, N. C. Jeong, S. Song, H.-j. Park, P. Tung Cao Thanh, R. Harder, B. Lim, G. Xiong, D. Ahn, I. McNulty, J. Kim, K. B. Yoon, I. K. Robinson and H. Kim, *Nature Mater.*, 2013, **12**, 729-734.
51. L. Adjianto, D. A. Bennett, C. Chen, A. S. Yu, M. Cargnello, P. Fornasiero, R. J. Gorte and J. M. Vohs, *Nano Lett.*, 2013, **13**, 2252-2257.
- 15 52. H. Wang, H. Guo, Y. Dai, D. Geng, Z. Han, D. Li, T. Yang, S. Ma, W. Liu and Z. Zhang, *Appl. Phys. Lett.*, 2012, **101**, 083116-083114.
53. S. Laurent, D. Forge, M. Port, A. Roch, C. Robic, L. Vander Elst and R. N. Muller, *Chem. Rev.*, 2008, **108**, 2064-2110.
54. X. Gong, S. Peng, W. Wen, P. Sheng and W. Li, *Adv. Funct. Mater.*, 2009, **19**, 292-297.
55. W. S. Seo, J. H. Lee, X. Sun, Y. Suzuki, D. Mann, Z. Liu, M. Terashima, P. C. Yang, M. V. McConnell, D. G. Nishimura and H. Dai, *Nat. Mater.*, 2006, **5**, 971-976.
- 20 56. J. Zhang, Y. Tang, K. Lee and M. Ouyang, *Nature*, 2010, **466**, 91-95.
57. X. Yu, J. Wan, Y. Shan, K. Chen and X. Han, *Chem. Mater.*, 2009, **21**, 4892-4898.
58. L. Wang, C. s. Clavero, Z. Huba, K. J. Carroll, E. E. Carpenter, D. Gu and R. A. Lukaszew, *Nano Lett.*, 2011, **11**, 1237-1240.
- 25 59. D. L. Peng, K. Sumiyama, T. J. Konno, T. Hihara and S. Yamamuro, *Phys. Rev. B.*, 1999, **60**, 2093-2100.
60. S. Yamamuro, K. Yamamoto, D. L. Peng, T. Hirayama and K. Sumiyama, *Appl. Phys. Lett.*, 2007, **90**, 242510.
61. R. Katoh, T. Hihara, D. L. Peng and K. Sumiyama, *Appl. Phys. Lett.*, 2005, **87**, 252501.
62. D. L. Peng, T. Hihara, K. Sumiyama and H. Morikawa, *J. Appl. Phys.*, 2002, **92**, 3075.
63. H. D. She, Y. Z. Chen, X. Z. Chen, K. Zhang, Z. Y. Wang and D. L. Peng, *J. Mater. Chem.*, 2012, **22**, 2757-2765.
- 30 64. H. Ow, D. R. Larson, M. Srivastava, B. A. Baird, W. W. Webb and U. Wiesner, *Nano Lett.*, 2005, **5**, 113-117.
65. F. Zhang, G. B. Braun, Y. Shi, Y. Zhang, X. Sun, N. O. Reich, D. Zhao and G. Stucky, *J. Am. Chem. Soc.*, 2010, **132**, 2850-2851.
66. L. A. Fredin, Z. Li, M. A. Ratner, M. T. Lanagan and T. J. Marks, *Adv. Mater.*, 2012, **24**, 5946-5953.
67. B. Shah, P. T. Yin, S. Ghoshal and K.-B. Lee, *Angew. Chem. Int. Ed.*, 2013, **52**, 6190-6195.
- 35 68. Z. Markova, A. B. Bourlinos, K. Safarova, K. Polakova, J. Tucek, I. Medrik, K. Siskova, J. Petr, M. Krysmann, E. P. Giannelis and R. Zboril, *J. Mater. Chem.*, 2012, **22**, 16219-16223.
69. M. M. Maye, J. Luo, L. Han, N. N. Kariuki and C. J. Zhong, *Gold Bulletin*, 2003, **36**, 75-82.
70. N. V. Long, Y. Yang, C. Minh Thi, N. V. Minh, Y. Cao and M. Nogami, *Nano Energy*, 2013, **2**, 636-676.
71. C.-Y. Wu, Y.-T. Liu, P.-C. Huang, T.-J. Mark Luo, C.-H. Lee, Y.-W. Yang, T.-C. Wen, T.-Y. Chen and T.-L. Lin, *Nanoscale*, 2013, **5**, 9181-9192.
- 40 72. J.-H. Lin and V. V. Gulians, *Appl. Catal. A. Gen.*, 2012, **445-446**, 187-194.
73. Y. Chen, B. Zhu, M. Yao, S. Wang and S. Zhang, *Catal. Commun.*, 2010, **11**, 1003-1007.
74. G. Huizhang Y. Chen, X. Chen, R. Wen, G.-Hui Yue, D.L. Peng, *Nanotechnol.*, 2011, **22**, 195604.
75. J.-M. Yan, X.-B. Zhang, T. Akita, M. Haruta and Q. Xu, *J. Am. Chem. Soc.*, 2010, **132**, 5326-5327.
- 45 76. H. Wang, M. Miyauchi, Y. Ishikawa, A. Pyatenko, N. Koshizaki, Y. Li, L. Li, X. Li, Y. Bando and D. Golberg, *J. Am. Chem. Soc.*, 2011, **133**, 19102-19109.
77. C. J. Zhong and M. M. Maye, *Adv. Mater.*, 2001, **13**, 1507-1511.
78. C. F. Zhou, Z. W. Liu, X. S. Du, D. R. G. Mitchell, Y. W. Mai, Y. S. Yan and S. Ringer, *Nanoscale Res. Lett.*, 2012, **7**, 1-11.
- 50 79. H. Peng, L. Xu, L. Zhang, K. Zhang, Y. Liu, H. Wu and P. Wu, *J. Mater. Chem.*, 2012, **22**, 14219-14227.
80. Z. Zhang, H. Che, Y. Wang, J. Gao, Y. Ping, Z. Zhong and F. Su, *Chem. Eng. J.*, 2012, **211**, 421-431.
81. T.-Y. Chen, T.-J. M. Luo, Y.-W. Yang, Y.-C. Wei, K.-W. Wang, T.-L. Lin, T.-C. Wen and C. H. Lee, *J. Phys. Chem. C*, 2012, **116**, 16969-16978.
82. Q. Tan, C. Du, G. Yin, P. Zuo, X. Cheng and M. Chen, *J. Catal.*, 2012, **295**, 217-222.
- 55 83. S. U. Son, Y. Jang, J. Park, H. B. Na, H. M. Park, H. J. Yun, J. Lee and T. Hyeon, *J. Am. Chem. Soc.*, 2004, **126**, 5026-5027.
84. D. Wang, H. L. Xin, H. Wang, Y. Yu, E. Rus, D. A. Muller, F. J. DiSalvo and H. D. Abruña, *Chem. Mater.*, 2012, **24**, 2274-2281.
85. Y. Xu, A. V. Ruban and M. Mavrikakis, *J. Am. Chem. Soc.*, 2004, **126**, 4717-4725.
- 60 86. B. Hammer and J. K. Nørskov, in *Advances in Catalysis*, ed. H. K. Bruce C. Gates, Academic Press, 2000, vol. 45, pp. 71-129.

87. F. Studt, F. Abild-Pedersen, Q. Wu, A. D. Jensen, B. Temel, J.-D. Grunwaldt and J. K. Nørskov, *J. Catal.*, 2012, **293**, 51-60.
88. M. Mavrikakis, B. Hammer and J. K. Nørskov, *Phys. Rev. Lett.*, 1998, **81**, 2819-2822.
89. B. Hammer, L. B. Hansen and J. K. Nørskov, *Phys. Rev. B.*, 1999, **59**, 7413-7421.
90. A. Ruban, B. Hammer, P. Stoltze, H. L. Skriver and J. K. Nørskov, *J. Mol. Catal. A: Chem.*, 1997, **115**, 421-429.
91. J. R. Kitchin, J. K. Nørskov, M. A. Barteau and J. G. Chen, *Phys. Rev. Lett.*, 2004, **93**, 156801.
92. W. Tang and G. Henkelman, *J. Chem. Phys.*, 2009, **130**, 194504-194506.
93. J. Wang, D. M. Do, G. K. Chuah and S. Jaenicke, *ChemCatChem*, 2013, **5**, 247-254.
94. K. Tedsree, T. Li, S. Jones, C. W. A. Chan, K. M. K. Yu, P. A. J. Bagot, E. A. Marquis, G. D. W. Smith and S. C. E. Tsang, *Nat. Nano.*, 2011, **6**, 302-307.
95. P. Strasser, S. Koh, T. Anniyev, J. Greeley, K. More, C. Yu, Z. Liu, S. Kaya, D. Nordlund, H. Ogasawara, M. F. Toney and A. Nilsson, *Nat. Chem.*, 2010, **2**, 454-460.
96. D. Wang and Y. Li, *J. Am. Chem. Soc.*, 2010, **132**, 6280-6281.
97. H. Z. Guo, Y. Z. Chen, X. Z. Chen, R. T. Wen, G. H. Yue and D. L. Peng, *Nanotechnol.*, 2011, **22**, 195604.
98. M. B. Gawande, H. Guo, A. K. Rathi, P. S. Branco, Y. Chen, R. S. Varma and D.-L. Peng, *RSC Adv.*, 2013, **3**, 1050-1054.
99. T. M. Ruhland, J. R. V. Lang, H. G. Alt and A. H. E. Müller, *E. J. Inorg. Chem.*, 2013, **2013**, 2146-2153.
100. A. Schätz, O. Reiser and W. J. Stark, *Chem. Eur. J.*, 2010, **16**, 8950-8967.
101. Z. Xu, Y. Hou and S. Sun, *J. Am. Chem. Soc.*, 2007, **129**, 8698-8699.
102. C. G. Tan and R. N. Grass, *Chem. Commun.*, 2008, **0**, 4297-4299.
103. T. Zhou, M. Lu, Z. Zhang, H. Gong, W. S. Chin and B. Liu, *Adv. Mater.*, 2010, **22**, 403-406.
104. T. Yao, T. Cui, J. Wu, Q. Chen, X. Yin, F. Cui and K. Sun, *Carbon*, 2012, **50**, 2287-2295.
105. Q. Zhang, I. Lee, J. B. Joo, F. Zaera and Y. Yin, *Acc. Chem. Res.*, 2012, **46**, 1816-1824.
106. T. M. Ruhland, J. R. V. Lang, H. G. Alt and A. H. E. Mueller, *Eur. J. Inorg. Chem.*, 2013, 2146-2153.
107. S. B. Kalidindi, U. Sanyal and B. R. Jagirdar, *Phys. Chem. Chem. Phys.*, 2008, **10**, 5870-5874.
108. L. Y. Wang, H. Y. Park, S. I. I. Lim, M. J. Schadt, D. Mott, J. Luo, X. Wang and C. J. Zhong, *J. Mater. Chem.*, 2008, **18**, 2629-2635.
109. X. Zhang and Z. Su, *Adv. Mater.*, 2012, **24**, 4574-4577.
110. J. Liu, X. Wei, Y. Yu, J. Song, X. Wang, A. Li, X.-W. Liu and W.-Q. Deng, *Chem. Commun.*, 2010, **46**, 1670-1672.
111. H.-L. Jiang, T. Akita and Q. Xu, *Chem. Commun.*, 2011, **47**, 10999-11001.
112. J. Wang, D. Dong-Minh, G.-K. Chuah and S. Jaenicke, *ChemCatChem*, 2013, **5**, 247-254.
113. S. Alayoglu and B. Eichhorn, *J. Am. Chem. Soc.*, 2008, **130**, 17479-17486.
114. J. X. Wang, H. Inada, L. Wu, Y. Zhu, Y. Choi, P. Liu, W.-P. Zhou and R. R. Adzic, *J. Am. Chem. Soc.*, 2009, **131**, 17298-17302.
115. M. Cargnello, M. Grzelczak, B. Rodriguez-Gonzalez, Z. Syrgiannis, K. Bakhmutsky, V. La Parola, L. M. Liz-Marzan, R. J. Gorte, M. Prato and P. Fornasiero, *J. Am. Chem. Soc.*, 2012, **134**, 11760-11766.
116. X. Cui, S. Wu, S. Jungwirth, Z. Chen, Z. Wang, L. Wang and Y. Li, *Nanotechnol.*, 2013, **24**, 295402.
117. J. Wang, Y.-L. Qin, X. Liu and X.-B. Zhang, *J. Mater. Chem.*, 2012, **22**, 12468-12470.
118. X. Guo, Q. Zhang, Y. H. Sun, Q. Zhao and J. Yang, *ACS Nano*, 2012, **6**, 1165-1175.
119. H. Wang, L. Chen, Y. Feng and H. Chen, *Acc. Chem. Res.*, 2013, **46**, 1636-1646.
120. T. Mitsudome and K. Kaneda, *ChemCatChem*, 2013, **5**, 1681-1691.
121. J.-H. Lin and V. V. Gulians, *Appl. Catal. A: Gen.*, 2012, **445**, 187-194.
122. R. Ghosh Chaudhuri and S. Paria, *Chem. Rev.*, 2011, **112**, 2373-2433.
123. D. X. Li, Q. He and J. B. Li, *Adv. Colloid Interface Sci.*, 2009, **149**, 28-38.
124. H. Zou, S. S. Wu and J. Shen, *Chem. Rev.*, 2008, **108**, 3893-3957.
125. C. Sanchez, B. Julian, P. Belleville and M. Popall, *J. Mater. Chem.*, 2005, **15**, 3559-3592.
126. W. Schartl, *Adv. Mater.*, 2000, **12**, 1899-1908.
127. R. Hao, R. J. Xing, Z. C. Xu, Y. L. Hou, S. Gao and S. H. Sun, *Adv. Mater.*, 2010, **22**, 2729-2742.
128. P. Reiss, M. Protiere and L. Li, *Small*, 2009, **5**, 154-168.
129. W. Schartl, *Nanoscale*, 2010, **2**, 829-843.
130. F. Caruso, *Adv. Mater.*, 2001, **13**, 11-22.
131. T. Mitsudome and K. Kaneda, *ChemCatChem*, **5**, 1681-1691.
132. H. Wang, L. Chen, Y. Feng and H. Chen, *Acc. Chem. Res.*, 2013, **46**, 1636-1646.
133. W. Li and D. Zhao, *Adv. Mater.*, 2013, **25**, 142-149.
134. W. W. Feng, Z. J. Fang, J. M. Yang, B. H. Zheng and Y. H. Jiang, *Carbohydr. Res.*, 2011, **346**, 352-356.
135. K. S. Kumar, V. B. Kumar and P. Paik, *J. Nanopart.*, 2013, **2013**, 24.
136. R. Silva, D. Voiry, M. Chhowalla and T. Asefa, *J. Am. Chem. Soc.*, 2013, **135**, 7823-7826.
137. S. Yoon and A. Manthiram, *J. Phys. Chem. C*, 2011, **115**, 9410-9416.
138. J. Shi, Z. Xiao, A. R. Votruba, C. Vilos and O. C. Farokhzad, *Angew. Chem. Int. Ed.*, 2011, **50**, 7027-7031.
139. H. Guo, R. Mao, D. Tian, W. Wang, D. Zhao, X. Yang and S. Wang, *J. Mater. Chem. A.*, 2013, **1**, 3652-3658.
140. Y. Chen, H. Chen, D. Zeng, Y. Tian, F. Chen, J. Feng and J. Shi, *ACS Nano*, 2010, **4**, 6001-6013.
141. W. Stöber, A. Fink and E. Bohn, *J. Colloid Interface Sci.*, 1968, **26**, 62-69.

142. D. Channei, B. Inceesungvorn, N. Wetchakun and S. Phanichphant, *J. Nanosci. Nanotechnol.*, 2014, **14**, 7756-7762.
143. H. Hoshi, W. Hao, Y. Fujita, A. Funayama, Y. Miyauchi, K. Hashimoto, K. Miyamoto, R. Iwasaki, Y. Sato, T. Kobayashi, H. Miyamoto, S. Yoshida, T. Mori, H. Kanagawa, E. Katsuyama, A. Fujie, K. Kitagawa, K. I. Nakayama, T. Kawamoto, M. Sano, K. Fukuda, I. Ohsawa, S. Ohta, H. Morioka, M. Matsumoto, K. Chiba, Y. Toyama and T. Miyamoto, *J. Bone Miner. Res.*, 2012, **27**, 2015-2023.
144. W. Gao, Y. Zhao, H. Chen, H. Chen, Y. Li, S. He, Y. Zhang, M. Wei, D. G. Evans and X. Duan, *Green Chem.*, 2015, **17**, 1525-1534.
145. M. Ristov, G. J. Sinadinovski and I. Grozdanov, *Thin Solids Films*, 1985, **123**, 63.
146. Y. F. Nicolau, *Appl. Surf. Sci.*, 1985, **22/23**, 1061.
147. V. P. Tolstoy, *Russ. Chem. Rev.*, 2006, **75**, 161.
148. H. Su, H. Xu, S. Gao, J. D. Dixon, Z. P. Aguilar, A. Y. Wang, J. Xu and J. Wang, *Nanoscale Res. Lett.*, 2010, **5**, 625-630.
149. J. Wei, A. Du, F. Jin, Z. Wang and X. Liu, *J. Magn. Magn. Mater.*, 2013, **340**, 70-75.
150. Y.-J. Chen, P. Gao, R.-X. Wang, C.-L. Zhu, L.-J. Wang, M.-S. Cao and H.-B. Jin, *J. Phys. Chem. C*, 2009, **113**, 10061-10064.
151. Y. Liu and Z. Tang, *Adv. Mater.*, 2013, **25**, 5819-5825.
152. W. Cha, N. C. Jeong, S. Song, H.-j. Park, T. C. Thanh Pham, R. Harder, B. Lim, G. Xiong, D. Ahn, I. McNulty, J. Kim, K. B. Yoon, I. K. Robinson and H. Kim, *Nat Mater*, 2013, **12**, 729-734.
153. S. Kandambeth, V. Venkatesh, D. B. Shinde, S. Kumari, A. Halder, S. Verma and R. Banerjee, *Nat Commun*, 2015, **6**, doi:10.1038/ncomms7786.
154. N. Zhang and Y.-J. Xu, *Chem. Mater.*, 2013, **25**, 1979-1988.
155. H. Guo, D. Tian, L. Liu, Y. Wang, Y. Guo and X. Yang, *J. Solid State Chem.*, 2013, **201**, 137-143.
156. S. Yoon and A. Manthiram, *J. Phys. Chem. C*, 2011, **115**, 9410-9416.
157. Q. Zhao, T. Tan, P. Qi, S. Wang, S. Bian, X. Li, Y. An and Z. Liu, *Appl. Surf. Sci.*, 2011, **257**, 3499-3503.
158. T. Tan, S. Wang, S. Bian and X. Li, *Adv. Mater. Res.*, 2009, **79-82**, 385-388.
159. S. Chandren and B. Ohtani, *J. Photochem. Photobiol. A*, 2012, **246**, 50-59.
160. S. Chandren and B. Ohtani, *Chem. Lett.*, 2012, **41**, 677-679.
161. J. Pan and F. Du, *Mater. Lett.*, 2009, **63**, 2126-2128.
162. X.-H. Zhang, X. Yi, J. Zhang, Z. Xie, J. Kang and L. Zheng, *Inorg. Chem.*, 2010, **49**, 10244-10246.
163. J. Yao, Y. Huang and H. Wang, *J. Mater. Chem.*, 2010, **20**, 9827-9831.
164. B. Yao, M. Liu, Z. Ma and C. Wang, *Adv. Mater. Res.*, 2011, **148-149**, 1331-1338.
165. K. Zhang, D. Q. Zhang, J. Liu, K. X. Ren, H. Luo, Y. J. Peng, G. S. Li and X. B. Yu, *CrystEngComm*, 2012, **14**, 700-707.
166. D. Han, P. Xu, X. Jing, J. Wang, D. Song, J. Liu and M. Zhang, *J. Solid State Chem.*, 2013, **203**, 60-67.
167. C. Guan, X. Xia, N. Meng, Z. Zeng, X. Cao, C. Soci, H. Zhang and H. J. Fan, *Energy Environ. Sci.*, 2012, **5**, 9085-9090.
168. R. Qiao, X. L. Zhang, R. Qiu, J. C. Kim and Y. S. Kang, *Chem. Eur. J.*, 2009, **15**, 1886-1892.
169. J. Cao and T. Matsoukas, *J. Nanopart. Res.*, 2004, **6**, 447-455.
170. Q. Xie, Y. Zhao, X. Chen, H. Liu, D. G. Evans and W. Yang, *Biomater.*, 2011, **32**, 6588-6594.
171. S.-W. Cao, Y.-J. Zhu, G.-F. Cheng and Y.-H. Huang, *J. Phys. Chem. Solids*, 2010, **71**, 1680-1683.
172. S.-W. Cao and Y.-J. Zhu, *J. Phys. Chem. C*, 2008, **112**, 12149-12156.
173. W. Wu, S. Zhang, F. Ren, X. Xiao, J. Zhou and C. Jiang, *Nanoscale*, 2011, **3**, 4676-4684.
174. N. S. Kim and J.-D. Kim, *J. Ind. Eng. Chem.*, 2012, **18**, 1721-1729.
175. Z. Li, X. Lai, H. Wang, D. Mao, C. Xing and D. Wang, *J. Phys. Chem. C*, 2009, **113**, 2792-2797.
176. F. Ye, H. Liu, J. Yang, H. Cao and J. Yang, *Dalton Trans.*, 2013, **42**, 12309-12316.
177. Y. Jiang, Y. Lu, D. Han, Q. Zhang and L. Niu, *Nanotechnol.*, 2012, **23**, 105609.
178. H. M. Song, D. H. Anjum, R. Sougrat, M. N. Hedhili and N. M. Khashab, *J. Mater. Chem.*, 2013, **22**, 25003-25010.
179. Y. Ding, B. Jin, G. Gu and X.-H. Xia, *J. Mater. Chem.*, 2009, **19**, 9141-9146.
180. Y. Ding and X.-H. Xia, *J. Nanosci. Nanotechnol.*, 2008, **8**, 1512-1517.
181. J. Li and H. C. Zeng, *Angew. Chem. Int. Ed.*, 2005, **44**, 4342-4345.
182. X. Li and L. Zhi, *Nanoscale*, 2013, **5**, 8864-8873 and references therein.
183. X. Li, P. Meduri, X. Chen, W. Qi, M. H. Engelhard, W. Xu, F. Ding, J. Xiao, W. Wang, C. Wang, J.-G. Zhang and J. Liu, *J. Mater. Chem.*, 2012, **22**, 11014-11017.
184. J. Wang, Y. Yu, L. Gu, C. Wang, K. Tang and J. Maier, *Nanoscale*, 2013, **5**, 2647-2650.
185. T. J. Longson, R. Bhowmick, C. Gu and B. A. Cruden, *J. Phys. Chem. C*, 2011, **115**, 12742-12750.
186. H. Guo, R. Mao, D. Tian, W. Wang, D. Zhao, X. Yang and S. Wang, *J. Mater. Chem. A*, 2013, **1**, 3652-3658.
187. Y. Yu, L. Gu, C. Wang, A. Dhanabalan, A. P. A. van and J. Maier, *Angew. Chem., Int. Ed.*, 2009, **48**, 6485-6489.
188. Q. Chen and K. Sieradzki, *Nature Mater.*, 2013, **12**, 1102-1106.
189. P. Weda, B. Trzebiecka, A. Dworak and C. B. Tsvetanov, *Polymer*, 2008, **49**, 1467-1474.
190. J.-J. Shi, Z.-Y. Xiao, A. R. Votruba, C. Vilos and O. C. Farokhzad, *Angew. Chem. Int. Ed.*, 2011, **50**, 7027-7031.
191. X. Yang, L. Chen, B. Huang, F. Bai and X. Yang, *Polymer*, 2009, **50**, 3556-3563.
192. M. Sasidharan and K. Nakashima, *Acc. Chem. Res.*, 2013, **12**, 1102-1106.
193. X. He, X. Ge, H. Liu, M. Wang and Z. Zhang, *Chem. Mater.*, 2005, **17**, 5891-5892.

194. L. Yang, P.W. May, L. Yin, "Sequential nucleation and growth of complex nanostructures by a two-step strategy", Chapter 12 in *Nanotechnology Nanofabrication, Patterning and Self Assembly*, edited by C.J. Dixon and O.W. Curtines (Nova Science Publishers, Inc., New York, USA, 2010), pp.409-433.
195. J. Prasek, J. Drbohlavova, J. Chomoucka, J. Hubalek, O. Jasek, V. Adam and R. Kizek, *J. Mater. Chem.*, 2011, **21**, 15872-15884.
196. M. F. L. De Volder, S. H. Tawfick, R. H. Baughman and A. J. Hart, *Science*, 2013, **339**, 535-539.
197. M. Terrones, *Annu. Rev. Mater. Sci.*, 2003, **33**, 419-501.
198. D. S. Su, S. Perathoner and G. Centi, *Chem. Rev.*, 2013, **113**, 5782-5816.
199. G. Meyer, *Recueil des Travaux Chimiques des Pays-Bas*, 1992, **111**, 413-413.
200. A. A. Popov, S. Yang and L. Dunsch, *Chem. Rev.*, 2013, **113**, 5989-6113.
201. B. B. Zhang, B. D. Chen, Y. L. Wang, F. F. Guo, Z. Q. Li and D. L. Shi, *J. Colloid Interface Sci.*, 2011, **353**, 426-432.
202. J. Kim, H. Choi, C. Nahm, C. Kim, J. I. Kim, W. Lee, S. Kang, B. Lee, T. Hwang, H. H. Park and B. Park, *Appl. Phys. Lett.*, 2013, **102**, 183901-183904.
203. Y. Ma, B. Zhang, M. Gu, S. Huang, X. Liu, B. Liu and C. Ni, *J. Appl. Polym. Sci.*, 2013, **130**, 1548-1553.
204. J. Bomm, A. Buechtemann, A. J. Chatten, R. Bose, D. J. Farrell, N. L. A. Chan, Y. Xiao, L. H. Slooff, T. Meyer, A. Meyer, S. W. G. J. H. M. van Sark and R. Koole, *Sol. Energy Mater. Sol. Cells*, 2011, **95**, 2087-2094.
205. J. J. Li, A. Wang, W. Guo, J. C. Keay, T. D. Mishima, M. B. Johnson and X. Peng, *J. Am. Chem. Soc.*, 2003, **125**, 12567-12575.
206. S. Xu, H. Shen, C. Zhou, H. Yuan, C. Liu, H. Wang, L. Ma and L. S. Li, *J. Phys. Chem. C*, 2011, **115**, 20876-20881.
207. H. Shen, H. Yuan, J. Z. Niu, S. Xu, C. Zhou, L. Ma and L. S. Li, *Nanotechnol.*, 2011, **22**, 375602.
208. H. Shen, C. Zhou, S. S. Xu, C. Yu, H. Wang, X. Chen and L. S. Li, *J. Mater. Chem.*, 2011, **21**, 6046-6053.
209. H. Shen, H. Wang, C. Zhou, J. Z. Niu, H. Yuan, L. Ma and L. S. Li, *Dalton Trans.*, 2011, **40**, 9180-9188.
210. J. Y. Woo, S. K. Tripathy, K. Kim and C.-S. Han, *Appl. Phys. Lett.*, 2012, **100**, 063105.
211. P.-T. Jing, X. Yuan, W.-Y. Ji, M. Ikezawa, X.-Y. Liu, L.-G. Zhang, J.-L. Zhao and Y. Masumoto, *Appl. Phys. Lett.*, 2011, **99**, 093106.
212. P. Jing, J. Zheng, M. Ikezawa, X. Liu, S. Lv, X. Kong, J. Zhao and Y. Masumoto, *J. Phys. Chem. C*, 2009, **113**, 13545-13550.
213. Y. Chen, J. Vela, H. Htoon, J. L. Casson, D. J. Werder, D. A. Bussian, V. I. Klimov and J. A. Hollingsworth, *J. Am. Chem. Soc.*, 2008, **130**, 5026-5027.
214. Y. Fu, T. T. Han, H. Agren, L. Lin, P. Chen, Y. Liu, G. Q. Tang, J. Wu, Y. Yue and N. Dai, *Appl. Phys. Lett.*, 2007, **90**, 173102.
215. J. Lim, S. Jun, E. Jang, H. Baik, H. Kim and J. Cho, *Adv. Mater.*, 2007, **19**, 1927-1932.
216. R. Xie, U. Kolb, J. Li, T. Basche and A. Mews, *J. Am. Chem. Soc.*, 2005, **127**, 7480-7488.
217. E. J. McLaurin, V. A. Vlaskin and D. R. Gamelin, *J. Am. Chem. Soc.*, 2011, **133**, 14978-14980.
218. A. Cros-Gagneux, F. Delpéch, C. Nayral, A. Cornejo, Y. Coppel and B. Chaudret, *J. Am. Chem. Soc.*, 2010, **132**, 18147-18157.
219. K. Tateno, G. Zhang, H. Gotoh and T. Sogawa, *J. Nanotechnol.*, 2012, 890607, 890608pp.
220. X. Li, D. Shen, J. Yang, C. Yao, R. Che, F. Zhang and D. Zhao, *Chem. Mater.*, 2012, **25**, 106-112.
221. Y. Masumoto, K. Goto, S. Tomimoto, P. Mohan, J. Motohisa and T. Fukui, *J. Lumin.*, 2013, **133**, 135-137.
222. E. Nakai, M. Yoshimura, K. Tomioka and T. Fukui, *Jpn. J. Appl. Phys.*, 2013, **52**, 055002.
223. M. Yoshimura, E. Nakai, K. Tomioka and T. Fukui, *Appl. Phys. Express*, 2013, **6**, 052301.
224. Y. Masumoto, Y. Hirata, P. Mohan, J. Motohisa and T. Fukui, *Appl. Phys. Lett.*, 2011, **98**, 211902.
225. K. Tomioka, J. Motohisa, S. Hara, K. Hiruma and T. Fukui, *Nano Lett.*, 2010, **10**, 1639-1644.
226. Y. Masumoto, K. Goto, S. Yoshida, Y. Sakuma, P. Mohan, J. Motohisa and T. Fukui, *Phys. Rev. B: Condens. Matter Mater. Phys.*, 2010, **82**, 075313.
227. P. Mohan, J. Motohisa and T. Fukui, *Appl. Phys. Lett.*, 2006, **88**, 133105.
228. K. Tomioka, M. Yoshimura and T. Fukui, *Nature*, 2012, **488**, 189-192.
229. G. Mariani, Z. Zhou, A. Scofield and D. L. Huffaker, *Nano Lett.*, 2013, **13**, 1632-1637.
230. C. Gutsche, A. Lysov, D. Braam, I. Regolin, G. Keller, Z.-A. Li, M. Geller, M. Spasova, W. Prost and F.-J. Tegude, *Adv. Funct. Mater.*, 2012, **22**, 929-936.
231. F. Qian, S. Gradecak, Y. Li, C.-Y. Wen and C. M. Lieber, *Nano Lett.*, 2005, **5**, 2287-2291.
232. H. Ko, Z. Zhang, Y.-L. Chueh, E. Saiz and A. Javey, *Angew. Chem., Int. Ed.*, 2010, **49**, 616-619.
233. D. Ruzmetov, V. P. Oleshko, P. M. Haney, H. J. Lezec, K. Karki, K. H. Baloch, A. K. Agrawal, A. V. Davydov, S. Krylyuk, Y. Liu, J. Y. Huang, M. Tanase, J. Cumings and A. A. Talin, *Nano Lett.*, 2012, **12**, 505-511.
234. S. A. Dayeh, A. V. Gin and S. T. Picraux, *Appl. Phys. Lett.*, 2011, **98**, 163112.
235. S. A. Dayeh, N. H. Mack, J.-Y. Huang and S. T. Picraux, *Appl. Phys. Lett.*, 2011, **99**, 023102.
236. M. Ben-Ishai and F. Patolsky, *Adv. Mater.*, 2009, **22**, 902-906.
237. I. M. Ben and F. Patolsky, *Angew. Chem., Int. Ed.*, 2009, **48**, 8699-8702.
238. T. J. Kempa, J. F. Cahoon, S.-K. Kim, R. W. Day, D. C. Bell, H.-G. Park and C. M. Lieber, *Proc. Natl. Acad. Sci. U. S. A.*, 2012, **109**, 1407-1412.
239. J. H. Shen, Y. H. Zhu, X. L. Yang, J. Zong and C. Z. Li, *Langmuir*, 2013, **29**, 690-695.

240. I. Y. Stetciura, A. V. Markin, A. N. Ponomarev, A. V. Yakimansky, T. S. Demina, C. Grandfils, D. V. Volodkin and D. A. Gorin, *Langmuir*, 2013, **29**, 4140-4147.
241. B. Peng, Q. Zhang, X. Liu, Y. Ji, H. V. Demir, C. H. A. Huan, T. C. Sum and Q. Xiong, *ACS Nano*, 2012, **6**, 6250-6259.
- 5 242. L. Catal, D. Brinzei, Y. Prado, A. Gloter, O. Stephan, G. Rogez and T. Mallah, *Angew. Chem. Int. Ed.*, 2009, **48**, 183-187.
243. N. Dia, L. Lisnard, Y. Prado, A. Gloter, O. Stephan, F. Brisset, H. Hafez, Z. Saad, C. Mathoniere, L. Catala and T. Mallah, *Inorg. Chem.*, 2013, **52**, 10264-10274.
244. L. Catala, D. Brinzei, Y. Prado, A. Gloter, O. Stéphan, G. Rogez and T. Mallah, *Angew. Chem. Int. Ed.*, 2009, **48**, 183-187.
- 10 245. K. X. Yao and H. C. Zeng, *J. Phys. Chem. C*, 2009, **113**, 1373-1385.
246. F. Wang, L.-D. Sun, W. Feng, H. Chen, M. H. Yeung, J. Wang and C.-H. Yan, *Small*, 2010, **6**, 2566-2575.
247. B. Rodriguez-Gonzalez, V. Salgueirino-Maceira, F. Garcia-Santamaria and L. M. Liz-Marzan, *Nano Lett.*, 2002, **2**, 471-473.
- 15 248. Z. Chen, Z. L. Wang, P. Zhan, J. H. Zhang, W. Y. Zhang, H. T. Wang and N. B. Ming, *Langmuir*, 2004, **20**, 3042-3046.
249. A. Knauer, A. Thete, S. Li, H. Romanus, A. Csaki, W. Fritzsche and J. M. Koehler, *Chem. Eng. J.*, 2011, **166**, 1164-1169.
250. A. Ray, Y.-E. K. Lee, G. Kim and R. Kopelman, *Small*, 2012, **8**, 2213-2221.
251. M. A. Quadir, M. R. Radowski, F. Kratz, K. Licha, P. Hauff and R. Haag, *J. Controlled Release*, 2008, **132**, 289-294.
- 20 252. S. Kuechler, M. R. Radowski, T. Blaschke, M. Dathe, J. Plendl, R. Haag, M. Schaefer-Korting and K. D. Kramer, *Eur. J. Pharm. Biopharm.*, 2009, **71**, 243-250.
253. J. Keilitz, M. R. Radowski, J.-D. Marty, R. Haag, F. Gauffre and C. Mingotaud, *Chem. Mater.*, 2008, **20**, 2423-2425.
254. C. Treiber, Q. M. Abdul, P. Voigt, M. Radowski, S. Xu, L.-M. Munter, T. A. Bayer, M. Schaefer, R. Haag and G. Multhaup, *Biochem.*, 2009, **48**, 4273-4284.
- 25 255. S. Saliba, C. V. Serrano, J. Keilitz, M. L. Kahn, C. Mingotaud, R. Haag and J. D. Marty, *Chem. Mater.*, 2010, **22**, 6301-6309.
256. M. Schwarze, J. Keilitz, S. Nowag, R. Y. Parapat, R. Haag and R. Schomacker, *Langmuir*, 2011, **27**, 6511-6518.
257. E. Fleige, B. Ziem, M. Grabolle, R. Haag and U. Resch-Genger, *Macromolecules*, 2012, **45**, 9452-9459.
258. J. Keilitz, M. Schwarze, S. Nowag, R. Schomaecker and R. Haag, *ChemCatChem*, 2010, **2**, 863-870.
- 30 259. S. Nowag, X.-S. Wang, J. Keilitz, A. Thomas and R. Haag, *ChemCatChem*, 2010, **2**, 807-811.
260. J. Keilitz, S. Nowag, J.-D. Marty and R. Haag, *Adv. Synth. Catal.*, 2010, **352**, 1503-1511.
261. N. Nagae and T. Tsukamoto, *Chromatogr.*, 2013, **34**, 41-47.
262. K. Lomsadze, G. Jibuti, T. Farkas and B. Chankvetadze, *J. Chromatogr. A*, 2012, **1234**, 50-55.
263. S. Fanali, G. D'Orazio, T. Farkas and B. Chankvetadze, *J. Chromatogr. A*, 2012, **1269**, 136-142.
- 35 264. F. Griitti, N. Tanaka and G. Guiochon, *J. Chromatogr. A*, 2012, **1236**, 28-41.
265. G. D'Orazio, S. Rocchi and S. Fanali, *J. Chromatogr. A*, 2012, **1255**, 277-285.
266. A. V. Biradar, A. A. Biradar and T. Asefa, *Langmuir*, 2011, **27**, 14408-14418.
267. Y.-L. Shi and T. Asefa, *Langmuir*, 2007, **23**, 9455-9462.
268. S. Das and T. Asefa, *Top. Catal.*, 2012, **55**, 587-594.
- 40 269. J.-S. Yu, S. B. Yoon, Y. J. Lee and K. B. Yoon, *J. Phys. Chem. B*, 2005, **109**, 7040-7045.
270. J.-S. Yu, *Rev. Adv. Mater. Sci.*, 2005, **10**, 341-346.
271. J.-R. Song, L.-X. Wen, L. Shao and J.-F. Chen, *Appl. Surf. Sci.*, 2006, **253**, 2678-2684.
272. Y. J. Chen, P. Gao, C. L. Zhu, R. X. Wang, L. J. Wang, M. S. Cao and X. Y. Fang, *J. Appl. Phys.*, 2009, **106**, 054303.
273. L.-H. Qian, Y. Ding, T. Fujita and M.-W. Chen, *Langmuir*, 2008, **24**, 4426-4429.
- 45 274. N. Du, Y. Chen, C. Zhai, H. Zhang and D. Yang, *Nanoscale*, 2013, **5**, 4744-4750.
275. X. Li, A. Dhanabalan, K. Bechtold and C. Wang, *Electrochem. Commun.*, 2010, **12**, 1222-1225.
276. X. Song, L. Gao and S. Mathur, *J. Phys. Chem. C*, 2011, **115**, 21730-21735.
277. L. Kuai, B. Geng, S. Wang and Y. Sang, *Chem. Eur. J.*, 2012, **18**, 9423-9429
278. C. Song, J. Du, J. Zhao, S. Feng, G. Du and Z. Zhu, *Chem. Mater.*, 2009, **21**, 1524-1530.
- 50 279. M. Gulfam, J.-M. Lee, J.-E. Kim, D.-W. Lim, E.-K. Lee and B.-G. Chung, *Langmuir*, 2011, **27**, 10993-10999.
280. X. Li, A. Dhanabalan, L. Gu and C. Wang, *Adv. Energy Mater.*, 2012, **2**, 238-244.
281. M. Hasan, S. B. Newcomb and K. M. Razeeb, *J. Electrochem. Soc.*, 2012, **159**, F203-F209.
282. X. Xia, J. Tu, Y. Zhang, X. Wang, C. Gu, X.-b. Zhao and H. J. Fan, *ACS Nano*, 2012, **6**, 5531-5538.
283. J. B. Wu, Z. G. Li, X. H. Huang and Y. Lin, *J. Power Sources*, 2012, **224**, 1-5.
- 55 284. D. Lu, L. Yang, Z. Tian, L. Wang and J. Zhang, *RSC Adv.*, 2012, **2**, 2783-2789.
285. A. Abbaspourrad, N. J. Carroll, S.-H. Kim and D. A. Weitz, *Adv. Mater.*, 2013, **25**, 3215-3221.
286. G. Van Tendeloo, S. Bals, S. Van Aert, J. Verbeeck and D. Van Dyck, *Adv. Mater.*, 2012, **24**, 5655-5675.
287. M. Zhao, K. Deng, L. He, Y. Liu, G. Li, H. Zhao and Z. Tang, *J. Am. Chem. Soc.*, 2014, **136**, 1738-1741.
288. C. Zhang, S. Li, T. Wang, G. Wu, X. Ma and J. Gong, *Chem. Commun.*, 2013, **49**, 10647-10649.
- 60 289. P. Shen, H. T. Zhang, H. Liu, J. Y. Xin, L. F. Fei, X. G. Luo, R. Z. Ma and S. J. Zhang, *J. Mater. Chem. A.*, 2015, **3**, 3456-3464.
290. S. Prabhudev, M. Bugnet, C. Bock and G. A. Botton, *ACS Nano*, 2013, **7**, 6103-6110.

291. Y.-Z. Chen, Q. Xu, S.-H. Yu and H.-L. Jiang, *Small*, 2015, **11**, 71-76.
292. F. Ke, L. Wang and J. Zhu, *Nanoscale*, 2015, **7**, 1201-1208.
293. D. Llamasa, M. Ruano, L. Martinez, A. Mayoral, E. Roman, M. Garcia-Hernandez and Y. Huttel, *Nanoscale*, 2014, **6**, 13483-13486.
- 5 294. J. Li, Z. Huang, M. Yang, L. Tan, X. Zhang, H. Gao, Y. Tang, Q. Ma and G. Wang, *New J. Chem.*, 2015, **39**, 2949-2955.
295. H.-L. Jiang, T. Akita, T. Ishida, M. Haruta and Q. Xu, *J. Am. Chem. Soc.*, 2011, **133**, 1304-1306.
296. T. A. G. Silva, E. Teixeira-Neto, N. López and L. M. Rossi, *Sci. Rep.*, 2014, **4**, 5766.
297. H. Liu, K. Tao, C. Xiong and S. Zhou, *Catal. Sci. Technol.*, 2015, **5**, 405-414.
- 10 298. Y.-Z. Chen, Q. Xu, S.-H. Yu and H.-L. Jiang, *Small*, 2015, **11**, doi: 10.1002/smll.201570005.
299. G. W. Kabalka and R. S. Varma, *Comprehensive Organic Synthesis*, ed. B. M. Trost and I. Fleming, Pergamon Press, Oxford, 1991, vol. 1998, p. 1363.
300. M. B. Gawande, A. K. Rathi, P. S. Branco, I. D. Nogueira, A. Velhinho, J. J. Shrikhande, U. U. Indulkar, R. V. Jayaram, C. A. A. Ghumman, N. Bundaleski and O. M. N. D. Teodoro, *Chem. Eur. J.*, 2012, **18**, 12628-12632.
- 15 301. M. B. Gawande, A. K. Rathi, P. S. Branco, T. M. Potewar, A. Velhinho, I. D. Nogueira, A. Tolstogousov, C. A. A. Ghumman and O. M. N. D. Teodoro, *RSC Adv.*, 2013, **3**, 3611-3617.
302. T. Ikariya and A. J. Blacker, *Acc. Chem. Res.*, 2007, **40**, 1300-1308.
303. R. H. Morris, *Chem. Soc. Rev.*, 2009, **38**, 2282-2291.
304. V. Polshettiwar, B. Baruwati and R. S. Varma, *Green Chem.*, 2009, **11**, 127-131.
- 20 305. I. N. Michaelides and D. J. Dixon, *Angew. Chem. Int. Ed.*, 2013, **52**, 806-808.
306. M. Yan, T. Jin, Y. Ishikawa, T. Minato, T. Fujita, L. Y. Chen, M. Bao, N. Asao, M. W. Chen and Y. Yamamoto, *J. Am. Chem. Soc.*, 2012, **134**, 17536-17542.
307. H. U. Blaser, C. Malan, B. Pugin, F. Spindler, H. Steiner and M. Studer, *Adv. Syn. Catal.*, 2003, **345**, 103-151.
308. W. Q. Jiang, Y. F. Zhou, Y. L. Zhang, S. H. Xuan and X. L. Gong, *Dalton Trans.*, 2012, **41**, 4594-4601.
- 25 309. R. Hudson, A. Riviere, C. M. Cirtiu, K. L. Luska and A. Moores, *Chem. Commun.*, 2012, **48**, 3360-3362.
310. Y. Han, D. Peng, Z. Xu, H. Wan, S. Zheng and D. Zhu, *Chem. Commun.*, 2013, **49**, 8350-8352.
311. P. Zhang, Y. Hu, B. Li, Q. Zhang, C. Zhou, H. Yu, X. Zhang, L. Chen, B. Eichhorn and S. Zhou, *ACS Catal.*, 2015, **5**, 1335-1343.
312. T. Mitsudome, Y. Mikami, M. Matoba, T. Mizugaki, K. Jitsukawa and K. Kaneda, *Angew. Chem. Int. Ed.*, 2012, **51**, 136-139.
- 30 313. T. Mitsudome, M. Matoba, T. Mizugaki, K. Jitsukawa and K. Kaneda, *Chem. Eur. J.*, 2013, **19**, 5255-5258.
314. J. R. L. Burwell, *Chem. Rev.*, 1957, **57**, 895-934.
315. 309. T. Mitsudome, Y. Takahashi, S. Ichikawa, T. Mizugaki, K. Jitsukawa and K. Kaneda, *Angew. Chem. Int. Ed.*, 2013, **52**, 1481-1485.
- 35 316. Y. Takahashi, N. Hashimoto, T. Hara, S. Shimazu, T. Mitsudome, T. Mizugaki, K. Jitsukawa and K. Kaneda, *Chem. Lett.*, 2011, **40**, 405-407.
317. R. A. W. Johnstone, A. H. Wilby and I. D. Entwistle, *Chem. Rev.*, 1985, **85**, 129-170.
318. H. S. Zhang, R. H. Jin, H. Yao, S. Tang, J. L. Zhuang, G. H. Liu and H. X. Li, *Chem. Commun.*, 2012, **48**, 7874-7876.
319. S. Garcia, R. M. Anderson, H. Celio, N. Dahal, A. Dolocan, J. P. Zhou and S. M. Humphrey, *Chem. Commun.*, 2013, **49**, 4241-4243.
- 40 320. N. Dahal, S. Garcia, J. Zhou and S. M. Humphrey, *ACS Nano*, 2012, **6**, 9433-9446.
321. Y. Wang, A. V. Biradar and T. Asefa, *ChemSusChem*, 2012, **5**, 132-139.
322. F. Tao, M. E. Grass, Y. Zhang, D. R. Butcher, J. R. Renzas, Z. Liu, J. Y. Chung, B. S. Mun, M. Salmeron and G. A. Somorjai, *Science*, 2008, **322**, 932-934.
- 45 323. R. Ferrando, J. Jellinek and R. L. Johnston, *Chem. Rev.*, 2008, **108**, 845-910.
324. Y.-T. Kim, H. Lee, H.-J. Kim and T.-H. Lim, *Chem. Commun.*, 2010, **46**, 2085-2087.
325. X.-C. Huang, Y.-Y. Lin, J.-P. Zhang and X.-M. Chen, *Angew. Chem. Int. Ed.*, 2006, **45**, 1557-1559.
326. K. Hayakawa, T. Yoshimura and K. Esumi, *Langmuir*, 2003, **19**, 5517-5521.
327. Y. Lu, Y. Mei, M. Drechsler and M. Ballauff, *Angew. Chem. Int. Ed.*, 2006, **45**, 813-816.
- 50 328. S. Jana, S. K. Ghosh, S. Nath, S. Pande, S. Praharaj, S. Panigrahi, S. Basu, T. Endo and T. Pal, *Appl. Catal. A Gen.*, 2006, **313**, 41-48.
329. J. Lee, J. C. Park and H. Song, *Adv. Mater.*, 2008, **20**, 1523-1528.
330. Q. Zhang, T. Zhang, J. Ge and Y. Yin, *Nano Lett.*, 2008, **8**, 2867-2871.
331. Q. Fu, F. Yang and X. Bao, *Acc. Chem. Res.*, 2013, **46**, 1692-1701.
- 55 332. G. E. O'Mahony, A. Ford and A. R. Maguire, *J. Sulf. Chem.*, 2013, **34**, 301-341.
333. K. Kaczorowska, Z. Kolarska, K. Mitka and P. Kowalski, *Tetrahedron*, 2005, **61**, 8315-8327.
334. Z.-A. Qiao, P. Zhang, S.-H. Chai, M. Chi, G. M. Veith, N. C. Gallego, M. Kidder and S. Dai, *J. Am. Chem. Soc.*, 2014, **136**, 11260-11263.
335. M. Shokouhimehr, K.-Y. Shin, J. S. Lee, M. J. Hackett, S. W. Jun, M. H. Oh, J. Jang and T. Hyeon, *J. Mater. Chem. A.*, 2014, **2**, 7593-7599.
- 60 336. S. Okada, K. Mori, T. Kamegawa, M. Che and H. Yamashita, *Chem. Eur. J.*, 2011, **17**, 9047-9051.
337. R. Diaz, J. Arbiol, A. Cirera, F. Sanz, F. Peiro, A. Cornet and J. R. Morante, *Chem. Mater.*, 2001, **13**, 4362-4366.

338. L. S. Zhong, J. S. Hu, Z. M. Cui, L. J. Wan and W. G. Song, *Chem. Mater.*, 2007, **19**, 4557-4562.
339. Z. Chen, Z. M. Cui, F. Niu, L. Jiang and W. G. Song, *Chem. Commun.*, 2010, **46**, 6524-6526.
340. M. Barmatova, I. Ivanchikova, O. Kholdeeva, A. Shmakov, V. Zaikovskii and M. Mel'gunov, *Catal. Lett.*, 2009, **127**, 75-82.
- 5 341. F. Mi, X. Chen, Y. Ma, S. Yin, F. Yuan and H. Zhang, *Chem. Commun.*, 2011, **47**, 12804-12806.
342. H. Deng, X. L. Li, Q. Peng, X. Wang, J. P. Chen and Y. D. Li, *Angew. Chem. Int. Ed.*, 2005, **44**, 2782-2785.
343. T. Fan, D. Pan and H. Zhang, *Ind. Eng. Chem. Res.*, 2011, **50**, 9009-9018.
344. T. Mitsudome, A. Noujima, T. Mizugaki, K. Jitsukawa and K. Kaneda, *Adv. Syn. Catal.*, 2009, **351**, 1890-1896.
345. A. M. Henning, J. Watt, P. J. Miedziak, S. Cheong, M. Santonastaso, M. Song, Y. Takeda, A. I. Kirkland, S. H. Taylor and R. D. Tilley, *Angew. Chem. Int. Ed.*, 2013, **52**, 1477-1480.
- 10 346. D. I. Enache, J. K. Edwards, P. Landon, B. Solsona-Espriu, A. F. Carley, A. A. Herzing, M. Watanabe, C. J. Kiely, D. W. Knight and G. J. Hutchings, *Science*, 2006, **311**, 362-365.
347. J. Chen, J. Qi, G. Li, F. Zheng, S. Li and Z. Tang, *Chem. Asian J.*, 2013, **8**, 694-699.
348. M.-F. Luo, P. Fang, M. He and Y.-L. Xie, *J. Mol. Catal. A: Chem.*, 2005, **239**, 243-248.
- 15 349. X. G. Guo, Q. Fu, Y. X. Ning, M. M. Wei, M. R. Li, S. Zhang, Z. Jiang and X. H. Bao, *J. Am. Chem. Soc.*, 2012, **134**, 12350-12353.
350. C. Z. Wu, Z. Y. Lim, C. Zhou, W. G. Wang, S. H. Zhou, H. F. Yin and Y. J. Zhu, *Chem. Commun.*, 2013, **49**, 3215-3217.
351. C. T. Kresge, M. E. Leonowicz, W. J. Roth, J. C. Vartuli and J. S. Beck, *Nature*, 1992, **359**, 710-712.
- 20 352. E. F. Iliopoulou, *Curr. Org. Synth.*, 2010, **7**, 587-598.
353. A. Suzuki, *Angew. Chem. Int. Ed.*, 2011, **50**, 6722-6737.
354. A. Suzuki and Y. Yamamoto, *Chem. Lett.*, 2011, **40**, 894-901.
355. H. A. Wegner and M. Auzias, *Angew. Chem. Int. Ed.*, 2011, **50**, 8236-8247.
356. M. Arpad, *Chem. Rev.*, 2011, **111**, 2251-2320.
- 25 357. P.-P. Fang, A. Jutand, Z.-Q. Tian and C. Amatore, *Angew. Chem. Int. Ed.*, 2011, **50**, 12184-12188.
358. A. Suzuki, *J. Organomet. Chem.*, 1999, **576**, 147-168.
359. F. Alonso, I. P. Beletskaya and M. Yus, *Tetrahedron*, 2008, **64**, 3047-3101.
360. O. Metin, S. F. Ho, C. Alp, H. Can, M. N. Mankin, M. S. Gultekin, M. Chi and S. Sun, *Nano Res.*, 2013, **6**, 10-18.
361. H. Q. Yang, G. Li and Z. C. Ma, *J. Mater. Chem.*, 2012, **22**, 6639-6648.
- 30 362. R. Chinchilla and C. Najera, *Chem. Soc. Rev.*, 2011, **40**, 5084-5121.
363. L. Zhang and H. Wang, *ACS Nano*, 2011, **5**, 3257-3267.
364. Y. Sui, W. Fu, Y. Zeng, H. Yang, Y. Zhang, H. Chen, Y. Li, M. Li and G. Zou, *Angew. Chem. Int. Ed.*, 2010, **49**, 4282-4285.
365. J. H. Kou, A. Saha, C. Bennett-Stamper and R. S. Varma, *Chem. Commun.*, 2012, **48**, 5862-5864.
- 35 366. J. Kou, A. Saha, C. Bennett-Stamper and R. S. Varma, *Chem. Commun.*, 2012, **48**, 5862-5864.
367. F. Haber, Kaiserliches Patentamt DE235421, 1911.
368. S. F. Yin, B. Q. Xu, X. P. Zhou and C. T. Au, *Appl. Catal. A: Gen.*, 2004, **277**, 1-9.
369. M. Feyen, C. Weidenthaler, R. Guettel, K. Schlichte, U. Holle, A.-H. Lu and F. Schueth, *Chem. Eur. J.*, 2011, **17**, 598-605.
- 40 370. P. Li, C. Y. Cao, Z. Chen, H. Liu, Y. Yu and W. G. Song, *Chem. Commun.*, 2012, **48**, 10541-10543.
371. H. Wang, H. Y. Jeong, M. Imura, L. Wang, L. Radhakrishnan, N. Fujita, T. Castle, O. Terasaki and Y. Yamauchi, *J. Am. Chem. Soc.*, 2011, **133**, 14526-14529.
372. H. Wang, S. Ishihara, K. Ariga and Y. Yamauchi, *J. Am. Chem. Soc.*, 2012, **134**, 10819-10821.
373. L. Wang and Y. Yamauchi, *J. Am. Chem. Soc.*, 2013, **135**, 16762-16765.
- 45 374. L. Wang, Y. Nemoto and Y. Yamauchi, *J. Am. Chem. Soc.*, 2011, **133**, 9674-9677.
375. K. Bakhmutsky, N. L. Wieder, M. Cargnello, B. Galloway, P. Fornasiero and R. J. Gorte, *ChemSusChem*, 2012, **5**, 140-148.
376. M. Cargnello, N. L. Wieder, T. Montini, R. J. Gorte and P. Fornasiero, *J. Am. Chem. Soc.*, 2010, **132**, 1402-1409.
377. J. Otera, Esterification: Methods, Reaction and Applications; Wiley- VCH: Weinheim, Germany, 2003.
- 50 378. K. Suzuki, T. Yamaguchi, K. Matsushita, C. Iitsuka, J. Miura, T. Akaogi and H. Ishida, *ACS Catal.*, 2013, **3**, 1845-1849.
379. K. Sato, M. Aoki and R. Noyori, *Science*, 1998, **281**, 1646-1647.
380. A. Castellán, J. C. J. Bart and S. Cavallaro, *Catal. Today*, 1991, **9**, 237-254.
381. A. K. Patra, A. Dutta and A. Bhaumik, *Chem. Eur. J.*, 2013, **19**, 12388-12395.
382. J. H. Park, K. M. Choi, J. H. Choi, D. K. Lee, H. J. Jeon, H. Y. Jeong and J. K. Kang, *Chem. Commun.*, 2012, **48**, 11002-11004.
- 55 383. J. Eastoe, M. J. Hollamby and L. Hudson, *Adv. Colloid Interface Sci.*, 2006, **128**, 5-15.
384. F. Heshmatpour, R. Abazari and S. Balalaie, *Tetrahedron*, 2012, **68**, 3001-3011.
385. N. Toshima and T. Yonezawa, *New J. Chem.*, 1998, **22**, 1179-1201.
386. M. Aizawa and J. M. Buriak, *Chem. Mater.*, 2007, **19**, 5090-5101.
- 60 387. B. Lim, M. Jiang, P. H. C. Camargo, E. C. Cho, J. Tao, X. Lu, Y. Zhu and Y. Xia, *Science*, 2009, **324**, 1302-1305.
388. S. P. S. Badawal, S. S. Giddey, C. Munnings, A. I. Bhatt and T. Hollenkamp, *Front. Chem.*, 2014, doi: 10.3389/fchem.2014.00079.

389. R. M. Crooks, M. Zhao, L. Sun, V. Chechik and L. K. Yeung, *Acc. Chem. Res.*, 2000, **34**, 181-190.
390. S. Mann, S. L. Burkett, S. A. Davis, C. E. Fowler, N. H. Mendelson, S. D. Sims, D. Walsh and N. T. Whilton, *Chem. Mater.*, 1997, **9**, 2300-2310.
391. P. Chandra, D. S. Doke, S. B. Umbarkar and A. V. Biradar, *J. Mater. Chem. A.*, 2014, **2**, 19060-19066.
- 5 392. Z. Peng and H. Yang, *Nano Today*, 2009, **4**, 143-164.
393. W. Niu and G. Xu, *Nano Today*, 2011, **6**, 265-285.
394. W. Du, Q. Wang, D. Saxner, N. A. Deskins, D. Su, J. E. Krzanowski, A. I. Frenkel and X. Teng, *J. Am. Chem. Soc.*, 2011, **133**, 15172-15183.
395. H. Ataee-Esfahani, L. Wang, Y. Nemoto and Y. Yamauchi, *Chem. Mater.*, 2010, **22**, 6310-6318.
- 10 396. R. Choi, S.-I. Choi, C. H. Choi, K. M. Nam, S. I. Woo, J. T. Park and S. W. Han, *Chem.-Eur. J.*, 2013, **19**, 8190-8198.
397. S. J. Hwang, S. J. Yoo, J. Shin, Y.-H. Cho, J. H. Jang, E. Cho, Y.-E. Sung, S. W. Nam, T.-H. Lim, S.-C. Lee and S.-K. Kim, *Sci. Rep.*, 2013, **3**, 1309.
398. Y. Kang, L. Qi, M. Li, R. E. Diaz, D. Su, R. R. Adzic, E. Stach, J. Li and C. B. Murray, *ACS Nano*, 2012, **6**, 2818-2825.
399. K. Sasaki, H. Naohara, Y. Cai, Y. M. Choi, P. Liu, M. B. Vukmirovic, J. X. Wang and R. R. Adzic, *Angew. Chem. Int. Ed.*, 2010, **49**, 8602-8607.
- 15 400. Q. T. Trinh, J. Yang, J. Y. Lee and M. Saeys, *J. Catal.*, 2012, **291**, 26-35.
401. D. Wang, H. L. Xin, R. Hovden, H. Wang, Y. Yu, D. A. Muller, F. J. DiSalvo and H. D. Abruna, *Nat. Mater.*, 2013, **12**, 81-87.
402. D. Wang, H. L. Xin, H. Wang, Y. Yu, E. Rus, D. A. Muller, F. J. DiSalvo and H. D. Abruna, *Chem. Mater.*, 2012, **24**, 2274-2281.
- 20 403. H. Yang, *Angew. Chem. Int. Ed.*, 2011, **50**, 2674-2676.
404. K. D. Beard, D. Borrelli, A. M. Cramer, D. Blom, J. W. Van Zee and J. R. Monnier, *ACS Nano*, 2009, **3**, 2841-2853.
405. Z. Liu, J. E. Hu, Q. Wang, K. Gaskell, A. I. Frenkel, G. S. Jackson and B. Eichhorn, *J. Am. Chem. Soc.*, 2009, **131**, 6924-6925.
- 25 406. Z. Liu, G. S. Jackson and B. W. Eichhorn, *Angew. Chem. Int. Ed.*, 2010, **49**, 3173-3176.
407. J. Luo, L. Wang, D. Mott, P. N. Njoki, Y. Lin, T. He, Z. Xu, B. N. Wanjana, I. I. S. Lim and C.-J. Zhong, *Adv. Mater.*, 2008, **20**, 4342-4347.
408. P. Mani, R. Srivastava and P. Strasser, *J. Phys. Chem. C*, 2008, **112**, 2770-2778.
409. J. Zhang, F. H. B. Lima, M. H. Shao, K. Sasaki, J. X. Wang, J. Hanson and R. R. Adzic, *J. Phys. Chem. B*, 2005, **109**, 22701-22704.
- 30 410. K. An, Q. Zhang, S. Alayoglu, N. Musselwhite, J.-Y. Shin and G. A. Somorjai, *Nano Lett.*, 2014, **14**, 4907-4912.
411. H. N. Nong, L. Gan, E. Willinger, D. Teschner and P. Strasser, *Chem. Sci.*, 2014, **5**, 2955-2963.
412. H. N. Nong, H.-S. Oh, T. Reier, E. Willinger, M.-G. Willinger, V. Petkov, D. Teschner and P. Strasser, *Angew. Chem. Int. Ed.*, 2015, **54**, 2975-2979.
- 35 413. B. Singh, B. Seddon, E. Dempsey, W. Redington and C. Dickinson, *Electroanalysis*, 2015, **27**, 135-143.
414. X. Huang and P. Jiang, *Adv. Mater.*, 2015, **27**, 546-554.
415. L. Arroyo-Ramirez, C. Chen, M. Cargnello, C. B. Murray, P. Fornasiero and R. J. Gorte, *J. Mater. Chem. A.*, 2014, **2**, 19509-19514.
416. Y. Wang, J. Liu, P. Wang, C. J. Werth and T. J. Strathmann, *ACS Catal.*, 2014, **4**, 3551-3559.
- 40 417. J. L. Zhang, M. B. Vukmirovic, Y. Xu, M. Mavrikakis and R. R. Adzic, *Angew. Chem. Int. Ed.*, 2005, **44**, 2132-2135.
418. F. H. B. Lima, J. Zhang, M. H. Shao, K. Sasaki, M. B. Vukmirovic, E. A. Ticianelli and R. R. Adzic, *J. Phys. Chem. C*, 2007, **111**, 404-410.
419. V. Stamenkovic, B. S. Mun, K. J. J. Mayrhofer, P. N. Ross, N. M. Markovic, J. Rossmeisl, J. Greeley and J. K. Nørskov, *Angew. Chem. Int. Ed.*, 2006, **45**, 2897-2901.
- 45 420. C. Wang, N. M. Markovic and V. R. Stamenkovic, *ACS Catal.*, 2012, **2**, 891-898.
421. P. Mani, R. Srivastava and P. Strasser, *J. Power Sources*, 2011, **196**, 666-673.
422. U. A. Paulus, A. Wokaun, G. G. Scherer, T. J. Schmidt, V. Stamenkovic, V. Radmilovic, N. M. Markovic and P. N. Ross, *J. Phys. Chem. B*, 2002, **106**, 4181-4191.
423. L. Yang, M. B. Vukmirovic, D. Su, K. Sasaki, J. A. Herron, M. Mavrikakis, S. Liao and R. R. Adzic, *J. Phys. Chem. C*, 2013, **117**, 1748-1753.
- 50 424. D. A. Cantane, F. E. R. Oliveira, S. F. Santos and F. H. B. Lima, *Appl. Catal. B-Environ.*, 2013, **136**, 351-360.
425. G. Zhang, Z.-G. Shao, W. Lu, H. Xiao, F. Xie, X. Qin, J. Li, F. Liu and B. Yi, *J. Phys. Chem. C*, 2013, **117**, 13413-13423.
426. K. A. Kuttiyiel, K. Sasaki, Y. M. Choi, D. Su, P. Liu and R. R. Adzic, *Nano Lett.*, 2012, **12**, 6266-6271.
- 55 427. Y. Zhang, Y.-C. Hsieh, V. Volkov, D. Su, W. An, R. Si, Y. Zhu, P. Liu, J. X. Wang and R. R. Adzic, *ACS Catal.*, 2014, **4**, 738-742.
428. X. Ge, L. Chen, J. Kang, T. Fujita, A. Hirata, W. Zhang, J. Jiang and M. Chen, *Adv. Funct. Mater.*, 2013, **23**, 4156-4162.
429. Y. Choi, K. A. Kuttiyiel, J. P. Labis, K. Sasaki, G.-G. Park, T.-H. Yang and R. R. Adzic, *Top. Catal.*, 2013, **56**, 1059-1064.
- 60 430. Z. Zhuang, W. Sheng and Y. Yan, *Adv. Mater.*, 2014, **26**, 3950-3955.

431. J. X. Wang, H. Inada, L. Wu, Y. Zhu, Y. Choi, P. Liu, W.-P. Zhou and R. R. Adzic, *J. Am. Chem. Soc.*, 2009, **131**, 17298-17302.
432. X. Sun, D. Li, Y. Ding, W. Zhu, S. Guo, Z. L. Wang and S. Sun, *J. Am. Chem. Soc.*, 2014, **136**, 5745-5749.
433. J.-N. Zheng, J.-J. Lv, S.-S. Li, M.-W. Xue, A.-J. Wang and J.-J. Feng, *J. Mater. Chem. A.*, 2014, **2**, 3445-3451.
- 5 434. S. Zhang, Y. Hao, D. Su, V. V. T. Doan-Nguyen, Y. Wu, J. Li, S. Sun and C. B. Murray, *J. Am. Chem. Soc.*, 2014, **136**, 15921-15924.
435. J.-J. Lv, J.-N. Zheng, Y.-Y. Wang, A.-J. Wang, L.-L. Chen and J.-J. Feng, *J. Power Sources*, 2014, **265**, 231-238.
436. F. Zheng, W.-T. Wong and K.-F. Yung, *Nano Res.*, 2014, **7**, 410-417.
437. Y. Kim, Y. W. Lee, M. Kim and S. W. Han, *Chem. Eur. J.*, 2014, **20**, 7901-7905.
- 10 438. V. L. Nguyen, M. Ohtaki, T. Matsubara, M. T. Cao and M. Nogami, *J. Phys. Chem. C*, 2012, **116**, 12265-12274.
439. N. V. Long, T. Asaka, T. Matsubara and M. Nogami, *Acta Mater.*, 2011, **59**, 2901-2907.
440. N. V. Long, M. Ohtaki, T. D. Hien, J. Randy and M. Nogami, *Electrochim. Acta*, 2011, **56**, 9133-9143.
441. B. B. Xiao, Y. F. Zhu, X. Y. Lang, Z. Wen and Q. Jiang, *Sci. Rep.*, 2014, **4**, 5205.
442. S. Guo, S. Zhang, D. Su and S. Sun, *J. Am. Chem. Soc.*, 2013, **135**, 13879-13884.
- 15 443. C. N. Brodsky, A. P. Young, K. C. Ng, C.-H. Kuo and C.-K. Tsung, *ACS Nano*, 2014, **8**, 9368-9378.
444. S. Guo, X. Zhang, W. Zhu, K. He, D. Su, A. Mendoza-Garcia, S. F. Ho, G. Lu and S. Sun, *J. Am. Chem. Soc.*, 2014, **136**, 15026-15033.
445. J.-J. Wang, Y.-T. Liu, I. L. Chen, Y.-W. Yang, T.-K. Yeh, C. H. Lee, C.-C. Hu, T.-C. Wen, T.-Y. Chen and T.-L. Lin, *J. Phys. Chem. C*, 2014, **118**, 2253-2262.
- 20 446. C. Feng, X. Pang, Y. He, B. Li and Z. Lin, *Chem. Mater.*, 2014, **26**, 6058-6067.
447. V. Gorshkov, V. Kuzmenko and V. Privman, *J. Phys. Chem. C*, 2014, **118**, 24959-24966.
448. L. Han, H. Liu, P. Cui, Z. Peng, S. Zhang and J. Yang, *Sci. Rep.*, 2014, **4**, 6414.
449. F. Liu, Y. Dong, W. Yang, J. Yu, Z. Xu and Y. Hou, *Chem. Eur. J.*, 2014, **20**, 15197-15202.
450. Y. Sun, H. Sai, F. von Stein, M. Riccio and U. Wiesner, *Chem. Mater.*, 2014, **26**, 5201-5207.
- 25 451. H. Zhu, A. Sigdel, S. Zhang, D. Su, Z. Xi, Q. Li and S. Sun, *Angew. Chem. Int. Ed.*, 2014, **53**, 12508-12512.
452. W. E. Mahmoud, L. M. Bronstein, F. Al-Hazmi, F. Al-Noaiser and A. A. Al-Ghamdi, *Langmuir*, 2013, **29**, 13095-13101.
453. D. Amram and E. Rabkin, *ACS Nano*, 2014, **8**, 10687-10693.
454. R. P. Chaudhary, S. K. Mohanty and A. R. Koymen, *Carbon*, 2014, **79**, 67-73.
- 30 455. S. I. Sanchez, M. W. Small, J.-M. Zuo and R. G. Nuzzo, *J. Am. Chem. Soc.*, 2009, **131**, 8683-8689.
456. S. H. Baker, M. Roy, S. C. Thornton, M. Qureshi and C. Binns, *J. Phys.: Condensed Matter*, 2010, **22**, 385301.
457. N. V. Long, T. Duy Hien, T. Asaka, M. Ohtaki and M. Nogami, *Int. J. Hydrogen Energy*, 2011, **36**, 8478-8491.
458. Y. Cho, W. H. Lee and H. Kim, *J. Mater. Chem. A.*, 2014, **2**, 11635-11641.
459. F. Pincella, Y. Song, T. Ochiai, K. Isozaki, K. Sakamoto and K. Miki, *Chem. Phys. Lett.*, 2014, **605**, 115-120.
- 35 460. T. A. G. Silva, E. Teixeira-Neto, N. Lopez and L. M. Rossi, *Sci. Rep.*, 2014, **4**, 5766.
461. B. T. Sneed, A. P. Young, D. Jalalpoor, M. C. Golden, S. Mao, Y. Jiang, Y. Wang and C.-K. Tsung, *ACS Nano*, 2014, **8**, 7239-7250.
462. J. Xiang, P. Li, H. Chong, L. Feng, F. Fu, Z. Wang, S. Zhang and M. Zhu, *Nano Res.*, 2014, **7**, 1337-1343.
463. L. Yang, J. Su, W. Luo and G. Cheng, *ChemCatChem*, 2014, **6**, 1617-1625.
- 40 464. A. V. Erokhin, E. S. Lokteva, A. Y. Yermakov, D. W. Boukhvalov, K. I. Maslakov, E. V. Golubina and M. A. Uimin, *Carbon*, 2014, **74**, 291-301.
465. Y. Mahara, H. Ishikawa, J. Ohyama, K. Sawabe, Y. Yamamoto, S. Arai and A. Satsuma, *Chem. Lett.*, 2014, **43**, 910-912.
466. C. Wu, H. Zhang, Y.-X. Wu, Q.-C. Zhuang, L.-L. Tian and X.-X. Zhang, *Electrochimica Acta*, 2014, **134**, 18-27.
- 45 467. M. Zhang, Q. Sheng, F. Nie and J. Zheng, *J. Electroanal. Chem.*, 2014, **730**, 10-15.
468. Y. Hu, Q. Zhang, J. Goebel, T. Zhang and Y. Yin, *Phys. Chem. Chem. Phys.*, 2010, **12**, 11836-11842.
469. Q. Zhang, J. Ge, J. Goebel, Y. Hu, Z. Lu and Y. Yin, *Nano Res.*, 2009, **2**, 583-591.
470. Q. Zhang, I. Lee, J. Ge, F. Zaera and Y. Yin, *Adv. Funct. Mater.*, 2010, **20**, 2201-2214.
471. M. A. Matin, J.-H. Jang and Y.-U. Kwon, *Int. J. Hydrogen Energy*, 2014, **39**, 3710-3718.
- 50 472. H. Zhang, Y. Yin, Y. Hu, C. Li, P. Wu, S. Wei and C. Cai, *J. Phys. Chem. C*, 2010, **114**, 11861-11867.
473. Y.-T. Yu and P. Dutta, *J. Solid State Chem.*, 2011, **184**, 312-316.
474. L. Yang, J. Su, W. Luo and G. Cheng, *Int. J. Hydrogen Energy*, 2014, **39**, 3360-3370.
475. S. W. Kang, Y. W. Lee, Y. Park, B.-S. Choi, J. W. Hong, K.-H. Park and S. W. Han, *ACS Nano*, 2013, **7**, 7945-7955.
476. X. Meng, L. Yang, N. Cao, C. Du, K. Hu, J. Su, W. Luo and G. Cheng, *ChemPlusChem*, 2014, **79**, 325-332.

55